

Fast Inverse Nonlinear Fourier Transformation using Exponential One-Step Methods, Part I: Darboux Transformation

V. Vaibhav

Delft Center for Systems and Control, Delft University of Technology, Mekelweg 2, 2628 CD Delft, The Netherlands

Abstract

This paper considers the non-Hermitian Zakharov-Shabat (ZS) scattering problem which forms the basis for defining the SU(2)-nonlinear Fourier transformation (NFT). The theoretical underpinnings of this generalization of the conventional Fourier transformation is quite well established in the Ablowitz-Kaup-Newell-Segur (AKNS) formalism; however, efficient numerical algorithms that could be employed in practical applications are still unavailable.

In this paper, we present a unified framework for the forward and inverse NFT using exponential one-step methods which are amenable to FFT-based fast polynomial arithmetic. Within this discrete framework, we propose a fast Darboux transformation (FDT) algorithm having an operational complexity of $\mathcal{O}(KN + N \log^2 N)$ such that the error in the computed N -samples of the K -soliton vanishes as $\mathcal{O}(N^{-p})$ where p is the order of convergence of the underlying one-step method. For fixed N , this algorithm outperforms the classical DT (CDT) algorithm which has a complexity of $\mathcal{O}(K^2 N)$. We further present extension of these algorithms to the general version of DT which allows one to add solitons to arbitrary profiles that are admissible as scattering potentials in the ZS-problem. The general CDT/FDT algorithms have the same operational complexity as that of the K -soliton case and the order of convergence matches that of the underlying one-step method. A comparative study of these algorithms is presented through exhaustive numerical tests.

Keywords: Inverse Nonlinear Fourier Transform, Fast Darboux Transformation, Inverse Scattering, Multi-solitons.

PACS: 02.30.Zz, 02.30.Ik, 42.81.Dp, 03.65.Nk

Notations

The set of real numbers (integers) is denoted by \mathbb{R} (\mathbb{Z}) and the set of non-zero positive real numbers (integers) by \mathbb{R}_+ (\mathbb{Z}_+). The set of complex numbers are denoted by \mathbb{C} , and, for $\zeta \in \mathbb{C}$, $\text{Re}(\zeta)$ and $\text{Im}(\zeta)$ refer to the real and the imaginary parts of ζ , respectively. The complex conjugate of $\zeta \in \mathbb{C}$ is denoted by ζ^* and $\sqrt{\zeta}$ denotes its square root with a positive real part. The upper-half (lower-half) of \mathbb{C} is denoted by \mathbb{C}_+ (\mathbb{C}_-) and its closure by $\overline{\mathbb{C}}_+$ ($\overline{\mathbb{C}}_-$). The set $\mathbb{D} = \{z \in \mathbb{C}, |z| < 1\}$ denotes an open unit disk in \mathbb{C} and $\overline{\mathbb{D}}$ denotes its closure. The set $\mathbb{T} = \{z \in \mathbb{C}, |z| = 1\}$

denotes the unit circle in \mathbb{C} . The Pauli's spin matrices are denoted by, σ_j , $j = 1, 2, 3$, which are defined as

$$\sigma_1 = \begin{pmatrix} 0 & 1 \\ 1 & 0 \end{pmatrix}, \quad \sigma_2 = \begin{pmatrix} 0 & -i \\ i & 0 \end{pmatrix}, \quad \sigma_3 = \begin{pmatrix} 1 & 0 \\ 0 & -1 \end{pmatrix},$$

where $i = \sqrt{-1}$. For uniformity of notations, we denote $\sigma_0 = \text{diag}(1, 1)$. Matrix transposition is denoted by $(\cdot)^\top$ and I denotes the identity matrix. For any two vectors $\mathbf{u}, \mathbf{v} \in \mathbb{C}^2$, $\mathcal{W}(\mathbf{u}, \mathbf{v}) \equiv (u_1 v_2 - u_2 v_1)$ denotes the Wronskian of the two vectors and $[A, B]$ stands for the commutator of two matrices A and B . Partial derivatives with respect to x are denoted by ∂_x or $(\cdot)_x$ while repeated derivatives by ∂_x^2 . The support of a function $f : \Omega \rightarrow \mathbb{R}$ in Ω is defined as $\text{supp } f = \overline{\{x \in \Omega \mid f(x) \neq 0\}}$. The Lebesgue spaces of

Email address: v.k.vaibhav@tudelft.nl (V. Vaibhav)

complex-valued functions defined in \mathbb{R} are denoted by L^p for $1 \leq p \leq \infty$ with their corresponding norm denoted by $\|\cdot\|_{L^p}$ or $\|\cdot\|_p$.

The inverse Fourier-Laplace transform of a function $F(\zeta)$ analytic in $\bar{\mathbb{C}}_+$ is defined as

$$f(\tau) = \frac{1}{2\pi} \int_{\Gamma} F(\zeta) e^{-i\zeta\tau} d\zeta,$$

where Γ is any contour parallel to the real line.

1. Introduction

This paper considers the two-component non-Hermitian scattering problem first studied by Zakharov and Shabat (ZS) [1], which forms the basis for defining the SU(2)-nonlinear Fourier transformation (NFT). For certain integrable nonlinear equations whose general description is provided by the AKNS-formalism [2, 3], the NFT offers a powerful means of solving the corresponding initial-value problem (IVP). One such example is the nonlinear Schrödinger equation (NSE) that is commonly used to model channels for optical fiber communication. The propagation of optical field in a loss-less single mode fiber under Kerr-type focusing nonlinearity is governed by the NSE [4, 5] which can be cast into the following standard form

$$i\partial_Z q = \partial_T^2 q + 2|q|^2 q, \quad (T, Z) \in \mathbb{R} \times \mathbb{R}_+, \quad (1)$$

where $q(T, Z)$ is a complex valued function associated with the slowly varying envelope of the electric field, $Z \in \mathbb{R}_+$ is the position along the fiber and T is the retarded time. This equation also provides a satisfactory description of optical pulse propagation in the guiding-center or path-averaged formulation [6–8] when more general scenarios such as presence of fiber losses, lumped or distributed periodic amplification are included in the mathematical model of the physical channel. The IVP corresponding to (1) consists in finding the evolved field $q(T, Z)$ for a given initial condition $q(T, 0)$ under vanishing boundary conditions. For a given initial condition $q(T, 0)$, the nonlinear Fourier spectrum consists of (i) a continuous part $\rho(\xi)$, $\xi \in \mathbb{R}$, and (ii) a discrete part given by $\mathfrak{S}_K = \{(\zeta_k, b_k) \in \mathbb{C}^2 \mid \text{Im } \zeta_k > 0, k = 1, 2, \dots, K\}$ which is an ordered pair of eigenvalues ζ_k and the respective norming constants b_k (see [2] or Sec. 2 for a complete

introduction). The discrete spectrum is associated with the solitonic components of the potential which will be referred to as *bound states* in the rest of this paper. The energy in these states does not disperse away as in the case of linear waves, a phenomenon which is adequately characterized by the term “bound states”. The evolution of the nonlinear Fourier (NF) spectrum depicted in Fig. 1 is reminiscent of evolution in a linear channel—a property which is attributed to the integrability of the nonlinear channel.

In passing, we also note that the ZS-problem appears in various other physical systems, for instance, grating-assisted co-directional couplers (GACCs), a device used to couple light between two different guided modes of an optical fiber (see [9, 10] and references therein), and, NMR spectroscopy where design of frequency selective pulses requires solution of a ZS-problem [11–13].

Amongst the key physical effects that affect the performance of an optical fiber communication system, namely, chromatic dispersion, Kerr-type nonlinearity and optical noise, it is the latter two that have become the principle factors limiting the spectral efficiency of wavelength-division-multiplexed (WDM) networks at high signal powers. The reason behind this is largely the transmission methodologies that assume a linear model of the channel. The NF spectrum, in contrast, offers a novel way of encoding information in optical pulses where the nonlinear effects are adequately taken into account as opposed to being treated as a source of signal distortion. The idea to use discrete eigenvalues of the NF spectrum was first proposed by Hasegawa and Nyu [14] which they termed as the *eigenvalue communication*. Recently, Yousefi and Kschischang [15] have proposed nonlinear signal multiplexing in multi-user channels in order to mitigate the problem of nonlinear cross-talk that occurs in WDM systems. We note that the most general modulation technique uses both the discrete as well as the continuous part of the NF spectrum which was recently demonstrated in [16]. We refer the reader to a comprehensive review article [17] and the references therein for an overview of the progress in theoretical as well as experimental aspects of various NFT-based optical communication methodologies.

In any NFT-based modulation technique, the importance of low-complexity NFT-algorithms cannot be over emphasized. In this two part paper, we focus on the development of fast algorithms for various modulation scenarios of a NFT-based transmission system. As noted in [17],

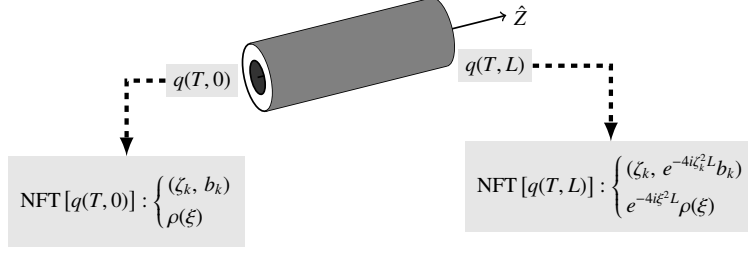


Figure 1: The figure shows evolution of the nonlinear Fourier spectrum along the length of the fiber. Here, the sequence (ζ_k, b_k) denotes the discrete spectrum and $\rho(\xi)$, $\xi \in \mathbb{R}$ is the continuous spectrum also known as the reflection coefficient.

many of the existing numerical approaches tend to become inaccurate as the signal power increases. While this maybe attributed to lack of numerical precision, it could also be numerical ill-conditioning or as a result of naive implementation. It is difficult to fully address these problems in this work, but let us remark that stability and convergence of the numerical algorithm plays a key role in determining its performance in realistic scenarios. We discuss these two aspects quite rigorously in this work.

Our primary goal here is to provide a theoretical foundation for the algorithms reported in [18] where we also showcased our preliminary results demonstrating the first fast inverse NFT. The specific problems for which we seek fast algorithms in this work are as follows:

Problem 1.1 (Generation of multi-solitons). *Given an arbitrary discrete spectrum \mathfrak{S}_K (K being its cardinality or, in other words, the number of bound states), compute the corresponding multi-soliton potential.*

Problem 1.2 (Addition of bound states). *Given an arbitrary potential $q_{seed}(x)$ referred to as the “seed” potential (assumed to be admissible as a scattering potential in the ZS-problem) and a given discrete spectrum \mathfrak{S}_K , compute the “augmented” potential such that its discrete spectrum is given by $\mathfrak{S}_{aug.} = \mathfrak{S}_{seed} \cup \mathfrak{S}_K$ where \mathfrak{S}_K is known to be disjoint with \mathfrak{S}_{seed} , the discrete spectrum of the seed potential.*

Problem 1.3 (Inversion of continuous spectrum). *Given an arbitrary continuous spectrum $\rho(\xi)$, $\xi \in \mathbb{R}$, such that there exists a positive constant $C > 0$ for which the estimate*

$$|\rho(\xi)| \leq \frac{C}{1 + |\xi|},$$

holds, compute the potential such that its continuous spectrum is $\rho(\xi)$ and the discrete spectrum is empty.

Problem 1.4 (Inverse NFT). *Given an arbitrary continuous spectrum $\rho(\xi)$, $\xi \in \mathbb{R}$, satisfying the estimate in Prob. 1.3 and a given discrete spectrum \mathfrak{S}_K , compute the potential such that its continuous spectrum is $\rho(\xi)$ and its discrete spectrum is \mathfrak{S}_K .*

The first two of these problems can be solved, at least in principle, using the Darboux transformations (DT) [19, 20]. The Prob. 1.1 can be solved with machine precision using DT with null-potential as the seed. The resulting complexity is $\mathcal{O}(K^2 N)$ where K is the number of eigenvalues and N is the number of samples of the potential. The scenario in Prob. 1.1 corresponds to the modulation of the discrete NF spectrum which has been explored by a number of groups [21–23] and it has also been experimentally demonstrated [24–29].

The Prob. 1.2 cannot be solved without resorting to numerical methods for the ZS-problem because the so called Jost solutions (which are required in DT) are not known in a closed form for any arbitrary seed potential. Prob. 1.3 and 1.4 will be treated in Part II of this paper. Note that a subclass of Prob. 1.3 is addressed in [30] which also deals with the Hermitian ZS-problem (which corresponds to defocussing type of nonlinearity for the NSE).

The numerical techniques for solving Prob. 1.1–1.4 developed in this work are based on exponential (linear) one-step methods [31, 32] for the discretization of the ZS-problem. The method yields a discrete framework for solving the ZS-problem which resembles the transfer matrix approach for solving wave-propagation problems in dielectric layered-media [33, Chap. 1]. These transfer

matrices have polynomial entries—a form that is amenable to the FFT-based polynomial arithmetic [34] and is also compatible with the layer-peeling algorithm [35]. All the methods considered in this article exhibit either a first order or a second order of convergence, i.e., the numerical errors vanish as $\mathcal{O}(N^{-p})$ where p is the order of the one-step method¹.

Within this discrete framework, we develop two algorithms: (a) the *classical Darboux transform* (CDT) which addresses Prob. 1.2, and, (b) the *fast Darboux transformation* (FDT) which addresses Prob. 1.1 and 1.2 both². The CDT algorithm is a direct numerical implementation of the DT in the continuum case where the seed Jost solutions are computed by numerically solving the scattering problem resulting in an overall complexity of $\mathcal{O}(K^2N)$. The FDT algorithm is entirely new and it is based on the pioneering work of Lubich on convolution quadrature [39–41]. In order to ensure compatibility with Lubich’s construction, we restricted ourselves to the implicit Euler method and the trapezoidal rule³. This algorithm has an operational complexity of $\mathcal{O}(N(K + \log^2 N))$ and an order of convergence that matches that of the underlying one-step method, i.e., $\mathcal{O}(N^{-p})$ where $p = 1$ (implicit Euler), $p = 2$ (trapezoidal rule). With increasing number of eigenvalues, FDT clearly outperforms CDT. The numerical tests and error analysis of the numerical scheme suggests that CDT is useful only for smaller number of eigenvalues. These tests further reveal that FDT is not only more accurate for the general case, it also has superior numerical conditioning with increasing number of eigenvalues as opposed to the CDT algorithm which be-

comes unstable.

1.1. Outline of the paper

This paper is organized as follows: In Sec. 2, we summarize the basic scattering theory and the Darboux transformation in the continuous regime.

The discrete scattering framework for the ZS-problem is developed in Sec. 3 where the numerical discretization in the spectral domain is described in Sec. 3.1, and, properties of the numerical Jost solutions are discussed in Sec. 3.2. We formulate the layer-peeling scheme in Sec. 3.3 which is based on the discrete framework developed in Sec. 3.1. Algorithmic aspects are addressed in Sec. 3.4 and 3.5 where we describe the sequential algorithm and its fast version obtained using a divide-and-conquer strategy, respectively. The sections 3.6 to 3.8 contain the main contribution of this paper: The method of inversion of continuous scattering coefficients using the Lubich’s method is discussed in Sec. 3.6. In Sec. 3.7, we apply the Lubich’s method to obtain the FDT algorithm for K -soliton potentials. Finally, the general version of the CDT algorithm and the FDT algorithm is discussed in Sec. 3.8.

The benchmarking methods that used for comparison are discussed in Sec. 4. The necessary and sufficient condition for discrete inverse scattering is discussed in Sec. 5. The stability and convergence analysis of the numerical schemes developed in earlier section is carried out in Sec. 6. The numerical experiments and results are discussed in the Sec. 7 which is followed by Sec. 8 which concludes the paper.

2. The AKNS System

In order to describe the fundamental basis of the nonlinear Fourier transform (NFT), we briefly review the scattering theory for a 2×2 AKNS system corresponding to the NSE. Because the NSE shows up in various disciplines, we choose to present the theory in a form that is independent of the context and conform to the way it appears in the classical texts on the scattering theory. For a complex valued field $q(x, t)$, we will work with the standard form of NSE which reads as

$$iq_t = q_{xx} + 2|q|^2q, \quad (x, t) \in \mathbb{R} \times \mathbb{R}_+, \quad (2)$$

¹The discrete system corresponding to Ablowitz-Ladik (AL) scattering problem [36, Chap. 3] is also amenable to FFT-based fast polynomial arithmetic and satisfies the layer-peeling property [37]; however, it does not illuminate on how to obtain a general recipe that could be applied to the ZS-problem in order to obtain a similar discrete system possessing a given order of convergence. The approach proposed in this article, on the other hand, translates into a general recipe for discretization of the ZS-problem using any linear one-step method to linear multistep methods [32] leading to a discrete system amenable to fast polynomial arithmetic and possessing a given order of convergence.

²It is worth noting that an alternative fast method of solving Prob. 1.1 is reported in [38] and it can be readily adapted to the discrete framework considered in this work. However, this method offers no control over the norming constants, therefore, we do not address this algorithm here.

³Both of these methods have an additional stability property known as the A-stability which makes them well suited for stiff ODEs [32].

where $t > 0$ is the evolution parameter identified as a *time-like* variable (this turns out to be the propagation distance Z for the fiber model) and $x \in \mathbb{R}$ is the domain over which the field is defined (which is the retarded time T for the fiber model). Henceforth, we closely follow the formalism developed in [2, 3] for the exposition in this article. The NFT of the complex-valued field $q(x, t)$ is introduced via the associated *Zakharov-Shabat scattering problem* [1] which can be stated as follows: Let $\zeta \in \mathbb{R}$ and $\mathbf{v} = (v_1, v_2)^\top \in \mathbb{C}^2$, then

$$\mathbf{v}_x = -i\zeta\sigma_3\mathbf{v} + U\mathbf{v}, \quad (3)$$

$$\mathbf{v}_t = 2i\zeta^2\sigma_3\mathbf{v} + [-2\zeta U + i\sigma_3(U^2 - U_x)]\mathbf{v}, \quad (4)$$

where

$$U = \begin{pmatrix} 0 & q(x, t) \\ r(x, t) & 0 \end{pmatrix}, \quad r(x, t) = -q^*(x, t), \quad (5)$$

is identified as the *scattering potential*. The second relation above corresponds to the focusing-type of nonlinearity for the NSE. The compatibility condition ($\mathbf{v}_{xt} = \mathbf{v}_{tx}$) between (3) and (4), assuming ζ is independent of t , produces the NSE as stated in (2).

The solution of the scattering problem (3), henceforth referred to as the ZS-problem, consists in finding the so called *scattering coefficients* which are defined through special solutions of (3) known as the *Jost solutions* described in the next subsection. These Jost solutions also play an important role in defining the *Darboux transformation* (DT) which is a powerful technique for constructing more complex potentials (as well as their Jost solutions) from simpler ones—this will be discussed in the final part of this section. There, we will be primarily interested in studying the form of DT which allows one to add bound states to a given potential.

2.1. Jost solutions

The *Jost solutions* are linearly independent solutions of (3) such that they have a plane-wave like behavior at $+\infty$ or $-\infty$. In the following, we set $t = 0$ and suppress the time-dependence of the solutions for the sake of brevity.

- *First kind:* The Jost solutions of the first kind, denoted by $\psi(x; \zeta)$ and $\bar{\psi}(x; \zeta)$, are the linearly independent solutions of (3) which have the following asymptotic behavior as $x \rightarrow \infty$: $\psi(x; \zeta)e^{-i\zeta x} \rightarrow (0, 1)^\top$ and $\bar{\psi}(x; \zeta)e^{i\zeta x} \rightarrow (1, 0)^\top$.

- *Second kind:* The Jost solutions of the second kind, denoted by $\phi(x; \zeta)$ and $\bar{\phi}(x; \zeta)$, are the linearly independent solutions of (3) which have the following asymptotic behavior as $x \rightarrow -\infty$: $\phi(x; \zeta)e^{i\zeta x} \rightarrow (1, 0)^\top$ and $\bar{\phi}(x; \zeta)e^{-i\zeta x} \rightarrow (0, -1)^\top$.

The evolution of the Jost solutions in time is governed by the equation (4) for $t \in \mathbb{R}_+$ under the asymptotic boundary conditions prescribed above. On account of the linear independence of ψ and $\bar{\psi}$, we have

$$\begin{aligned} \phi(x; \zeta) &= a(\zeta)\bar{\psi}(x; \zeta) + b(\zeta)\psi(x; \zeta), \\ \bar{\phi}(x; \zeta) &= -\bar{a}(\zeta)\psi(x; \zeta) + \bar{b}(\zeta)\bar{\psi}(x; \zeta). \end{aligned}$$

Similarly, using the pair ϕ and $\bar{\phi}$, we have

$$\begin{aligned} \psi(x; \zeta) &= -a(\zeta)\bar{\phi}(x; \zeta) + \bar{b}(\zeta)\phi(x; \zeta), \\ \bar{\psi}(x; \zeta) &= \bar{a}(\zeta)\phi(x; \zeta) + b(\zeta)\bar{\phi}(x; \zeta). \end{aligned}$$

The coefficients appearing in the equations above can be written in terms of the Jost solutions by using the Wronskian relations⁴:

$$\begin{aligned} a(\zeta) &= \mathcal{W}(\phi, \psi), & b(\zeta) &= \mathcal{W}(\bar{\psi}, \phi), \\ \bar{a}(\zeta) &= \mathcal{W}(\bar{\phi}, \bar{\psi}), & \bar{b}(\zeta) &= \mathcal{W}(\bar{\phi}, \psi). \end{aligned} \quad (6)$$

These coefficients are known as the *scattering coefficients* and the process of computing them is referred to as *forward scattering*. As it turns out, we would also be interested in studying the analytic continuation of the Jost solutions with respect to ζ , which in turn also determines the analytic continuation of the scattering coefficients. The motivation behind this is threefold: First, the inversion of the scattering coefficients cannot be done in general by knowing the value of the scattering coefficients over the real line (i.e. $\zeta \in \mathbb{R}$). Second, the knowledge of analyticity and decay properties of these functions in the complex plane allows us to establish certain theoretical estimates with greater ease. Lastly, in many cases, the knowledge

⁴For any pair of linearly independent vectors, $\mathbf{v}, \mathbf{u} \in \mathbb{C}^2$, their Wronskian which is defined as

$$\mathcal{W}(\mathbf{u}, \mathbf{v}) = (\mathbf{u}, \mathbf{v}) = u_1 v_2 - v_1 u_2,$$

is non-zero. If \mathbf{u}, \mathbf{v} also qualify as Jost solutions, then their Wronskian is independent of x [2].

of the analytic form introduces a certain redundancy in the system that can be exploited by the numerical algorithms to improve its numerical conditioning and stability.

In order to discuss the analytic continuation of the Jost solution with respect to ζ , let us specify the following two classes of functions for the scattering potential (at $t = 0$): Let $q(\cdot, 0) \in L^1$ such that $\text{supp } q(\cdot, 0) \subset \Omega = [L_1, L_2]$ or $|q(x, 0)| \leq C \exp[-2d|x|]$ almost everywhere in \mathbb{R} for some constants $C > 0$ and $d > 0$. In the former case, the Jost solutions have analytic continuation in whole of the complex plane with respect to ζ . Consequently, the scattering coefficients $a(\zeta)$, $b(\zeta)$, $\bar{a}(\zeta)$, $\bar{b}(\zeta)$ are analytic functions of $\zeta \in \mathbb{C}$. In the latter case, the analyticity property can be summarized as follows [2, Sec. IV.A]: The functions $e^{-i\zeta x}\psi$ and $e^{i\zeta x}\phi$ are analytic in the half-space $\{\zeta \in \mathbb{C} \mid \text{Im } \zeta > -d\}$. The functions $e^{i\zeta x}\bar{\psi}$ and $e^{-i\zeta x}\bar{\phi}$ are analytic in the half-space $\{\zeta \in \mathbb{C} \mid \text{Im } \zeta < d\}$. In this case, the coefficient $a(\zeta)$ is analytic for $\text{Im } \zeta > -d$ while the coefficient $b(\zeta)$ is analytic in the strip defined by $-d < \text{Im } \zeta < d$. More will be said about the analyticity and decay properties of the scattering coefficients in Sec. 6.1.

Furthermore, the symmetry properties

$$\bar{\psi}(x; \zeta) = \begin{pmatrix} \psi_2^*(x; \zeta^*) \\ -\psi_1^*(x; \zeta^*) \end{pmatrix}, \quad \bar{\phi}(x; \zeta) = \begin{pmatrix} \phi_2^*(x; \zeta^*) \\ -\phi_1^*(x; \zeta^*) \end{pmatrix}, \quad (7)$$

yield the relations $\bar{a}(\zeta) = a^*(\zeta^*)$ and $\bar{b}(\zeta) = b^*(\zeta^*)$.

2.2. Scattering data and the nonlinear Fourier spectrum

The scattering coefficients introduced in the last section together with certain quantities defined below that facilitate the recovery of the scattering potential are collectively referred to as the *scattering data*. The *nonlinear Fourier spectrum* can then be defined as any of the subsets which qualify as the “primordial” scattering data [2, App. 5], i.e., the minimal set of quantities sufficient to determine the scattering potential, uniquely.

In general, the nonlinear Fourier spectrum for the potential $q(x, 0)$ comprises a *discrete* and a *continuous spectrum*. The discrete spectrum consists of the so called *eigenvalues* $\zeta_k \in \mathbb{C}_+$, such that $a(\zeta_k) = 0$, and, the *normalizing constants* b_k such that $\phi(x; \zeta_k) = b_k \psi(x; \zeta_k)$. For convenience, let the discrete spectrum be denoted by the set

$$\mathfrak{S}_K = \{(\zeta_k, b_k) \in \mathbb{C}^2 \mid \text{Im } \zeta_k > 0, k = 1, 2, \dots, K\}. \quad (8)$$

For compactly supported potentials, $b_k = b(\zeta_k)$. Note that some authors choose to define the discrete spectrum using the pair (ζ_k, ρ_k) where $\rho_k = b_k/\dot{a}(\zeta_k)$ is known as the *spectral amplitude* corresponding to ζ_k (\dot{a} denotes the derivative of a).

The continuous spectrum, also referred to as the *reflection coefficient*, is defined by $\rho(\xi) = b(\xi)/a(\xi)$ for $\xi \in \mathbb{R}$. The coefficient $a(\zeta)$ and consequently the discrete eigenvalues do not evolve in time. The rest of the scattering data evolves according to the relations $b_k(t) = b_k e^{-4i\zeta_k^2 t}$ and $\rho(\xi, t) = \rho(\xi) e^{-4i\xi^2 t}$.

2.3. The Darboux transformation

The *Darboux transformation* provides a purely algebraic means of adding bound states to a seed solution [19, 20, 42]. In doing so the b -coefficient of the potential remains invariant [19] while the a -coefficient gets modified to reflect the addition of the bound states. In particular, starting from the “vacuum” solution (i.e. the solution for the null-potential), one can compute reflectionless potentials also referred to as the multi-soliton or, more precisely, the K -soliton potential with the desired discrete spectrum. The Darboux transformation is carried out by means of *Darboux matrices* which is described in the following paragraphs.

Let \mathfrak{S}_K as defined by (8) be the discrete spectrum to be added to the seed potential. Define the matrix form of the Jost solutions as

$$v(x, t; \zeta) = (\phi, \psi) = \begin{pmatrix} \phi_1 & \psi_1 \\ \phi_2 & \psi_2 \end{pmatrix}. \quad (9)$$

The augmented matrix Jost solution $v_K(x, t; \zeta)$ can be obtained from the seed solution $v_0(x, t; \zeta)$ using the Darboux matrix as

$$v_K(x, t; \zeta) = \mu_K(\zeta) D_K(x, t; \zeta, \mathfrak{S}_K) v_0(x, t; \zeta), \quad \zeta \in \overline{\mathbb{C}}_+,$$

where $\mu_K(\zeta)$ is to be determined. In the following, we summarize the approach proposed by Neugebauer and Meinel [42] which requires the Darboux matrix to be written as

$$D_K(x, t; \zeta, \mathfrak{S}_K) = \sum_{k=0}^K D_k^{(K)}(x, t; \mathfrak{S}_K) \zeta^k,$$

where the coefficient matrices are such that (for the special case $r = -q^*$) $d_K^{(K)} = \sigma_0$ and

$$D_k^{(K)} = \begin{pmatrix} d_0^{(k,K)} & d_1^{(k,K)} \\ -d_1^{(k,K)*} & d_0^{(k,K)*} \end{pmatrix}, \quad k = 0, 1, \dots, K-1.$$

From the Wronskian relation, we know $a_0(\zeta) = \det[v_0]$; hence, it follows that

$$\begin{aligned} a_K(\zeta) &= \det[v_K(x, t; \zeta)] \\ &= [\mu_K(\zeta)]^2 \det[D_K(x, t; \zeta, \mathfrak{S}_K)] a_0(\zeta). \end{aligned}$$

It is shown in [42] that $\det[D_K(x, t; \zeta, \mathfrak{S}_K)]$ is independent of (x, t) . Further, the symmetry imposed by the condition $r = -q^*$, requires

$$\det[D_K(x, t; \zeta, \mathfrak{S}_K)] = \prod_{k=1}^K (\zeta - \zeta_k)(\zeta - \zeta_k^*),$$

which combined with the fact that [19]

$$a_K(\zeta) = a_0(\zeta) \prod_{k=1}^K \left(\frac{\zeta - \zeta_k^*}{\zeta - \zeta_k} \right),$$

yields

$$\mu_K(\zeta) = \prod_{k=1}^K \frac{1}{(\zeta - \zeta_k^*)}.$$

From $\phi_K(x, t; \zeta_k) = b_k(t)\psi_K(x, t; \zeta_k)$, we have

$$D_K(x, t; \zeta_k, \mathfrak{S}_K)[\phi_0(x, t; \zeta_k) - b_k(t)\psi_0(x, t; \zeta_k)] = 0. \quad (10)$$

Note that $\phi_0(x, t; \zeta_k) - b_k(t)\psi_0(x, t; \zeta_k) \neq 0$ on account of $a_0(\zeta_k) \neq 0$, i.e., ζ_k is not an eigenvalue of the seed potential. The $2K$ system of equations in (10) can be used to compute the $2K$ unknown coefficients of the Darboux matrix. Let U_K and U_0 correspond to the augmented potential q_K and the seed potential q_0 , respectively; then

$$\begin{aligned} U_K &= U_0 - i[D_{K-1}^{(K)}, \sigma_3] \\ &= U_0 + \begin{pmatrix} 0 & 2id_1^{(K-1,K)} \\ 2id_1^{(K-1,K)*} & 0 \end{pmatrix}. \end{aligned}$$

2.3.1. Darboux matrix of degree one

For the sake of simplicity, let us consider the seed solution with empty discrete spectra. Let us define the

successive discrete spectra $\emptyset = \mathfrak{S}_0 \subset \mathfrak{S}_1 \subset \mathfrak{S}_2 \subset \dots \subset \mathfrak{S}_K$ such that $\mathfrak{S}_j = \{(\zeta_j, b_j)\} \cup \mathfrak{S}_{j-1}$ for $j = 1, 2, \dots, K$ where (ζ_j, b_j) are distinct elements of \mathfrak{S}_K .

For single bound state, described by \mathfrak{S}_1 , putting

$$\beta_0(x, t; \zeta_1, b_1) = \frac{\phi_1^{(0)}(x, t; \zeta_1) - b_1(t)\psi_1^{(0)}(x, t; \zeta_1)}{\phi_2^{(0)}(x, t; \zeta_1) - b_1(t)\psi_2^{(0)}(x, t; \zeta_1)},$$

the solution of the corresponding linear system (10) yields the Darboux matrix of degree one given by

$$\begin{aligned} D_1(x, t; \zeta, \mathfrak{S}_1|\mathfrak{S}_0) &= \zeta\sigma_0 - \begin{pmatrix} \beta_0 & 1 \\ 1 & -\beta_0^* \end{pmatrix} \begin{pmatrix} \zeta_1 & 0 \\ 0 & \zeta_1^* \end{pmatrix} \begin{pmatrix} \beta_0 & 1 \\ 1 & -\beta_0^* \end{pmatrix}^{-1} \\ &= \zeta\sigma_0 - \frac{1}{1 + |\beta_0|^2} \begin{pmatrix} |\beta_0|^2\zeta_1 + \zeta_1^* & (\zeta_1 - \zeta_1^*)\beta_0 \\ (\zeta_1 - \zeta_1^*)\beta_0^* & \zeta_1 + \zeta_1^*|\beta_0|^2 \end{pmatrix}. \end{aligned} \quad (11)$$

The augmented potential then works out as

$$q_1(x, t) = q_0(x, t) - 2i \frac{(\zeta_1 - \zeta_1^*)\beta_0}{1 + |\beta_0|^2}. \quad (12)$$

The Jost solutions for this new potential can be obtained via the Darboux matrix and the entire procedure can be repeated for adding another bound state to the augmented potential. Suppressing the x and t dependence for the sake of brevity, it follows that the Darboux matrix of degree $K > 1$ can be factorized into Darboux matrices of degree one as

$$\begin{aligned} D_K(\zeta, \mathfrak{S}_K|\mathfrak{S}_0) &= D_1(\zeta, \mathfrak{S}_K|\mathfrak{S}_{K-1}) \\ &\quad \times D_1(\zeta, \mathfrak{S}_{K-1}|\mathfrak{S}_{K-2}) \times \dots \times D_1(\zeta, \mathfrak{S}_1|\mathfrak{S}_0), \end{aligned}$$

where $D_1(\zeta, \mathfrak{S}_j|\mathfrak{S}_{j-1})$, $j = 1, \dots, K$ are the successive Darboux matrices of degree one with the convention that $(\zeta_j, b_j) = \mathfrak{S}_j \cap \mathfrak{S}_{j-1}$ is the bound state being added to the seed solution whose discrete spectra is \mathfrak{S}_{j-1} . Using the expression in (11), we have

$$\begin{aligned} D_1(\zeta, \mathfrak{S}_j|\mathfrak{S}_{j-1}) &= \zeta\sigma_0 - \\ &\quad \frac{1}{1 + |\beta_{j-1}|^2} \begin{pmatrix} |\beta_{j-1}|^2\zeta_j + \zeta_j^* & (\zeta_j - \zeta_j^*)\beta_{j-1} \\ (\zeta_j - \zeta_j^*)\beta_{j-1}^* & \zeta_j + \zeta_j^*|\beta_{j-1}|^2 \end{pmatrix}, \end{aligned}$$

where

$$\beta_{j-1}(\zeta_j, b_j) = \frac{\phi_1^{(j-1)}(\zeta_j) - b_j\psi_1^{(j-1)}(\zeta_j)}{\phi_2^{(j-1)}(\zeta_j) - b_j\psi_2^{(j-1)}(\zeta_j)},$$

for $(\zeta_j, b_j) \in \mathfrak{S}_K$ and the successive Jost solutions, $v_j = (\phi_j, \psi_j)$, needed in this ratio are computed as

$$v_j = \frac{1}{(\zeta - \zeta_j)} D_1(\zeta, \mathfrak{S}_j | \mathfrak{S}_{j-1}) v_{j-1}.$$

The successive potentials are given by

$$q_j = q_{j-1} - 2i \frac{(\zeta_j - \zeta_j^*) \beta_{j-1}}{1 + |\beta_{j-1}|^2}.$$

See Fig. 2 for a schematic representation of the DT.

If the seed Jost solution $v_0(x, t; \zeta)$ corresponding to the seed potential $q_0(x, t)$ is known, then the Darboux transformations can be readily carried out over any set of grid points $\{x_n\} \subset \mathbb{R}$ in order to compute the augmented potential at these grid points. The resulting order of operational complexity, excluding the cost of evaluating the seed potential and the seed Jost solution, works out to be $\mathcal{O}(K^2 N)$ where N is the number of samples of the augmented potential. For the special case of K -solitons, the seed potential as well as the seed Jost solutions are trivially known; therefore, this method provides us with an algorithm for computing the K -soliton potentials with machine precision. In general, closed form solutions are rarely known for arbitrary potentials; nevertheless, this procedure can be carried out with numerically computed Jost solutions in any discrete framework. This scheme will be referred to as the *classical Darboux transformation* (CDT) in the rest of the article. The error analysis of this method is carried out in Sec. 6.5.

For multi-solitons, the asymptotic form of the potential as $x \rightarrow \infty$ works out to be

$$q_k(x, t) \sim 2i \sum_{j=1}^k \frac{(\zeta_j - \zeta_j^*)}{a_{j-1}^*(\zeta_j)} b_j^*(t) e^{-2i\zeta_j^* x},$$

and as $x \rightarrow -\infty$

$$q_k(x, t) \sim 2i \sum_{j=1}^k \frac{(\zeta_j - \zeta_j^*)}{a_{j-1}(\zeta_j)} \frac{1}{b_j(t)} e^{-2i\zeta_j x},$$

where $a_j(\zeta) = a(\zeta; \mathfrak{S}_j)$ are the successive a -coefficients. Therefore, $q_k(x, t)$ exhibits exponential decay with a decay constant that is given by $d_k = \min_{1 \leq j \leq k} \text{Im} \zeta_j$. This observation allows us to conclude that round off errors in the CDT scheme can be minimized if the eigenvalues

are “added” in the decreasing order of the magnitude of their imaginary parts [43]. Further, the knowledge of the decay constant can be used to choose an optimal computational domain so that the numerical errors due to domain truncation is minimized (see Sec. 7.1.1).

2.3.2. Effective support of multi-soliton potentials

A multi-soliton potential has an unbounded support, therefore, in any practical application it is mandatory to introduce an effective support with desired energy content. Posing conversely, one may also be interested in choosing the discrete spectrum which leads to a prescribed effective support with desired energy content initially or over a finite duration of evolution.

In case of multi-solitons, the energy content of the side lobe which we wish to truncate is trivially available in the CDT scheme and it can be used as a truncation criteria. Let χ_Ω denote the characteristic function of Ω and let $[-L, L]$ ($L > 0$) be the domain that needs to be determined so that

$$\|q_K \chi_{(-\infty, -L]}\|_{L^2}^2 + \|q_K \chi_{[L, \infty)}\|_{L^2}^2 = \epsilon \|q_K\|_{L^2}^2. \quad (13)$$

Suppressing the dependence on t for the sake of brevity, the asymptotic expansion of $\phi_K(-L; \zeta) e^{-i\zeta L}$ with respect to ζ yields [2, Sec. IV.A]

$$\|q_K \chi_{(-\infty, -L]}\|_{L^2}^2 = \sum_{j=1}^K \frac{4 \text{Im}(\zeta_j)}{[1 + |\beta_{j-1}(-L; \zeta_j, b_j)|^{-2}]}, \quad (14)$$

and that corresponding to $\psi_K(L; \zeta) e^{-i\zeta L}$ yields

$$\|q_K \chi_{[L, \infty)}\|_{L^2}^2 = \sum_{j=1}^K \frac{4 \text{Im}(\zeta_j)}{[1 + |\beta_{j-1}(L; \zeta_j, b_j)|^2]}. \quad (15)$$

These relationships are also known as the *nonlinear Parseval's relationships*. Asymptotic estimates when $L \gg 1$ can be easily obtained from the above relations:

$$\begin{aligned} \|q_K \chi_{(-\infty, -L]}\|_{L^2}^2 &\sim \sum_{j=1}^K \frac{4 \text{Im}(\zeta_j)}{|a_{j-1}(\zeta_j)|^2} \frac{1}{|b_j|^2} e^{-4 \text{Im}(\zeta_j) L}, \\ \|q_K \chi_{[L, \infty)}\|_{L^2}^2 &\sim \sum_{j=1}^K \frac{4 \text{Im}(\zeta_j)}{|a_{j-1}(\zeta_j)|^2} |b_j|^2 e^{-4 \text{Im}(\zeta_j) L}. \end{aligned}$$

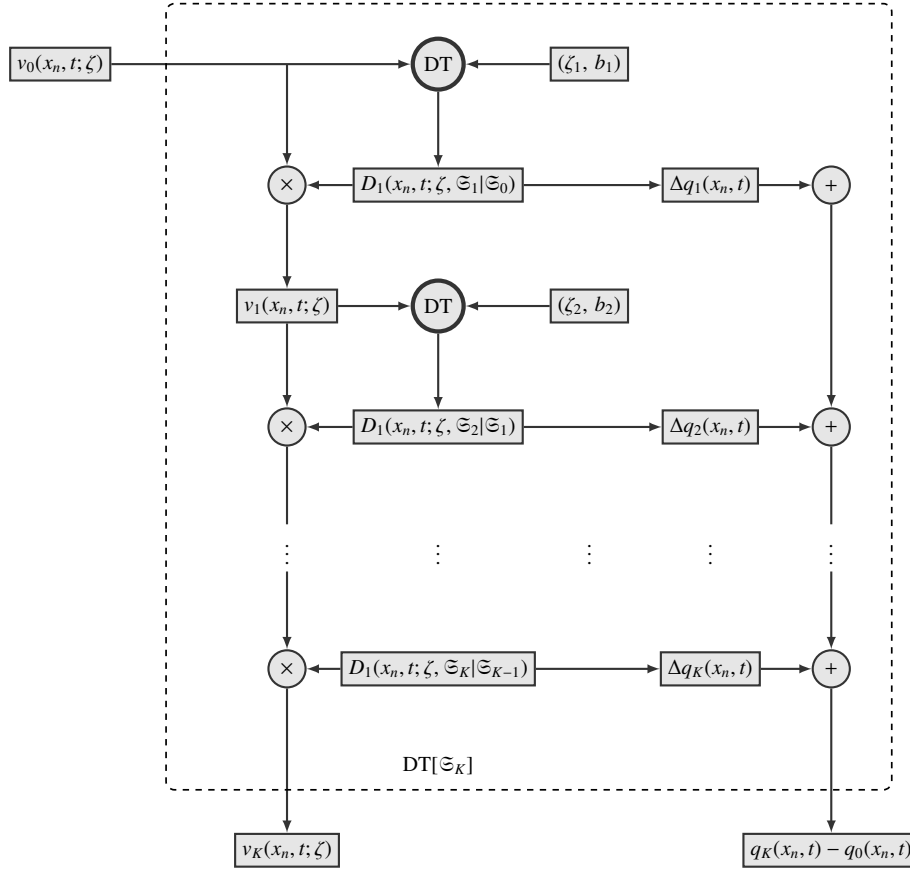


Figure 2: The figure shows the schematic of the classical Darboux transformation for a given discrete spectrum, Ξ_K , where the discrete spectrum of the seed solution is empty, i.e. $\Xi_0 = \emptyset$, and the given grid point, x_n . The part enclosed within broken lines is referred to as the complete DT-block (labeled as $\text{DT}[\Xi_K]$). The sole input to this block is the seed Jost solution, $v_0(x_n, t; \zeta)$. The output of the DT-block consists of the augmented Jost solution, $v_K(x_n, t; \zeta)$, and the difference between the augmented and the seed potential, $q_K(x_n, t) - q_0(x_n, t)$. Here, $\Delta q_j(x_n, t) = q_j(x_n, t) - q_{j-1}(x_n, t)$ and $\Xi_j = \Xi_{j-1} \cup \{(\zeta_j, b_j)\}$ with $\Xi_1 = \{(\zeta_1, b_1)\} \cup \Xi_0$ where (ζ_j, b_j) , $j = 1, 2, \dots, K$ are the distinct elements of Ξ_K (see Sec. 2.2).

This allows us to obtain an asymptotic formula for the effective support of a K -soliton potential. Define $L = L(\epsilon; \Xi_K) > 0$ such that

$$\|q_K \chi_{[-L, L]}\|_{L^2}^2 = (1 - \epsilon) \|q_K\|_{L^2}^2 = 4(1 - \epsilon) \sum_{j=1}^K \eta_j,$$

then

$$L \approx W = \frac{1}{2\eta_{\min}} \log \left[\frac{\sum_{j=1}^K \omega_j \eta_j}{\epsilon \sum_{j=1}^K \eta_j} \right], \quad (16)$$

under the assumption $\epsilon \sum_{j=1}^K \eta_j \ll \sum_{j=1}^K \omega_j \eta_j$ where

$$\omega_j = \frac{1}{|a_{j-1}(\zeta_j)|^2} \left(|b_j|^2 + \frac{1}{|b_j|^2} \right).$$

Finally, let us note that a binary search algorithm (bisection method) can be devised to solve the nonlinear equation (13) for $L = L(\epsilon, \Xi_K)$ where $[0, W]$ can be taken as the bracketing interval for the root⁵. The complexity of

⁵Numerical tests indicates that $[-W, W]$ tends to over estimate the effective support.

such an algorithm (for fixed t) works out to be $\mathcal{O}(mK^2)$ where m is the number of bisection steps needed.

2.3.3. Scattering coefficients of a truncated multi-soliton

Let $x = 0$ be taken as the point of truncation. Then a multi-soliton potential can be seen as comprising a left-sided profile (supported in $\mathbb{R}_- \cup \{0\}$) and a right-sided profile (supported in $\{0\} \cup \mathbb{R}_+$). The respective scattering coefficients of each of the truncated potentials turn out to be a rational function of ζ . These observations were already made by several authors [12, 13, 44–46] and a number of different methods do exist for inversion of the scattering data which exploit the rational character of the truncated scattering coefficients. Our numerical scheme also exploits this property; therefore, we discuss this case in some detail below.

Let us consider the left-sided profile, denoted by $q^{(-)}(x, t)$. The Jost solution $\phi^{(-)}(x, t; \zeta)$ at $x = 0$ can be computed using the Darboux transformation as described above. The Jost solution $\psi^{(-)}(x, t; \zeta)$ at $x = 0$ corresponds to that of a null-potential, i.e., $\psi^{(-)}(0, t; \zeta) = (0, 1)^T$. The scattering coefficients for the left-sided profile, therefore, works out to be

$$a^{(-)}(\zeta, t) = \phi_1^{(-)}(0, t; \zeta), \quad b^{(-)}(\zeta, t) = \phi_2^{(-)}(0, t; \zeta).$$

This corresponds to the first column of the Darboux matrix $D_K(0, t; \zeta, \Xi_K)$, therefore, a purely rational function of ζ analytic in $\overline{\mathbb{C}}_+$. Now, let us consider the right-sided profile, denoted by $q^{(+)}(x, t)$. The Jost solution $\psi^{(+)}(x, t; \zeta)$ at $x = 0$ can be computed using the Darboux transformation as before while the Jost solution $\phi^{(+)}(x, t; \zeta)$ at $x = 0$ is given by $\phi^{(+)}(0, t; \zeta) = (1, 0)^T$. Therefore, the relevant scattering coefficients for the right-sided profile works out to be

$$a^{(+)}(\zeta, t) = \psi_2^{(+)}(0, t; \zeta), \quad \bar{b}^{(+)}(\zeta, t) = \psi_1^{(+)}(0, t; \zeta).$$

This corresponds to the second column of the Darboux matrix $D_K(0, t; \zeta, \Xi_K)$ and, therefore, a purely rational function of ζ analytic in $\overline{\mathbb{C}}_+$.

Remark 2.1 (Conjugation and reflection). *The inverse scattering problem for the right-sided profile can be transformed to that of a left-sided profile in the following way: putting $y = -x$, we have*

$$\begin{aligned} v_y(-y; \zeta) &= i\zeta\sigma_3 v(-y; \zeta) - U(-y)v(-y; \zeta), \\ w_y &= -i\zeta\sigma_3 w + U^*(-y)w, \end{aligned}$$

where $w(y) = \sigma_1 v(-y; \zeta)$. Denote the Jost solutions of the new system (i.e. with potential $U^*(-y)$) by $\Psi(y; \zeta)$, $\bar{\Psi}(y; \zeta)$ (first kind) and $\Phi(y; \zeta)$, $\bar{\Phi}(y; \zeta)$ (second kind), then

$$\begin{aligned} \Psi(y; \zeta) &= \sigma_1 \phi(-y; \zeta), & \bar{\Psi}(y; \zeta) &= -\sigma_1 \bar{\phi}(-y; \zeta), \\ \Phi(y; \zeta) &= \sigma_1 \psi(-y; \zeta), & \bar{\Phi}(y; \zeta) &= -\sigma_1 \bar{\psi}(-y; \zeta). \end{aligned}$$

Let $A(\zeta)$, $B(\zeta)$, $\bar{A}(\zeta)$ and $\bar{B}(\zeta)$ be the scattering coefficients for the new system, then

$$\begin{aligned} A(\zeta) &= \mathcal{W}(\Phi, \Psi) = a(\zeta), & \bar{A}(\zeta) &= \mathcal{W}(\bar{\Phi}, \bar{\Psi}) = \bar{a}(\zeta), \\ B(\zeta) &= \mathcal{W}(\bar{\Psi}, \Phi) = \bar{b}(\zeta), & \bar{B}(\zeta) &= \mathcal{W}(\bar{\Phi}, \Psi) = b(\zeta). \end{aligned}$$

The discrete eigenvalues do not change, however, the norming constants change as $B_k = 1/b_k$. Now, the scattering coefficients for the left-sided profile obtained as result of truncating the new potential from the right at $x = 0$ work out to be

$$\begin{aligned} A^{(-)}(\zeta, t) &= \Phi_1(0, t; \zeta) = \psi_2(0, t; \zeta), \\ B^{(-)}(\zeta, t) &= \Phi_2(0, t; \zeta) = \psi_1(0, t; \zeta). \end{aligned}$$

Therefore, an implementation for the case of left-sided profile is sufficient to solve problems of general nature encountered in forward/inverse NFT.

Remark 2.2 (Translation). *Let us note that there is no loss of generality in choosing the point of truncation to be $x = 0$ on account of the translational properties of the discrete spectrum. If we wish to choose the point of truncation to be $x = x_0$, we can consider the transformation $x = y + x_0$. Define the new potential to be $\tilde{U}(y) = U(y + x_0)$ so that*

$$\begin{aligned} v_y(y + x_0; \zeta) &= -i\zeta\sigma_3 v(y + x_0; \zeta) + U(y + x_0)v(y + x_0; \zeta), \\ w_y &= -i\zeta\sigma_3 w + \tilde{U}(y)w, \end{aligned}$$

where $w(y; \zeta) = v(y + x_0; \zeta)$. Denote the Jost solutions of the new system by $\Psi(y; \zeta)$, $\bar{\Psi}(y; \zeta)$ (first kind) and $\Phi(y; \zeta)$, $\bar{\Phi}(y; \zeta)$ (second kind), then

$$\begin{aligned} \Psi(y; \zeta) &= \psi(y + x_0; \zeta)e^{-i\zeta x_0}, & \bar{\Psi}(y; \zeta) &= \bar{\psi}(y + x_0; \zeta)e^{i\zeta x_0}, \\ \Phi(y; \zeta) &= \phi(y + x_0; \zeta)e^{i\zeta x_0}, & \bar{\Phi}(y; \zeta) &= \bar{\phi}(y + x_0; \zeta)e^{-i\zeta x_0}. \end{aligned}$$

Let $A(\zeta)$, $B(\zeta)$, $\bar{A}(\zeta)$ and $\bar{B}(\zeta)$ be the scattering coefficients for the new system, then

$$\begin{aligned} A(\zeta) &= \mathcal{W}(\Phi, \Psi) = a(\zeta), & B(\zeta) &= \mathcal{W}(\bar{\Psi}, \Phi) = b(\zeta)e^{2i\zeta x_0}, \\ \bar{A}(\zeta) &= \mathcal{W}(\bar{\Phi}, \bar{\Psi}) = \bar{a}(\zeta), & \bar{B}(\zeta) &= \mathcal{W}(\bar{\Phi}, \Psi) = \bar{b}(\zeta)e^{-2i\zeta x_0}. \end{aligned}$$

The discrete eigenvalues do not change, however, the norming constants change as $B_k = b_k e^{-2i\zeta_k x_0}$.

3. Discrete Forward and Inverse Scattering

In this section, we discuss certain discretization schemes for the scattering problem in (3) such that they are amenable to FFT-based fast polynomial arithmetic [34]. This method of obtaining a discrete scattering problem is referred to as the *spectral-domain* approach⁶. We begin with the transformation $\tilde{\mathbf{v}} = e^{i\sigma_3 \zeta x} \mathbf{v}$ so that (3) becomes

$$\partial_x [e^{i\sigma_3 \zeta x} \mathbf{v}] = e^{i\sigma_3 \zeta x} U e^{-i\sigma_3 \zeta x} [e^{i\sigma_3 \zeta x} \mathbf{v}],$$

or,

$$\begin{aligned} \tilde{\mathbf{v}}_x &= \tilde{U} \tilde{\mathbf{v}}, \\ \tilde{U} &= e^{i\sigma_3 \zeta x} U e^{-i\sigma_3 \zeta x} = \begin{pmatrix} 0 & q e^{2i\zeta x} \\ r e^{-2i\zeta x} & 0 \end{pmatrix}. \end{aligned} \quad (17)$$

The next step is to apply linear one-step method [32] to (17) in order to setup a recurrence relation initialized by the given initial condition. Let us note that the method of numerical integration just described above is identified as the *exponential integrator* based on linear one-step methods, in particular, the integrating factor (IF) method [31]. One of the advantages of the transformation carried out above in arriving at (17) is that the “vacuum” solution obtained from the discrete problem is exact.

Remark 3.1. *In the literature, the usage of the terms “forward scattering” and “inverse scattering” is not made precise; for instance, “forward scattering” could refer to computation of the scattering coefficients a and b or the nonlinear Fourier spectrum. In order to avoid any confusion arising in the usage of these terms, we follow the convention that the term “forward scattering” refers to the computation of the Jost solutions while the term “inverse scattering” refers to the process of recovering the samples of the scattering potential from (the polynomial form of) the Jost solutions. Note that in almost all cases, knowledge of the Jost solutions trivially allows one to compute the truncated discrete scattering coefficients and vice versa, therefore, no confusion should arise in what constitutes as input to the inverse scattering process.*

⁶See [35] for alternative approaches.

3.1. Discretization in the spectral-domain

In order to discuss various discretization schemes, we take an equispaced grid defined by $x_n = L_1 + nh$, $n = 0, 1, \dots, N$, with $x_N = L_2$ where h is the grid spacing. Define $\ell_-, \ell_+ \in \mathbb{R}$ such that $h\ell_- = -L_1$, $h\ell_+ = L_2$. Further, let us define $z = e^{i\zeta h}$ and treat ζ as a fixed parameter. For the potential functions sampled on the grid, we set $q_n = q(x_n, t)$, $r_n = r(x_n, t)$ where the time-dependence is suppressed. Using the same convention, $U_n = U(x_n, t)$ and $\tilde{U}_n = \tilde{U}(x_n, t)$.

3.1.1. Forward Euler method

The forward Euler (FE) method is the simplest of the finite-difference schemes. It can be stated as

$$\begin{aligned} \tilde{\mathbf{v}}_{n+1} &= (\sigma_0 + \tilde{U}_n) \tilde{\mathbf{v}}_n, \\ \mathbf{v}_{n+1} &= e^{-i\sigma_3 \zeta h} (\sigma_0 + U_n) \mathbf{v}_n. \end{aligned}$$

Setting $Q_n = hq_n$, $R_n = hr_n$ and $\Theta_n = (1 - Q_n R_n)$, we have

$$\mathbf{v}_{n+1} = z^{-1} \begin{pmatrix} 1 & Q_n \\ z^2 R_n & z^2 \end{pmatrix} \mathbf{v}_n = z^{-1} M_{n+1}(z^2) \mathbf{v}_n, \quad (18)$$

or, equivalently,

$$\frac{z^{-1}}{\Theta_n} \begin{pmatrix} z^2 & -Q_n \\ -z^2 R_n & 1 \end{pmatrix} \mathbf{v}_{n+1} = \mathbf{v}_n. \quad (19)$$

Let us note that the transfer matrix can be transformed to a form that resembles that of the implicit Euler method described in the next section: Putting $\mathbf{w}_n = e^{i\sigma_3 \zeta h} \mathbf{v}_n$, we have

$$\mathbf{w}_{n+1} = z^{-1} \begin{pmatrix} 1 & z^2 Q_n \\ R_n & z^2 \end{pmatrix} \mathbf{w}_n. \quad (20)$$

3.1.2. Implicit Euler method

The backward difference formula of order one (BDF1) is also known as the implicit Euler method. The discretization of (17) using this method reads as

$$\begin{aligned} \tilde{\mathbf{v}}_{n+1} &= (\sigma_0 - h\tilde{U}_{n+1})^{-1} \tilde{\mathbf{v}}_n, \\ \mathbf{v}_{n+1} &= (\sigma_0 - hU_{n+1})^{-1} e^{-i\sigma_3 \zeta h} \mathbf{v}_n. \end{aligned}$$

Setting $Q_n = hq_n$, $R_n = hr_n$ and $\Theta_n = (1 - Q_n R_n)$, this scheme can be stated as follows:

$$\mathbf{v}_{n+1} = \frac{z^{-1}}{\Theta_{n+1}} \begin{pmatrix} 1 & z^2 Q_{n+1} \\ R_{n+1} & z^2 \end{pmatrix} \mathbf{v}_n = z^{-1} M_{n+1}(z^2) \mathbf{v}_n, \quad (21)$$

or, equivalently,

$$z^{-1} \begin{pmatrix} z^2 & -z^2 Q_{n+1} \\ -R_{n+1} & 1 \end{pmatrix} \mathbf{v}_{n+1} = \mathbf{v}_n.$$

3.1.3. Trapezoidal rule

The trapezoidal rule (TR) happens to be one of the most popular methods of integrating ODEs numerically. The discretization of (17) using this method reads as

$$\begin{aligned} \tilde{\mathbf{v}}_{n+1} &= \left(\sigma_0 - \frac{h}{2} \tilde{U}_{n+1} \right)^{-1} \left(\sigma_0 + \frac{h}{2} \tilde{U}_n \right) \tilde{\mathbf{v}}_n, \\ \mathbf{v}_{n+1} &= \left(\sigma_0 - \frac{h}{2} U_{n+1} \right)^{-1} e^{-i\sigma_3 \zeta h} \left(\sigma_0 + \frac{h}{2} U_n \right) \mathbf{v}_n. \end{aligned}$$

Setting $2Q_n = hq_n$, $2R_n = hr_n$ and $\Theta_n = 1 - Q_n R_n$, this scheme can be stated as follows:

$$\begin{aligned} \mathbf{v}_{n+1} &= \frac{z^{-1}}{\Theta_{n+1}} \begin{pmatrix} 1 + z^2 Q_{n+1} R_n & z^2 Q_{n+1} + Q_n \\ R_{n+1} + z^2 R_n & R_{n+1} Q_n + z^2 \end{pmatrix} \mathbf{v}_n \\ &= z^{-1} M_{n+1}(z^2) \mathbf{v}_n, \end{aligned} \quad (22)$$

or, equivalently,

$$\frac{z^{-1}}{\Theta_n} \begin{pmatrix} R_{n+1} Q_n + z^2 & -z^2 Q_{n+1} - Q_n \\ -R_{n+1} - z^2 R_n & 1 + z^2 Q_{n+1} R_n \end{pmatrix} \mathbf{v}_{n+1} = \mathbf{v}_n.$$

3.2. Jost solutions and scattering coefficients

In order to express the discrete approximation to the Jost solutions, let us define the vector-valued polynomial

$$\mathbf{P}_n(z) = \begin{pmatrix} P_1^{(n)}(z) \\ P_2^{(n)}(z) \end{pmatrix} = \sum_{k=0}^n \mathbf{P}_k^{(n)} z^k = \sum_{k=0}^n \begin{pmatrix} P_{1,k}^{(n)} \\ P_{2,k}^{(n)} \end{pmatrix} z^k. \quad (23)$$

The Jost solutions ψ and ϕ , for the forward/implicit Euler method and the trapezoidal rule, can be written in the form

$$\psi_n = z^{\ell_+} z^{-m} \mathbf{S}_m(z^2), \quad \phi_n = z^{\ell_-} z^{-n} \mathbf{P}_n(z^2), \quad (24)$$

where $m + n = N$. Note that the expressions above correspond to the boundary conditions $\psi_N = z^{\ell_+} (0, 1)^\top$ and $\phi_0 = z^{\ell_-} (1, 0)^\top$ which translate to $\mathbf{S}_0 = (0, 1)^\top$ and $\mathbf{P}_0 = (1, 0)^\top$, respectively. The other Jost solutions, $\bar{\psi}_n$ and $\bar{\phi}_n$, can be written as

$$\begin{aligned} \bar{\psi}_n &= z^{-\ell_+} z^m (i\sigma_2) \mathbf{S}_m^*(1/z^{*2}), \\ \bar{\phi}_n &= z^{-\ell_-} z^n (i\sigma_2) \mathbf{P}_n^*(1/z^{*2}). \end{aligned}$$

The recurrence relation for the polynomial functions defined in (24) take the form

$$\begin{aligned} \mathbf{S}_{m+1}(z^2) &= \tilde{M}_n(z^2) \mathbf{S}_m(z^2), \\ \mathbf{P}_{n+1}(z^2) &= M_{n+1}(z^2) \mathbf{P}_n(z^2), \end{aligned} \quad (25)$$

where $M_{n+1}(z^2)$ with its inverse $z^{-2} \tilde{M}_{n+1}(z^2)$ is determined by the respective discretization scheme. The discrete approximation to the scattering coefficients is obtained from the scattered field: $\phi_N = (a_N z^{-\ell_+}, b_N z^{\ell_+})^\top$ yields

$$a_N(z^2) = P_1^{(N)}(z^2), \quad b_N(z^2) = (z^2)^{-\ell_+} P_2^{(N)}(z^2). \quad (26)$$

and $\psi_0 = (\bar{b}_N z^{\ell_-}, a_N z^{-\ell_-})^\top$ yields

$$a_N(z^2) = S_2^{(N)}(z^2), \quad \bar{b}_N(z^2) = (z^2)^{-\ell_-} S_1^{(N)}(z^2). \quad (27)$$

The quantities a_N , b_N and \bar{b}_N above are referred to as the *discrete scattering coefficients*. Note that these coefficients can only be defined for $\text{Re } \zeta \in [-\pi/2h, \pi/2h]$.

Remark 3.2. For the sake of brevity, we may occasionally refer to the polynomials $\mathbf{S}_m(z^2)$ and $\mathbf{P}_n(z^2)$ (as opposed to ψ_n and ϕ_n) as the (discrete) Jost solutions.

3.2.1. Discrete spectrum

The eigenvalues are computed by forming $a_N(z^2)$ and employing a suitable root-finding algorithm (see [47] and the references therein for more details). It turns out that the computation of the norming constants by evaluating b_N is ill-conditioned on account of the vanishingly small contribution from the solitonic components of the potential. Note that addition of bound states leaves b -coefficients invariant; therefore, recovery of the norming constant from $b(\zeta)$ cannot be expected to succeed in all cases. In order to remedy this problem, we use the general definition of the norming constants⁷: To this end, we proceed by computing the truncated scattering coefficients. Consider the case of potentials truncated from the right,

⁷Similar approach is reported in [23] and [48], however, it is not emphasized in these papers that the norming constants are never defined to be a value of $b(\zeta)$ unless it is guaranteed to be analytic in \mathbb{C}_+ . Note that the study of the errors introduced by the numerical discretization also provides significant insight into why the evaluation of $b_N(z^2)$ at complex values of ζ is ill-conditioned (see Sec. 6.3).

i.e., $q^{(-)}(x) = \theta(x_1 - x)q(x)$ where x_1 is the point of truncation and $\theta(x)$ is the Heaviside step function. The new potential now supported in $(-\infty, x_1]$ is interpreted as left-sided with respect to x_1 . The scattering coefficient can be stated in terms of the Jost solutions of the original potential as [44]

$$a^{(-)}(\zeta) = \phi_1(x_1; \zeta)e^{i\zeta x_1}, \quad b^{(-)}(\zeta) = \phi_2(x_1; \zeta)e^{-i\zeta x_1}. \quad (28)$$

Similarly, for potentials truncated from the left, we have

$$a^{(+)}(\zeta) = \psi_2(x_1; \zeta)e^{-i\zeta x_1}, \quad \bar{b}^{(+)}(\zeta) = \psi_1(x_1; \zeta)e^{i\zeta x_1}. \quad (29)$$

Denoting the corresponding discrete scattering coefficients by $a_n^{(-)}$, $b_n^{(-)}$, $a_m^{(+)}$ and $\bar{b}_m^{(+)}$, where $m + n = \ell_- + \ell_+$, we have

$$\begin{aligned} \phi_n &= \begin{pmatrix} z^{\ell_- - n} a_n^{(-)} \\ z^{-\ell_- + n} b_n^{(-)} \end{pmatrix} = z^{\ell_-} z^{-n} \mathbf{P}_n(z^2), \\ \psi_n &= \begin{pmatrix} z^{-\ell_+ + m} \bar{b}_m^{(+)} \\ z^{\ell_+ - m} a_m^{(+)} \end{pmatrix} = z^{\ell_+} z^{-m} \mathbf{S}_m(z^2), \end{aligned}$$

where $m = N - n$. Here n can be chosen to be $N/2$. Once an admissible root, z_k , of $a_N(z^2)$ that corresponds to a soliton is determined⁸, the corresponding norming constant is obtained via the proportionality of ϕ_n and ψ_n which translates to

$$\begin{aligned} b_k &= \frac{b_n^{(-)}(z_k^2)}{a_m^{(+)}(z_k^2)} = (z^2)^{\ell_- - n} \frac{P_2^{(n)}(z_k^2)}{S_2^{(m)}(z_k^2)}, \\ \frac{1}{b_k} &= \frac{\bar{b}_m^{(+)}(z_k^2)}{a_n^{(-)}(z_k^2)} = (z^2)^{\ell_+ - m} \frac{S_1^{(m)}(z_k^2)}{P_1^{(n)}(z_k^2)}. \end{aligned} \quad (30)$$

The truncated potential does not share discrete eigenvalues with the original potential; therefore, $a_m^{(+)}(z_k^2) \neq 0$ and $a_n^{(-)}(z_k^2) \neq 0$. The computation of the truncated scattering coefficients can be accomplished by direct evaluation of transfer matrices and subsequently forming the cumulative product leading to an operational complexity of $\mathcal{O}(N)$ for each eigenvalue (see Sec. 3.4.1).

It must be noted that our fast algorithm for forward scattering as discussed Sec. 3.5.1 is entirely compatible

with the approach suggested here. The scattering coefficients are easily obtainable from the truncated scattering coefficients using the Wronskian relations given in Sec. 2.1 as

$$\begin{aligned} a_N(z^2) &= \mathcal{W}(\phi_n, \psi_n) = \mathcal{W}(\mathbf{P}_n(z^2), \mathbf{S}_m(z^2)), \\ b_N(z^2) &= \mathcal{W}(\bar{\psi}_n, \phi_n) = (z^4)^{(\ell_- - n)} \mathbf{P}_n(z^2) \cdot \mathbf{S}_m^*(1/z^{*2}), \\ \bar{b}_N(z^2) &= \mathcal{W}(\bar{\phi}_n, \psi_n) = (z^4)^{(\ell_+ - m)} \mathbf{P}_n^*(1/z^{*2}) \cdot \mathbf{S}_m(z^2). \end{aligned} \quad (31)$$

Every polynomial multiplication involved above can be carried out efficiently using the FFT algorithm (see Sec. 3.5.1).

3.3. Inversion of discrete scattering coefficients

In this section, we consider the problem of recovering the discrete samples of the scattering potential from the discrete scattering coefficients known in the polynomial form. This step is referred to as the *discrete inverse scattering* step. Starting from the recurrence relation (25), we develop a layer-peeling algorithm similar to that reported by Brenne and Skaar [10]. The common aspect of the layer-peeling step for all kinds of discretization schemes is that using nothing but the knowledge of $\mathbf{P}_{n+1}(z^2)$, one should be able to retrieve the samples of the potential needed to compute the transfer matrix $\bar{\mathbf{M}}_{n+1}(z^2)$ so that the entire step can be repeated with $\mathbf{P}_n(z^2)$ until all the samples of the potential are recovered (as illustrated in Fig. 3b). In the following, we summarize the main results which facilitate the layer-peeling step corresponding to the each of the discretization schemes introduced so far. A detailed study of the recurrence relation and the proof of the necessary and sufficient conditions for discrete inverse scattering is provided in Sec. 5.

3.3.1. Forward Euler method

The recurrence relation for the forward Euler method yields

$$P_{1,0}^{(n+1)} = 1. \quad (32)$$

The layer-peeling algorithm based on the forward Euler method uses the relation

$$R_n = \frac{P_{2,1}^{(n+1)}}{P_{1,0}^{(n+1)}}, \quad (33)$$

⁸Given that $z_k = \exp[i\zeta_k h]$ and $\text{Im } \zeta_k > 0$, we must have $|z_k| < 1$.

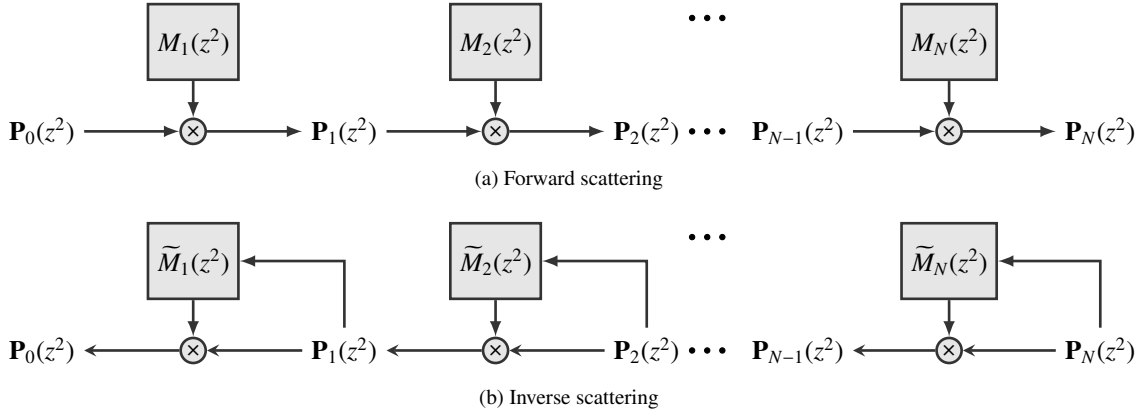


Figure 3: The figure depicts the sequential discrete forward and inverse scattering algorithms. The inverse scattering algorithm which is also known as the layer-peeling algorithm consists using $P_{n+1}(z^2)$ to determine the transfer matrix $\tilde{M}_{n+1}(z^2)$ so that the entire step can be repeated with $P_n(z^2)$ as depicted in the lower diagram.

where $P_{1,0}^{(n+1)} \neq 0$ on account of (32). As evident from (18), the transfer matrix, $M_{n+1}(z^2)$, connecting $P_n(z^2)$ and P_{n+1} is therefore completely determined by R_n (with $Q_n = -R_n^*$).

3.3.2. Implicit Euler method

The recurrence relation for the implicit Euler method yields

$$P_{1,0}^{(n+1)} = \prod_{k=1}^{n+1} \Theta_k^{-1} > 0, \quad P_{n+1}^{(n+1)} = 0. \quad (34)$$

The layer-peeling algorithm based on the implicit Euler method uses the relation

$$R_{n+1} = \frac{P_{2,0}^{(n+1)}}{P_{1,0}^{(n+1)}}, \quad (35)$$

where $P_{1,0}^{(n+1)} \neq 0$ on account of (34). As evident from (21), the transfer matrix, $M_{n+1}(z^2)$, connecting $P_n(z^2)$ and P_{n+1} is therefore completely determined by R_{n+1} (with $Q_{n+1} = -R_{n+1}^*$).

3.3.3. Trapezoidal rule

Let us assume $Q_0 = 0$. The recurrence relation for the trapezoidal rule yields

$$P_{1,0}^{(n+1)} = \Theta_{n+1}^{-1} \prod_{k=1}^n \left(\frac{1 + Q_k R_k}{1 - Q_k R_k} \right) = \Theta_{n+1}^{-1} \prod_{k=1}^n \left(\frac{2 - \Theta_k}{\Theta_k} \right), \quad (36)$$

$$P_{n+1}^{(n+1)} = 0,$$

where the last relationship follows from the assumption $Q_0 = 0$. For sufficiently small h , it is reasonable to assume that $1 + Q_n R_n = 2 - \Theta_n > 0$ so that $P_{1,0}^{(n)} > 0$ (it also implies that $|Q_n| = |R_n| < 1$). The layer-peeling algorithm based on the trapezoidal scheme uses the relations

$$R_{n+1} = \frac{P_{2,0}^{(n+1)}}{P_{1,0}^{(n+1)}}, \quad R_n = \frac{\chi}{1 + \sqrt{1 + |\chi|^2}}, \quad (37)$$

where

$$\chi = \frac{P_{2,1}^{(n+1)} - R_{n+1} P_{1,1}^{(n+1)}}{P_{1,0}^{(n+1)} - Q_{n+1} P_{2,0}^{(n+1)}}.$$

Note that $P_{1,0}^{(n+1)} \neq 0$ and $P_{1,0}^{(n+1)} - Q_{n+1} P_{2,0}^{(n+1)} \neq 0$. As evident from (22), the transfer matrix, $M_{n+1}(z^2)$, connecting $P_n(z^2)$ and P_{n+1} is completely determined by the samples R_{n+1} and R_n (with $Q_{n+1} = -R_{n+1}^*$ and $Q_n = -R_n^*$).

3.4. Sequential algorithm

3.4.1. Forward scattering

The computation of the Jost solution for a given value of the spectral parameter, $\zeta \in \mathbb{C}$ is considered here as the forward scattering step. The direct use of the recurrence relations obtained in Sec. 6.2 gives us a sequential algorithm (see the illustration in Fig. 3a). If $\varpi(n)$, $n \in \mathbb{Z}_+$, denotes the complexity of computing the Jost solution $P_n(z^2)$ for a given ζ , then $\varpi(n+1) = 4 + \varpi(n)$, counting only the multiplications involved. This recurrence relation yields $\varpi(n) = 4n$. It must be noted that the sequential algorithms can be useful for computing norming constants as discussed in Sec. 3.2.1 if the eigenvalues are known beforehand. If good initial guesses are known for the eigenvalues, search based methods such as Newton's method of finding the eigenvalues can also benefit from sequential algorithms [47].

The sequential algorithm for computing the polynomial coefficients of $P_n(z^2)$ can also be obtained in the same manner where transfer matrices are now treated as polynomial matrices. If $\varpi(n)$ denotes the complexity of computing the polynomial coefficients for the Jost solution $P_n(z^2)$, then $\varpi(n+1) = 4(n+1) + \varpi(n)$, counting only the multiplications involved. This yields $\varpi(n) = 2(n+1)(n+2) = \mathcal{O}(n^2)$ which is extremely prohibitive for large number of samples. This task can be accomplished much more efficiently using a divide-and-conquer strategy together with FFT-based fast polynomial arithmetic as described in Sec. 3.5.1.

3.4.2. Inverse scattering

The inverse scattering step here refers to the retrieval of the samples of the scattering potential from the known polynomial form of the discrete scattering coefficients. This can be accomplished by a sequential layer-peeling algorithm as described in Sec. 3.3 (see the illustration in Fig. 3b). If $\varpi(n)$, $n \in \mathbb{Z}_+$, denotes the complexity of inversion of $P_n(z^2)$, then $\varpi(n) = 4(n+1) + \varpi(n-1)$ counting only the multiplications. This again yields a complexity of $\mathcal{O}(n^2)$. This task can also be accomplished much more efficiently using a divide-and-conquer strategy together with FFT-based fast polynomial arithmetic as described in Sec. 3.5.2.

3.5. Fast algorithm: A divide-and-conquer strategy

3.5.1. Forward scattering

The scattering algorithm consists in forming cumulative product of, say N , transfer matrices. Given that the transfer matrices have polynomial entries (of maximum degree one), one can use FFT-based polynomial multiplication [34] to obtain a fast forward scattering algorithm. In this article we restrict ourselves to the case where N is a power of 2. Most efficient use of the FFT-based multiplication can be made if we use a divide-and-conquer strategy as in [37] where products are formed pair-wise culminating in the full transfer matrix. The complexity of obtaining the cumulative transfer matrix from n transfer matrices, denoted by $\varpi(n)$, then satisfies the recurrence relation

$$\varpi(n) = 8\nu(n) + 2\varpi(n/2),$$

where $\nu(n) = n(3 \log_2 2n + 2)$ is the complexity of multiplying two polynomials of degree $n-1$ using the FFT algorithm. The number of pairs is given by $l = \log_2 N$ so that the recurrence relation yields

$$\varpi(N) = 2^l \varpi(1) + 8 \sum_{k=0}^{l-1} 2^k \nu(2^{l-k}),$$

which simplifies to

$$\varpi(N) = N\varpi(1) + 4N[3(\log_2 N)^2 + 13 \log_2 N].$$

Therefore, the complexity of the forward scattering algorithm is $\mathcal{O}(N \log^2 N)$. Note that $\varpi(1)$ denotes the cost of obtaining each of the transfer matrices.

Evaluation of $P_N(z^2)$ at an arbitrary complex point can be done using Horner's method which has the complexity of $\mathcal{O}(N)$. However, multipoint evaluation at $M (\geq N)$ Fourier nodes can be carried out with complexity $\mathcal{O}(M \log M)$ where M is a power of 2.

3.5.2. Inverse scattering

In this section, we describe how to obtain a fast layer-peeling algorithm by adapting McClary's approach [38, 49] for our discrete inverse scattering problem. Consider the grid $(x_n)_{0 \leq n \leq N}$ and let us label the segment $[x_n, x_{n+1}]$ by $n+1$ for $n < N$. Recall that the inverse of the transfer matrix $M_n(z^2)$ is $z^{-2} \tilde{M}_n(z^2)$. The cumulative transfer matrix from the n -th segment to the $(n-m+1)$ -th segment is

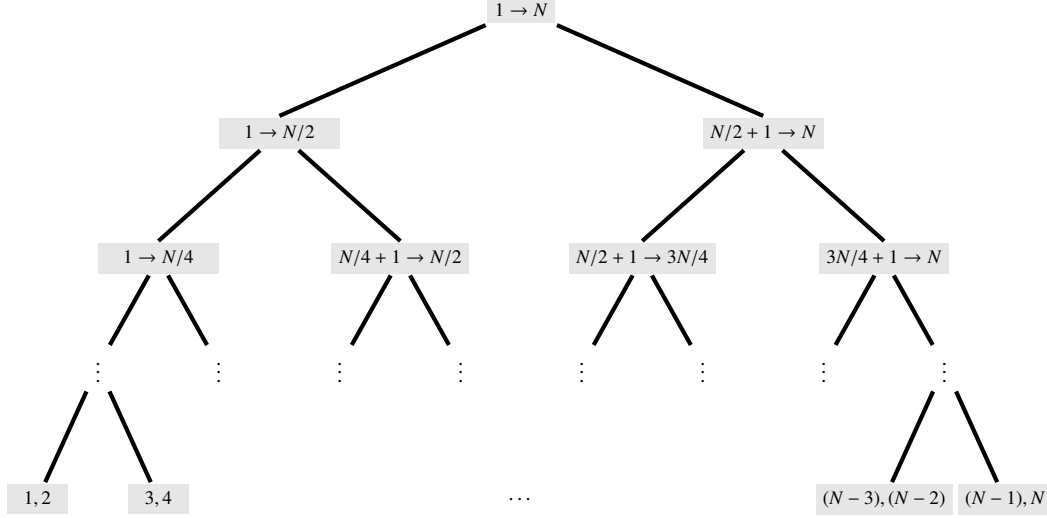


Figure 4: The figure shows the binary-tree structure obtained as a result of applying a divide-and-conquer strategy to the conventional layer-peeling method. The node label depicts the range of indices of the segments/layers ordered from left to right in the computational domain.

given by

$$z^{-2} \tilde{M}_{n-m+1}(z^2) \times \dots \times z^{-2} \tilde{M}_{n-1}(z^2) \times z^{-2} \tilde{M}_n(z^2) \\ = z^{-2m} \tilde{M}_{n-m+1, \dots, n-1, n}(z^2).$$

Note that in order to determine the transfer matrices for last l segments starting from the n -th segment, it is sufficient to have a partial knowledge of the Jost solution, more specifically⁹, $\{\mathbf{P}_n\}_{l+1}$, where $\{\cdot\}_l$ denotes truncation after first l coefficients. Let the complimentary polynomial vector be defined as

$$\{\mathbf{P}_n(z^2)\}_l^c = z^{-2l} (\mathbf{P}_n(z^2) - \{\mathbf{P}_n(z^2)\}_l),$$

and consider the inverse propagation relation in terms of the inverse of the transfer matrices:

$$\mathbf{P}_{n-m}(z^2) = z^{-2m} \tilde{M}_{n-m+1, \dots, n-1, n}(z^2) \times \\ \left(\{\mathbf{P}_n(z^2)\}_{l+1} + z^{2(l+1)} \{\mathbf{P}_n(z^2)\}_l^c \right).$$

For every $m > 0$, the first two coefficients of the polynomial $\mathbf{P}_{n-m}(z^2)$ are required in order to determine the transfer matrix for the segment $n-m$; therefore, $2(l+1-m) > 0$

ensures that no contribution comes from the complimentary polynomial in computing these first two coefficients. It then follows that the transfer matrices

$$\tilde{M}_n(z^2), \tilde{M}_{n-1}(z^2), \dots, \tilde{M}_{n-l+1}(z^2)$$

can be determined without needing the complimentary polynomial $\{\mathbf{P}_n(z^2)\}_{l+1}^c$. Once the matrices are determined, the Jost solution needed to determine the transfer matrices for $n-l$ segments works out to be

$$\mathbf{P}_{n-l+1}(z^2) = z^{-2l} \tilde{M}_{n-l+1, \dots, n-1, n}(z^2) \mathbf{P}_n(z^2).$$

All polynomial multiplications can be carried out using the FFT-algorithm. The observations made above makes it clear that a divide-and-conquer strategy can be easily devised in order to speed up the layer-peeling algorithm. For the inversion of the discrete scattering coefficients, we start with the associated Jost solution $\mathbf{P}_N(z^2)$ where N is a power of 2, we devise a divide-and-conquer strategy that reduces the original problem into two equal size (in terms of number of segments) subproblems¹⁰. The algorithm can be described as follows:

⁹We discuss the case where the underlying one-step method is the trapezoidal rule on account of the fact that the corresponding transfer matrix is the most general among the methods considered in this article.

¹⁰Note that the analysis in Sec. 3.3 reveals that the number of coefficients associated with $\mathbf{P}_N(z^2)$ is exactly N .

- i. Define a binary tree with the number of levels given by $l = \log_2 N$ (see Fig. 4). Every parent node forks into two child nodes eventually terminating the tree at the leaf nodes.
- ii. Associate N segments with the root node which is assumed to be at the level zero. Number of segments associated with every child node is half of that of the parent node. If $S(k)$ denotes the number of segments associated with nodes at the k -th level, then $S(k) = N2^{-k}$ for $k = 0, 1, \dots, l-1$.
- iii. Every node in the binary tree is labeled by the index-coordinates (j, k) where k is the level and j being the horizontal position of the node from the left in any particular level, say k , so that $0 \leq j \leq k$. If the index of the last segment associated with a given node (j, k) is denoted by N_{jk} , then $N_{jk} = 2^j S(k)$.
- iv. All polynomial products to be formed at any node at the k -th level requires executing an FFT-algorithm for vectors of length no more than $2S(k)$.
- v. The segments associated with a node dictate the associated cumulative transfer matrix and the Jost solution (with the required number of coefficients) needed in order to determine the entries of constituting transfer matrices. For the node (j, k) , the associated cumulative transfer matrix is

$$z^{-2n} \widetilde{M}_{N_{jk}-n+1, \dots, N_{jk}-1, N_{jk}}(z^2), \quad n = S(k),$$

and the associated Jost solution is $\{P_{N_{jk}}(z^2)\}_{n+1}$.

- vi. Our algorithm requires exactly two types of operations to be carried out at every node except for the leaf nodes. The first is the computation of the cumulative transfer matrix once the constituting matrices are known at the child nodes. The second is computing the Jost solution needed by any of the child nodes. Both of these operations boil down to polynomial multiplications, therefore, it can be carried out efficiently using the FFT-algorithm. The samples of the potential are determined at the leaf nodes.

Denoting the complexity of multiplying two polynomials of degree $n-1$ (via the FFT-algorithm) by $v(n)$, the

recurrence relation for the complexity of the fast layer-peeling procedure, denoted by $\varpi(n)$ (where $n = S(k)$, the number of segments at level k), can be stated as

$$\varpi(n) = 4v(n) + 8v(n) + 2\varpi(n/2).$$

The first term on the RHS corresponds to the determination of Jost solution for the second child node assuming that the Jost solution is known at the parent node and the cumulative transfer matrix is known at the first child node. The second term corresponds to the determination of the cumulative transfer matrix at the corresponding parent node using the transfer matrices of the child nodes. Observing

$$\varpi(N) = 2^{l-1} \varpi(2) + 12 \sum_{k=0}^{l-2} 2^k v(2^{l-k}) - 8v(N),$$

where the last term on RHS is a correction for the root node since the determination of the cumulative transfer matrix at the root level is unnecessary. Using $v(n) = n(3 \log_2 2n + 2)$, we have

$$\varpi(N) = (N/2)\varpi(2) + 6N[3(\log_2 N)^2 + 13 \log_2 N - 68/3],$$

valid for $N \geq 4$ where $\varpi(2)$ refers to the cost of executing the leaf node. Therefore, the fast layer-peeling algorithm has the complexity of $\mathcal{O}(N \log^2 N)$.

3.6. Inversion of scattering coefficients

Let us assume that the scattering coefficients $a(\zeta)$ and $b(\zeta)$ are analytic in $\overline{\mathbb{C}}_+$ such that for some $C > 0$, we have

$$|a(\zeta) - 1| \leq \frac{C}{1 + |\zeta|}, \quad |\check{b}(\zeta)| \leq \frac{C}{1 + |\zeta|}, \quad \zeta \in \overline{\mathbb{C}}_+,$$

where $\check{b}(\zeta) = b(\zeta)e^{2i\zeta L_2}$. The precise conditions under which such a situation may arise is discussed in theorems 6.2 and 6.3. We further assume that the potential is supported in a domain of the form $(-\infty, L_2]$ or $[L_1, L_2]$. In this section, we would like to develop a method to compute the discrete scattering coefficients from the analytic form of the scattering coefficients so that the corresponding inverse problem can be solved numerically using the layer-peeling algorithm discussed in Sec. 3.3. It turns out that this task can be efficiently accomplished using the

method developed by Lubich [39] which is used in computing the quadrature weights for convolution-type integrals.

Introduce the function $\delta(z)$ as in [39] which corresponds to the A-stable one-step methods, namely, BDF1 and TR:

$$\delta(z) = \begin{cases} (1-z) & \text{(BDF1),} \\ 2\frac{(1-z)}{1+z} & \text{(TR).} \end{cases} \quad (38)$$

Putting $z = e^{i\zeta h}$, let us define the coefficients a_k and \check{b}_k as

$$a\left(\frac{i\delta(z^2)}{2h}\right) = 1 + \sum_{k=0}^{\infty} a_k z^{2k}, \quad \check{b}\left(\frac{i\delta(z^2)}{2h}\right) = \sum_{k=0}^{\infty} \check{b}_k z^{2k}.$$

The coefficients can be obtained using the Cauchy integrals

$$\begin{aligned} a_k &= \frac{1}{2\pi i} \oint_{|z|=\varrho} \left[a\left(\frac{i\delta(z)}{2h}\right) - 1 \right] z^{-k-1} dz, \\ \check{b}_k &= \frac{1}{2\pi i} \oint_{|z|=\varrho} \left[\check{b}\left(\frac{i\delta(z)}{2h}\right) \right] z^{-k-1} dz, \end{aligned} \quad (39)$$

which can be easily computed using FFT. Note that the zeroth coefficient can be computed exactly as

$$a_0 = \left[a\left(\frac{i\delta(0)}{2h}\right) - 1 \right], \quad \check{b}_0 = \left[\check{b}\left(\frac{i\delta(0)}{2h}\right) \right]. \quad (40)$$

On account of the decay property of the scattering coefficients with respect to ζ , $a_0 = \mathcal{O}(h)$ and $\check{b}_0 = \mathcal{O}(h)$.

Let $f_k(h)$ denote either a_k or \check{b}_k and let $F(z^2)$ represent the corresponding integrand in (39). Following [40], we obtain the approximation $f_k(h; M)$ for $f_k(h)$ as

$$f_k(h; M) = \frac{1}{MQ^k} \sum_{j=0}^{M-1} F_j e^{-i\frac{2\pi jk}{M}},$$

where $F_j = F(\varrho e^{-i\frac{2\pi jk}{M}})$. Choosing $\varrho \leq 1$ ensures that $\text{Im } \zeta \geq 0$. In order to achieve an accuracy of $\mathcal{O}(\epsilon)$ for computing $f_k(h; M)$ for $k = 0, 1, \dots, N$ choose $\log \varrho = (1/N) \log \epsilon$ and $M = N \log(1/\epsilon)$. The Lubich's method, therefore, delivers discrete scattering coefficients with $\mathcal{O}(M \log M)$ complexity excluding the cost of function evaluations.

Remark 3.3. If it is known that the scattering coefficients are also analytic in \mathbb{C}_- , say, in the strip $\mathbb{S}_-(\mu) = \{\zeta \in$

$\mathbb{C}_- | \text{Im } \zeta \geq -\mu\}$, then Cauchy's estimate can be used to show that the Lubich coefficients decay exponentially with k . Let $\Gamma = \{z \in \mathbb{C} | |z| = \varrho, \varrho > 1\}$ be such that $[i\delta(z)/2h] \in \overline{\mathbb{C}}_+ \cup \mathbb{S}(\mu)$ for all $z \in \Gamma$. Then, Cauchy's estimate gives

$$|f_k(h)| \leq \varrho^{-k} \max_{z \in \Gamma} \left| f\left(\frac{i\delta(z)}{2h}\right) \right|,$$

where $f(\zeta)$ stands for $a(\zeta)$ or $\check{b}(\zeta)$ and $f_k(h)$ denotes the k -th Lubich coefficients.

3.6.1. Relationship with inverse Fourier-Laplace transform

Define the functions $\alpha(\tau)$ and $\beta(\tau)$ as

$$\begin{aligned} \alpha(\tau) &= \frac{1}{2\pi} \int_{-\infty}^{\infty} [a(\zeta) - 1] e^{-i\zeta\tau} d\zeta, \\ \beta(\tau) &= \frac{1}{2\pi} \int_{-\infty}^{\infty} \check{b}(\zeta) e^{-i\zeta\tau} d\zeta. \end{aligned} \quad (41)$$

Note that for $\tau < 0$, the contour can be closed in \mathbb{C}_+ and the integrals would evaluate to zero, therefore $\alpha(\tau)$ and $\beta(\tau)$ are causal. According to [39, Theorem 4.1], the coefficients a_k and \check{b}_k approximate the quantities $(2h)\alpha(2hk)$ and $(2h)\beta(2hk)$ up to $\mathcal{O}(h^{p+1})$, respectively, for $k > 0$ (note that the zeroth coefficient is given by (40) which merely requires function evaluation).

If accurate values of the quantities $2h\alpha(2hk)$ and $2h\beta(2hk)$ are available, then it provides an alternative means to obtain the Lubich coefficients. However, for better agreement with the true Lubich coefficients, one should choose $k > N_{\text{th}}$ where $N_{\text{th}} > 0$ is a suitably chosen threshold.

3.7. Inversion of rational scattering coefficients: Truncated multi-solitons

In order to obtain a fast version of the Darboux transformations (DT) for generating multi-solitons (Problem 1.1) we would like to employ the scattering coefficients obtained as a result of truncation of a K -soliton potential at $x = 0$. As shown in Sec. 2.3.3, the scattering coefficients are rational functions of ζ with no poles in $\overline{\mathbb{C}}_+$. Therefore, the Lubich's method of obtaining discrete scattering coefficients as described in Sec. 3.6 is also applicable here. It must be noted that in order to obtain the complete K -soliton potential at a given time t , the truncation must be done after computing the time-evolved Darboux matrix.

Discrete inverse scattering proceeds by computing the polynomial vector $\mathbf{P}_N(z^2)$ associated with the discrete scattering coefficients. Without the loss of generality, we assume that the truncation is done at $x = 0$ (see Remark 2.2). Let the discrete spectrum of the K -soliton be \mathfrak{S}_K as defined in Sec. 2.2. Using the notations introduced in Sec. 2.3.1 and setting $N_1 = N/2 \in \mathbb{Z}_+$, for the left-sided profile, we have

$$\begin{aligned} P_1^{(N_1)}(z^2) &= \left\{ \mu_K \left(\frac{i\delta(z^2)}{2h} \right) \left[D_K \left(0, t; \frac{i\delta(z^2)}{2h}, \mathfrak{S}_K \right) \right]_{11} \right\}_{N_1}, \\ P_2^{(N_1)}(z^2) &= \left\{ \mu_K \left(\frac{i\delta(z^2)}{2h} \right) \left[D_K \left(0, t; \frac{i\delta(z^2)}{2h}, \mathfrak{S}_K \right) \right]_{21} \right\}_{N_1}, \end{aligned}$$

where truncation after N_1 terms is implied by the notation $\{\cdot\}_{N_1}$. This determines $U(x)$ for $x < 0$. The right-sided profile can be generated using the transformation described in Remark 2.1 so that

$$\begin{aligned} P_1^{(N_1)}(z^2) &= \left\{ \mu_K \left(\frac{i\delta(z^2)}{2h} \right) \left[D_K \left(0, t; \frac{i\delta(z^2)}{2h}, \mathfrak{S}_K \right) \right]_{22} \right\}_{N_1}, \\ P_2^{(N_1)}(z^2) &= \left\{ \mu_K \left(\frac{i\delta(z^2)}{2h} \right) \left[D_K \left(0, t; \frac{i\delta(z^2)}{2h}, \mathfrak{S}_K \right) \right]_{12} \right\}_{N_1}. \end{aligned}$$

This would determine $U^*(-x)$ for $x < 0$. Combining the two parts determines the complete multi-soliton potential. Note that the foregoing description also applies to any set of rational functions which qualify as scattering coefficients of a left-sided or a right-sided profile, respectively.

The operational complexity of this algorithm can be computed by taking into account the complexity of DT at $x = 0$, which is $\mathcal{O}(K^2)$, and the complexity of computation of Lubich coefficients which is $\mathcal{O}(KM) + \mathcal{O}(M \log M)$ where M is the number of nodes used in evaluating the Cauchy integral. Given that $K \ll M$ and $M = \mathcal{O}(N)$, the overall complexity of generating the multi-soliton including the layer-peeling step works out to be $\mathcal{O}(N(K + \log^2 N))$. The algorithm presented in this section is referred to as the *fast Darboux transformation* (FDT) algorithm. As pointed out in Sec. 2.3.1, the CDT algorithm offers machine precision for computing K -soliton potentials with an operational complexity of $\mathcal{O}(K^2N)$. The fundamental difference between the CDT and the FDT algorithm is depicted in Fig. 5 where it is evident that by avoiding DT-iterations at each of the grid points (except at $x = 0$) and using the fast LP algorithm, a lower complexity order algorithm can be obtained.

For any rational function, if the poles and residues are known then resolution into partial fractions offers a straightforward means of computing the inverse Fourier-Laplace transform. Let us apply this method to the problem of generating multi-solitons as discussed in the last paragraph: Poles of the Jost solutions are known to be ζ_k^* (where ζ_k are the discrete eigenvalues), therefore, the resolution of the Darboux matrix into partial fractions reads as

$$\begin{aligned} \mu_K(\zeta) D_K(0, t; \zeta, \mathfrak{S}_K) \\ = \sigma_0 + \sum_{k=1}^K \frac{\text{Res}[\mu_K, \zeta_k^*]}{\zeta - \zeta_k^*} D_K(0, t; \zeta_k^*, \mathfrak{S}_K). \end{aligned} \quad (42)$$

The inversion of $(\zeta - \zeta_k^*)^{-1}$ leads to terms of the form $-ie^{-i\zeta_k^* \tau}$, therefore, the quantities $e^{-2ih\zeta_k^*}$ must be computed beforehand. Excluding the cost of computing the K exponentials, the complexity of this algorithm is $\mathcal{O}(KN)$ where N is the number of samples in the τ -domain. In practice, replacing Lubich coefficients with that obtained by resolution into partial-fractions leads to increase in error and even failure to converge; however, for larger values of the index, the agreement between the two improves allowing us to reduce the overall complexity of computing the discrete coefficients $\mathbf{P}_k^{(N_1)}$ by switching to the faster algorithm for $k > N_{\text{th}}$ where $N_{\text{th}} > 0$ is a suitably chosen threshold.

Before we conclude this section, it is worth mentioning that the case treated by Rourke *et al.* [12, 13] of rational reflection coefficient $\rho(\zeta)$ proceeds by reducing the problem to an equivalent problem of generating multi-solitons on a given half-space. Therefore, such cases are amenable to the method discussed in this article.

3.8. General Darboux transformation: Addition of bound states

In this section, we address Problem 1.2 introduced in the beginning of this article. To this end, let us note that the general Darboux transformation consists in adding a given discrete spectrum \mathfrak{S}_K (as defined in Sec. 2.2) to a given seed potential, $q_{\text{seed}} = q_0(x)$, which is assumed to be admissible as a scattering potential in the ZS-problem. The two algorithms developed for this purpose, namely, the classical Darboux transformation (CDT) and the fast Darboux transformation (FDT) meant to carry out the

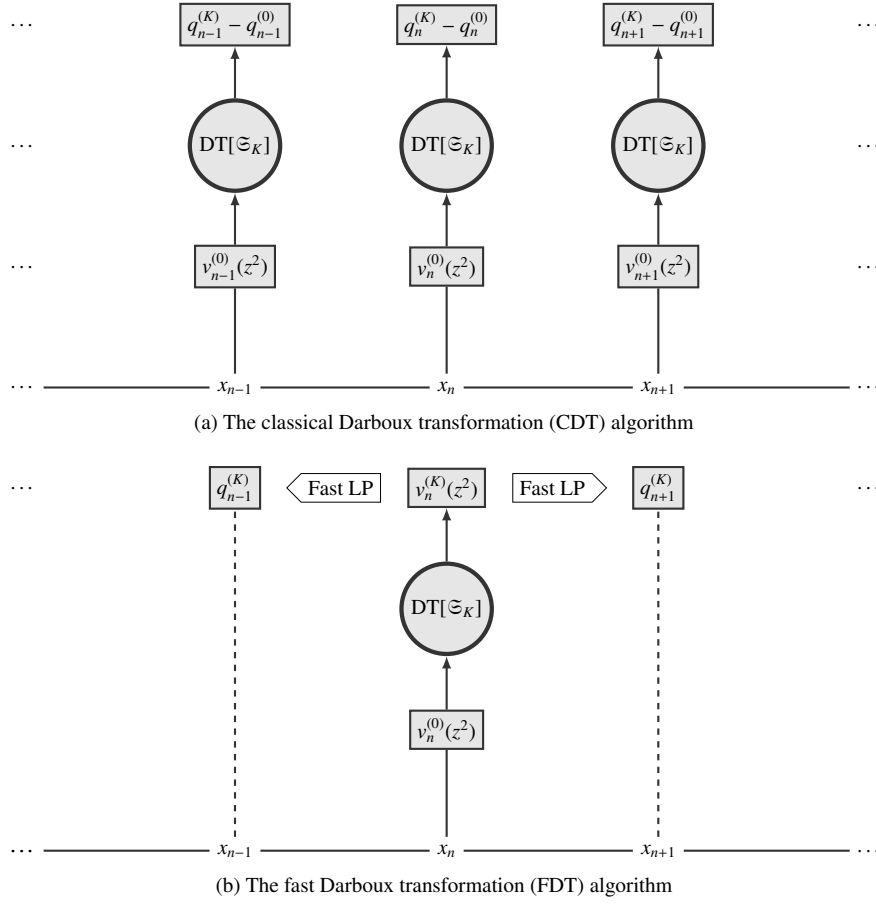


Figure 5: The figure depicts the CDT and the FDT algorithm for computing the augmented potential, $q_n^{(K)}$ (which is the discrete approximation to $q_K(x_n)$), by adding a given discrete spectrum, ξ_K , to the seed potential, $q_n^{(0)} = q_0(x_n)$. The DT-block, labeled as $DT[\xi_K]$, is described in Fig. 2. The quantities $v_n^{(j)}(z^2)$ refer to the discrete approximation of $v_j(x_n, 0; \zeta)$ in Fig. 2.

general Darboux transformation are described in the following subsections. For the sake of brevity of presentation, we restrict ourselves to the case $t = 0$.

3.8.1. The CDT algorithm

The basic idea behind the CDT algorithm is described in Sec. 2.3.1 and also depicted in Fig. 5a. In the discrete framework developed in Sec. 6.2, the seed Jost solutions (which need to be evaluated at the eigenvalues ζ_j to be added) can be computed via the sequential algorithm discussed in Sec. 3.4.1. Using the notations introduced in Sec. 2.3.1 and Sec. 3.2.1, and, introducing $\beta_n^{(j-1)}(z_j)$ as

the discrete approximation to $\beta_{j-1}(x_n, 0; \zeta_j)$, we have

$$\beta_n^{(j-1)}(z_j) = \frac{P_1^{(n,j-1)}(z_j^2) - (z_j^2)^{-\ell_-+n} b_j S_1^{(m,j-1)}(z_j^2)}{P_2^{(n,j-1)}(z_j^2) - (z_j^2)^{-\ell_-+n} b_j S_2^{(m,j-1)}(z_j^2)}, \quad (43)$$

where $(\zeta_j, b_j) \in \xi_K$, $m+n = N$ and $z_j = e^{2i\zeta_j h}$. Noting that $v_n^{(j)} = (P_n^{(j)}, S_n^{(j)})$, the rest of the steps involved are similar to that discussed in Sec. 2.3.1.

The operational complexity of computing the seed Jost solutions at K eigenvalues using the sequential algorithm is $\mathcal{O}(KN)$ so that the overall complexity of the CDT algorithm is $\mathcal{O}(K^2N)$. A final remark that we would like

to make with regard to the CDT algorithm is that numerical computation of the Jost solutions for complex values of the spectral parameter ζ tends to become inaccurate on account of the ζ -dependence of the truncation error coefficient as discussed in Sec. 6.2. It is therefore recommended that $\text{Im } \zeta_k$ is kept below a certain threshold.

3.8.2. The FDT algorithm

The fundamental idea of the FDT algorithm is the same as that described in Sec. 3.7 which considers the problem of adding bound states, described by \mathfrak{S}_K , to a null seed potential. The difference merely lies in how we compute the seed Jost solutions required in the DT-iterations at $x = 0$ for a general seed potential. Following Sec. 2.3.1 and 3.2.1, note that evaluation of the Jost solutions at $\zeta = \zeta_j$ amounts to evaluating the approximating polynomial at $z_j = e^{2i\zeta_j h}$ (setting $x = 0$ and $t = 0$), so that the recursive step for computing the β -coefficients reads as

$$\beta_0^{(j-1)}(z_j) = \frac{P_1^{(\ell_-, j-1)}(z_j^2) - b_j S_1^{(\ell_+, j-1)}(z_j^2)}{P_2^{(\ell_-, j-1)}(z_j^2) - b_j S_2^{(\ell_+, j-1)}(z_j^2)}. \quad (44)$$

where we have assumed $\ell_-, \ell_+ \in \mathbb{Z}$ for simplicity and $(\zeta_j, b_j) \in \mathfrak{S}_K$. Noting that $v_n^{(j)} = (\mathbf{P}_{\ell_-}^{(j)}, \mathbf{S}_{\ell_+}^{(j)})$, other steps of the iteration are identical to that described in Sec. 2.3.1. Here, our objective is not to follow the conventional Darboux transformation but merely obtain the truncated scattering coefficients (for the left-sided and the right-sided potential) at the origin so that a fast layer-peeling algorithm can be used to compute the samples of the augmented potential.

The operational complexity of this algorithm can be worked out as follows: The cost of computing the Jost solutions (as a polynomial vector) is $\mathcal{O}(N \log^2 N)$ and the cost of evaluation of the Jost solutions using Horner's scheme is $\mathcal{O}(N)$ for each of the eigenvalues so that the overall complexity of computing the discrete truncated scattering coefficient at $x = 0$ is $\mathcal{O}(K^2) + \mathcal{O}(KM) + \mathcal{O}(M \log M) + \mathcal{O}(N \log^2 N)$ where M is the number of nodes used in evaluating the Cauchy integral, N is the number of samples of the potential and K is the number of eigenvalues to be added. Observing that $K \ll M$, N and $M = \mathcal{O}(N)$, the overall complexity is effectively $\mathcal{O}(N(K + \log^2 N))$ including the layer-peeling step.

The convergence behavior of the FDT algorithm is studied in the Sec. 6.5 where it is shown that the Darboux matrices can be computed with the same order of accuracy as that of the underlying one-step method used in the computation of the Jost solutions of the seed potential. Further, the global order of convergence matches that of the underlying one-step method for the computation of Lubich coefficients or the layer-peeling algorithm depending on which of the two is lower.

Finally, let us conclude this section by pointing out that if a fast and sufficiently accurate means of inversion of continuous spectrum (i.e., no bound states present) is available then a fast inverse scattering algorithm can be easily obtained for the general cases using the FDT algorithm outlined in this section. The first results in this direction are reported in [18] where the trapezoidal rule is used to develop two algorithms of complexity $\mathcal{O}(N(K + \log^2 N))$ that exhibit a convergence behavior of $\mathcal{O}(N^{-2})$.

4. Benchmarking methods

In this section, we discuss two of the conventional methods which are widely used for solving scattering problems. We would like to benchmark our method against these known methods. Unlike the linear one-step methods, here we employ a staggered grid configuration given by $(x_{n+1/2})_{0 \leq n < N}$ such that $x_{n+1/2} = x_n + h/2$.

4.1. Magnus integrator

By applying the Magnus method with one-point Gaussian quadrature (see [50–52]) to the original ZS-problem in (3), we obtain

$$\mathbf{v}_{n+1} = e^{-i\zeta\sigma_3 h + U_{n+1/2} h} \mathbf{v}_n. \quad (45)$$

The exponential operator can be computed exactly as

$$e^{-i\zeta\sigma_3 h + U_{n+1/2} h} = \begin{pmatrix} \cosh(\Gamma) - \frac{i\zeta h}{\Gamma} \sinh(\Gamma) & \frac{Q_{n+1/2}}{\Gamma} \sinh(\Gamma) \\ \frac{R_{n+1/2}}{\Gamma} \sinh(\Gamma) & \cosh(\Gamma) + \frac{i\zeta h}{\Gamma} \sinh(\Gamma) \end{pmatrix}, \quad (46)$$

where $\Gamma = \sqrt{Q_{n+1/2} R_{n+1/2} - \zeta^2 h^2}$ where $Q_{n+1/2} = hq(x_n + h/2, t)$ and $R_{n+1/2} = hr(x_n + h/2, t)$. We refer to this integrator as “MG1” signifying Magnus integrator with one-point Gauss quadrature. This method is also referred to as

the exponential mid-point rule in the literature and it can be shown to be consistent and stable with an order $p = 2$. Additionally, it also forms the part of the Lie-group methods [51, 53] as it retains the $SU(2)$ structure of the Jost solution $v = (\phi, \bar{\phi})$ for $\zeta \in \mathbb{R}$. It must be noted that this method is specially suited for highly oscillatory problems and has been employed by several authors to solve forward scattering problems [54, 55]. Finally, let us mention that the method of computing the norming constants as described in Sec. 3.2.1 can also be adapted to MG1.

4.2. Split-Magnus method

A further simplification obtained by applying Strang-type splitting [56] to the exponential operator provides the right discrete framework for the layer-peeling algorithm. This simplification is achieved as follows:

$$e^{-i\zeta\sigma_3 h + U_{n+1/2}h} = e^{-i\zeta\sigma_3 h/2} e^{U_{n+1/2}h} e^{-i\zeta\sigma_3 h/2} + \mathcal{O}(h^3). \quad (47)$$

The order of approximation is determined by applying the Baker-Campbell-Hausdorff (BCH) formula to the exponential operators [53, Chapter 4]. Setting $\Gamma = \sqrt{Q_{n+1/2}R_{n+1/2}}$,

$$\begin{aligned} e^{U_{n+1/2}h} &= \begin{pmatrix} \cosh \Gamma & Q_{n+1/2} \frac{\sinh \Gamma}{\Gamma} \\ R_{n+1/2} \frac{\sinh \Gamma}{\Gamma} & \cosh \Gamma \end{pmatrix} \\ &= \frac{1}{\sqrt{1 - \tanh^2 \Gamma}} \begin{pmatrix} 1 & Q_{n+1/2} \frac{\tanh \Gamma}{\Gamma} \\ R_{n+1/2} \frac{\tanh \Gamma}{\Gamma} & 1 \end{pmatrix} \\ &= \frac{1}{\sqrt{1 - \Gamma^2}} \begin{pmatrix} 1 & Q_{n+1/2} \\ R_{n+1/2} & 1 \end{pmatrix} + \mathcal{O}(h^3). \end{aligned}$$

Therefore, the discretization scheme works out to be

$$v_{n+1} = \frac{1}{\Theta_{n+1/2}^{1/2}} \begin{pmatrix} z^{-1} & Q_{n+1/2} \\ R_{n+1/2} & z \end{pmatrix} v_n, \quad (48)$$

where $\Theta_{n+1/2} = (1 - Q_{n+1/2}R_{n+1/2}) > 0$. This form has been used by a number of authors in connection with the conventional layer-peeling algorithm [9, 10, 57] as well as for the fast version of the layer-peeling algorithm [37, 38]. By employing the transformation $w_n = e^{i\zeta\sigma_3 h/2} v_n$, we obtain

$$\begin{aligned} w_{n+1} &= \frac{z^{-1}}{\Theta_{n+1/2}^{1/2}} \begin{pmatrix} 1 & z^2 Q_{n+1/2} \\ R_{n+1/2} & z^2 \end{pmatrix} w_n \\ &= z^{-1} M_{n+1}(z^2) w_n, \end{aligned} \quad (49)$$

which maybe viewed as a modification of the implicit Euler scheme. The integration scheme thus obtained is referred to as the split-Magnus (SM) method. The inverse relationship is given by

$$\frac{z^{-1}}{\Theta_{n+1/2}^{1/2}} \begin{pmatrix} z^2 & -z^2 Q_{n+1/2} \\ -R_{n+1/2} & 1 \end{pmatrix} w_{n+1} = w_n. \quad (50)$$

The Jost solution can be put in to the form

$$\begin{aligned} \psi_n &= z^{\ell_+} z^{-m} \begin{pmatrix} z^{-1} & 0 \\ 0 & 1 \end{pmatrix} S_m(z^2), \\ \phi_n &= z^{\ell_-} z^{-n} \begin{pmatrix} 1 & 0 \\ 0 & z \end{pmatrix} P_n(z^2), \end{aligned} \quad (51)$$

where $S_m(z^2)$ and $P_n(z^2)$ obey the same kind of transfer matrix relation as in (25) with initial condition $S_0 = (0, 1)^\top$ and $P_0 = (1, 0)^\top$. The scattering coefficients work out to be

$$\begin{aligned} a_N(z^2) &= P_1^{(N)}(z^2), & b_N(z) &= z^{-2\ell_++1} P_2^{(N)}(z^2), \\ a_N(z^2) &= S_2^{(N)}(z^2), & \bar{b}_N(z) &= z^{-2\ell_- - 1} S_1^{(N)}(z^2). \end{aligned} \quad (52)$$

The layer-peeling property can be stated as $R_{n+1/2} = P_{2,0}^{(n+1)} / P_{1,0}^{(n+1)}$ with the following additional constraints:

$$P_{1,0}^{(n+1)} = \prod_{k=1}^{n+1} \Theta_k^{-1/2} > 0, \quad P_{n+1}^{(n+1)} = 0. \quad (53)$$

Lastly, the formula for computing norming constants given by

$$\begin{aligned} b_k &= (z_k^2)^{\ell_- - n} \frac{z_k P_2^{(n)}(z_k^2)}{S_2^{(m)}(z_k^2)}, \\ \frac{1}{b_k} &= (z_k^2)^{\ell_+ - m} \frac{S_1^{(m)}(z_k^2)}{z_k P_1^{(n)}(z_k^2)}. \end{aligned} \quad (54)$$

Lastly, we note that a staggered grid configuration may prove superior for potentials with jump discontinuity at any grid point because the sampling of the potential at the points of discontinuity is avoided.

Remark 4.1. It must be noted that the CDT and the FDT algorithms are incompatible with the staggered grid configuration, therefore, the SM integrator is ruled out for all DT-related algorithms.

5. Discrete inverse scattering: Necessary and sufficient condition

In this section, we study the necessary and sufficient condition for the inversion of the discrete scattering coefficients within the framework of the numerical discretization introduced in Sec. 3. Let $\{(\cdot)_k\}_{k=1}^N$ denote a sequence of quantities such as scalars, vectors or matrices.

Definition 5.1. Let d be a non-negative integer. A polynomial $P_n(z)$ defined as in (23) (with coefficients $P_k^{(n)} \in \mathbb{C}^2$, $k = 0, 1, \dots, n$) is said to belong to the class $P(d; \mathbb{C}^2)$ if $\deg[P_n(z)] \leq d$ and, for all $z \in \mathbb{T}$, we have

$$P_n(z) \cdot P_n^*(z) = 1, \quad (55)$$

with $P_{1,0}^{(n)} \in \mathbb{R}_+$.

For any $P_n(z) \in P(d; \mathbb{C}^2)$, on equating the coefficient of the zeroth degree term on LHS and RHS of (55), we obtain

$$\sum_{k=0}^n P_k^{(n)} \cdot P_k^{(n)*} = \sum_{k=0}^n \left[|P_{1,k}^{(n)}|^2 + |P_{2,k}^{(n)}|^2 \right] = 1.$$

Therefore, $|P_{1,k}^{(n)}| \leq 1$ and $|P_{2,k}^{(n)}| \leq 1$ for $k = 0, 1, \dots, n$. Note that the condition $P_{1,0}^{(n)} \in \mathbb{R}_+$ ensures that there are no constant phase factors in $P_n(z)$ because the relation (55) is insensitive to constant phase factors.

Definition 5.2 (Para-conjugate). For any scalar valued complex function, $f(z)$, we define $\bar{f}(z) = f^*(1/z^*)$. For any vector valued complex function, $\mathbf{f}(z) = (f_1(z), f_2(z))^T$, we define

$$\bar{\mathbf{f}}(z) = i\sigma_2 \mathbf{f}^*(1/z^*) = \begin{pmatrix} \bar{f}_2(z) \\ -\bar{f}_1(z) \end{pmatrix}.$$

For a matrix valued function, $M(z)$, we define

$$\bar{M}(z) = i\sigma_2 M^*(1/z^*) (i\sigma_2)^\dagger = \sigma_2 M^*(1/z^*) \sigma_2$$

so that the operation $\bar{(\cdot)}$ is distributive over matrix-vector and matrix-matrix products.

Based on the discrete formulation of the ZS-problem in Sec. 3, we identified a discrete representation of the Jost

solution which can also be stated in the form (leaving out the factors independent of n)

$$w_n = \begin{pmatrix} z^{-n} P_n(z^2), z^n \bar{P}_n(z^2) \end{pmatrix}, \quad (56)$$

such that the column vectors are linearly independent for all $z \in \mathbb{C}$. This implies, $\det[w_n] \neq 0$. In fact, the determinant must turn out to be independent of z^2 so that we may put $\det[w_n] = W_n$ which translates into the constraint¹¹

$$\det \begin{bmatrix} P_n(z^2), \bar{P}_n(z^2) \end{bmatrix} = -P_n(z^2) \cdot P_n^*(1/z^{*2}) = W_n.$$

For $z \in \mathbb{T}$,

$$P_n(z^2) \cdot P_n^*(z^2) = -W_n > 0. \quad (57)$$

This condition is necessary for w_n , defined by (56), to be a Jost solution. Further, it is easy to verify that w_n satisfies the relation

$$\bar{w}_n = \sigma_2 \begin{pmatrix} z^n \bar{P}_n(z), z^{-n} P_n(z^2) \end{pmatrix} \sigma_2 = -w_n \quad (58)$$

Finally, let us note that $\tilde{w}_n = w_n / \sqrt{-W_n}$ forms a $SU(2)$ -valued sequence for $z \in \mathbb{T}$.

The discrete scattering problem will be assumed to be stated in the form of a recurrence relation which reads as

$$w_{n+1} = z^{-1} M_{n+1}(z^2) w_n, \quad (59)$$

where $M_n(z^2)$ is a polynomial matrix of degree one. Note that w_n as defined by (56) satisfies the relation $\bar{w}_n = -w_n$, therefore, in order that w_{n+1} be a Jost solution, we must have $z^{-1} M_{n+1}(z^2) = z \bar{M}_{n+1}(z^2)$. This relationship expands to

$$\begin{pmatrix} m_{11}^{(n)}(z^2) & m_{12}^{(n)}(z^2) \\ m_{21}^{(n)}(z^2) & m_{22}^{(n)}(z^2) \end{pmatrix} = z^2 \begin{pmatrix} \bar{m}_{22}^{(n)}(z^2) & -\bar{m}_{21}^{(n)}(z^2) \\ -\bar{m}_{12}^{(n)}(z^2) & \bar{m}_{11}^{(n)}(z^2) \end{pmatrix} \quad (60)$$

and $\det[M_n(z^2)] = z^2 C_n$ where C_n is independent of z . Introducing the functions

$$m_j^{(n)}(z^2) = m_{j,0}^{(n)} + m_{j,1}^{(n)} z^2, \quad j = 1, 2, \quad (61)$$

it follows that the general form of the transfer matrix (of degree one in z^2) can be written as

$$M_n(z^2) = \begin{pmatrix} m_1^{(n)}(z^2) & -z^2 \bar{m}_2^{(n)}(z^2) \\ m_2^{(n)}(z^2) & z^2 \bar{m}_1^{(n)}(z^2) \end{pmatrix} \quad (62)$$

¹¹Given that $\det[w_n]$ is a polynomial, the only way $\det[w_n] \neq 0$ is when it is a polynomial of degree zero.

with

$$\begin{aligned} C_n &= |m_{1,0}^{(n)}|^2 + |m_{2,0}^{(n)}|^2 + |m_{1,1}^{(n)}|^2 + |m_{2,1}^{(n)}|^2, \\ m_{1,0}^{(n)} m_{1,1}^{(n)*} + m_{2,0}^{(n)} m_{2,1}^{(n)*} &= 0. \end{aligned} \quad (63)$$

Let the inverse of $M_n(z^2)$ be denoted by $z^{-2} \widetilde{M}_n(z^2)$ which also satisfies a similar symmetry relation as in (60) and

$$z^{-2} \widetilde{M}_n(z^2) = \frac{z^{-2}}{C_n} \begin{pmatrix} z^2 \overline{m}_1^{(n)}(z^2) & z^2 \overline{m}_2^{(n)}(z^2) \\ -\overline{m}_2^{(n)}(z^2) & \overline{m}_1^{(n)}(z^2) \end{pmatrix}$$

so that $\widetilde{M}_n = z^2 \overline{M}_n$. Further, it is straightforward to verify that, for $z \in \mathbb{T}$, the matrices $z^{-1} M_n / \sqrt{C_n}$ and $z^{-1} \widetilde{M}_n / \sqrt{C_n}$ are elements of $SU(2)$. The discrete scattering problem in its unitary form reads as

$$\frac{w_{n+1}}{\sqrt{-W_{n+1}}} = \frac{z^{-1}}{\sqrt{C_{n+1}}} M_{n+1}(z^2) \frac{w_n}{\sqrt{-W_n}}. \quad (64)$$

Introducing $\mu_n, A_n, B_n \in \mathbb{C}$, the independent elements of transfer matrix can be put into the form

$$\begin{aligned} m_1^{(n)}(z^2) &= \mu_n(1 - z^2 A_n^* B_n), \\ m_2^{(n)}(z^2) &= \mu_n(A_n + B_n z^2), \end{aligned} \quad (65)$$

so that

$$C_n = |\mu_n|^2 (1 + |A_n|^2)(1 + |B_n|^2). \quad (66)$$

Setting $\mu_n = |\mu_n| e^{i\theta_n}$, the transfer matrix admits of the following factorization

$$M_n = |\mu_n| \begin{pmatrix} 1 & -A_n^* \\ A_n & 1 \end{pmatrix} \begin{pmatrix} 1 & 0 \\ 0 & z^2 \end{pmatrix} \begin{pmatrix} 1 & -B_n^* \\ B_n & 1 \end{pmatrix} e^{i\sigma_3 \theta_n}. \quad (67)$$

For the cases considered in this article, $\theta_n = 0$, therefore, we assume $\mu_n \in \mathbb{R}_+$ so that it does not play a role in the unitary form of the transfer matrix for $z \in \mathbb{T}$. For a given initial condition and fixed sequence of transfer matrices, the recurrence relation (59) leads to a unique polynomial associated with the Jost solution w_n . In particular, the following result is straightforward:

Lemma 5.1. *Let N be a finite positive integer. Let the vectors $\mathbf{A} = (A_1, A_2, \dots, A_N)$, $\mathbf{B} = (B_1, B_2, \dots, B_N) \in \mathbb{C}^N$ and $\boldsymbol{\mu} = (\mu_1, \mu_2, \dots, \mu_N) \in \mathbb{R}_+^N$ define $\{M_n(z^2)\}_{n=1}^N$ through (67). Let $w_0 = \sigma_1$, then the recurrence relation (59) determines a sequence of Jost solutions $\{w_n\}_{n=1}^N$ such that for every n ($1 \leq n \leq N$) there exists a unique polynomial $P_n(z^2)$ associated with w_n .*

Now let us consider an arbitrary polynomial $P_n(z^2)$ satisfying (57) for $n \geq 0$. Assume $P_n(z^2)/\sqrt{-W_n} \in \mathcal{P}(n; \mathbb{C}^2)$ and let $P_{n+1}(z^2)$ be associated with w_{n+1} . To understand the properties of the polynomial $P_{n+1}(z^2)$, we consider the recurrence relation (59). Equating the coefficients of the zeroth degree term on the RHS and the LHS of (59), we have

$$\begin{aligned} P_{1,0}^{(n+1)} &= \mu_{n+1} (P_{1,0}^{(n)} - B_{n+1}^* P_{2,0}^{(n)}), \\ P_{2,0}^{(n+1)} &= \mu_{n+1} A_{n+1} (P_{1,0}^{(n)} - B_{n+1}^* P_{2,0}^{(n)}). \end{aligned} \quad (68)$$

It is straightforward to see that

$$A_{n+1} = \frac{P_{2,0}^{(n+1)}}{P_{1,0}^{(n+1)}} \quad (69)$$

and

$$P_{1,0}^{(n+1)} = \mu_{n+1} \left(1 - B_{n+1}^* \frac{P_{2,0}^{(n)}}{P_{1,0}^{(n)}} \right) P_{1,0}^{(n)}.$$

Therefore, in order that $P_{n+1}(z^2)/\sqrt{-W_{n+1}} \in \mathcal{P}(n+1; \mathbb{C}^2)$ where $W_{n+1} = \det[w_{n+1}] = C_{n+1} W_n$, we must have

$$1 - B_{n+1}^* \frac{P_{2,0}^{(n)}}{P_{1,0}^{(n)}} \in \mathbb{R}_+.$$

Lemma 5.2. *Under the assumption of the previous lemma, setting $W_n = \det[w_n]$, the polynomial $P_n(z^2)/\sqrt{-W_n} \in \mathcal{P}(n; \mathbb{C}^2)$ if and only if the sequence $\{(A_n, B_n)\}_{n=1}^N$ satisfies the constraint $(1 - A_n B_{n+1}^*) \in \mathbb{R}_+$ for $1 \leq n < N$. If $B_1 = 0$, then $P_n(z^2)/\sqrt{-W_n} \in \mathcal{P}(n-1; \mathbb{C}^2)$.*

Proof. Using the recurrence relation (68) and the property (69) for all $n \geq 0$, it is straightforward to see that

$$\begin{aligned} P_{1,0}^{(n+1)} &= \mu_{n+1} (1 - A_n B_{n+1}^*) P_{1,0}^{(n)} \\ &= \mu_1 \prod_{k=1}^n \mu_{k+1} (1 - A_k B_{k+1}^*), \end{aligned} \quad (70)$$

for $n > 0$ while $P_{1,0}^{(1)} = \mu_1$. The proof of the first part of the lemma follows from this relation.

For the second part, equating the coefficients of $(z^2)^{n+1}$ on the RHS and the LHS of (59), we have

$$\begin{aligned} P_{1,n+1}^{(n+1)} &= -\mu_{n+1} A_{n+1}^* (B_{n+1} P_{1,n}^{(n)} + P_{2,n}^{(n)}), \\ P_{2,n+1}^{(n+1)} &= \mu_{n+1} (B_{n+1} P_{1,n}^{(n)} + P_{2,n}^{(n)}), \end{aligned}$$

for $n \geq 0$. These relations yield

$$\begin{aligned} P_{1,n+1}^{(n+1)} &= -\mu_{n+1} A_{n+1}^* P_{2,n+1}^{(n+1)}, \\ P_{2,n+1}^{(n+1)} &= \mu_1 B_1 \prod_{k=1}^n \mu_{k+1} (1 - B_{k+1} A_k^*). \end{aligned} \quad (71)$$

for $n > 0$ while $P_{1,1}^{(1)} = -\mu_1 A_1^* B_1$ and $P_{2,1}^{(1)} = \mu_1 B_1$. Therefore, if $B_1 = 0$ then $P_n^{(n)} = 0$ for $1 \leq n \leq N$. \square

Next we would like to analyze the inverse problem described as follows: Given an arbitrary polynomial $P_{n+1}(z^2)$ associated with w_{n+1} satisfying

$$P_{n+1}(z^2) \cdot P_{n+1}^*(z^2) = -W_{n+1} > 0, \quad (72)$$

for $n \geq 0$ such that $P_{n+1}(z^2)/\sqrt{-W_{n+1}} \in \mathcal{P}(n+1; \mathbb{C}^2)$. Find a polynomial $P_n(z^2)$ associated with w_n and a transfer matrix $M_{n+1}(z^2)$ such that w_n , defined by

$$w_n = z^{-1} \tilde{M}_{n+1}(z^2) w_{n+1}, \quad (73)$$

is a Jost solution. Again, equating the coefficients of the zeroth degree term on the RHS and the LHS of (59), we get the recurrence relation (69). Equating the coefficients of z^2 on the RHS and the LHS of (59), we obtain

$$\begin{aligned} P_{1,1}^{(n+1)} &= \mu_{n+1} (P_{1,1}^{(n)} - A_{n+1}^* B_{n+1} P_{1,0}^{(n)}) \\ &\quad - \mu_{n+1} (B_{n+1}^* P_{2,1}^{(n)} + A_{n+1}^* P_{2,0}^{(n)}), \\ P_{2,1}^{(n+1)} &= \mu_{n+1} (A_{n+1} P_{1,1}^{(n)} + B_{n+1} P_{1,0}^{(n)}) \\ &\quad + \mu_{n+1} (P_{2,0}^{(n)} - A_{n+1} B_{n+1}^* P_{2,1}^{(n)}). \end{aligned}$$

This yields

$$P_{2,1}^{(n+1)} - A_{n+1} P_{1,1}^{(n+1)} = \mu_{n+1} (1 + |A_{n+1}|^2) (P_{2,0}^{(n)} + B_{n+1} P_{1,0}^{(n)}),$$

so that using (68) we have

$$\frac{P_{2,0}^{(n)} + B_{n+1} P_{1,0}^{(n)}}{P_{1,0}^{(n)} - B_{n+1}^* P_{2,0}^{(n)}} = \chi_{n+1} \quad (74)$$

where

$$\chi_{n+1} = \frac{P_{2,1}^{(n+1)} - A_{n+1} P_{1,1}^{(n+1)}}{(1 + |A_{n+1}|^2) P_{1,0}^{(n+1)}}. \quad (75)$$

First, we find that the parameter A_{n+1} of $M_{n+1}(z^2)$ must be set according to (69). Note that this condition implies that

the lowest degree term on the RHS of (73) is the zeroth degree term so that

$$P_0^{(n)} = \frac{\mu_{n+1} (1 + |A_{n+1}|^2)}{C_{n+1}} \left(\frac{1 + B_{n+1}^* \chi_{n+1}}{\chi_{n+1} - B_{n+1}} \right) P_{1,0}^{(n+1)}. \quad (76)$$

In order to compute B_{n+1} , we introduce a free parameter, $\lambda_n = P_{2,0}^{(n)}/P_{1,0}^{(n)}$, so that from (74), we have

$$B_{n+1} = \frac{1 + |\lambda_n|^2}{1 - |\chi_{n+1}|^2 |\lambda_n|^2} \chi_{n+1} - \frac{1 + |\chi_{n+1}|^2}{1 - |\chi_{n+1}|^2 |\lambda_n|^2} \lambda_n. \quad (77)$$

Now, let us observe that

$$\begin{aligned} 1 + B_{n+1}^* \chi_{n+1} &= \frac{1 + |\chi_{n+1}|^2}{1 - |\chi_{n+1}|^2 |\lambda_n|^2} (1 - \chi_{n+1} \lambda_n^*), \\ \chi_{n+1} - B_{n+1} &= \frac{1 + |\chi_{n+1}|^2}{1 - |\chi_{n+1}|^2 |\lambda_n|^2} (1 - \chi_{n+1} \lambda_n^*) \lambda_n, \end{aligned}$$

and

$$1 - B_{n+1}^* \lambda_n = \frac{1 + |\lambda_n|^2}{1 - |\chi_{n+1}|^2 |\lambda_n|^2} (1 - \chi_{n+1}^* \lambda_n)$$

so that

$$1 + |B_{n+1}|^2 = \frac{(1 + |\lambda_n|^2)(1 + |\chi_{n+1}|^2)}{(1 - |\chi_{n+1}|^2 |\lambda_n|^2)^2} |1 - \chi_{n+1}^* \lambda_n|^2.$$

Now the zeroth degree coefficient given by (76) simplifies to

$$P_0^{(n)} = \frac{(1 - |\chi_{n+1}|^2 |\lambda_n|^2)}{\mu_{n+1} (1 + |\lambda_n|^2)} \frac{P_{1,0}^{(n+1)}}{(1 - \chi_{n+1}^* \lambda_n)} \left(\frac{1}{\lambda_n} \right). \quad (78)$$

Therefore, in order that $P_n(z^2)/\sqrt{-W_n} \in \mathcal{P}(n; \mathbb{C}^2)$ where $W_n = W_{n+1}/C_{n+1}$, we must have

$$\frac{1 - \chi_{n+1}^* \lambda_n}{1 - |\chi_{n+1}| |\lambda_n|} \in \mathbb{R}_+. \quad (79)$$

The above condition can be enforced by setting $\lambda_n = \chi_{n+1} \omega_n$ where we restrict ourselves to the case $\omega_n \in \mathbb{R}$, $\omega_n \geq 0$. Under this condition, the expressions for B_{n+1} and $P_0^{(n)}$ simplifies to

$$B_{n+1} = \frac{(1 - \omega_n) \chi_{n+1}}{1 + |\chi_{n+1}|^2 \omega_n} \quad (80)$$

and

$$\mathbf{P}_0^{(n)} = \frac{1 + |\chi_{n+1}|^2 \omega_n}{1 + |\chi_{n+1}|^2 \omega_n^2} \begin{pmatrix} 1 \\ \omega_n \chi_{n+1} \end{pmatrix} \mu_{n+1}^{-1} \mathbf{P}_{1,0}^{(n+1)}, \quad (81)$$

respectively. Clearly, the transfer matrix $M_{n+1}(z^2)$ as well as the polynomial $\mathbf{P}_n(z^2)$ is not unique as it depends on a free parameter $\omega_n \geq 0$. Note that the parameter μ_{n+1} turns out to be merely a scale factor which does not play a role in the unitary form of the discrete scattering problem. Finally, let us observe that in order to predict the highest degree term that is non-zero in $\mathbf{P}_n(z^2)$, the recurrence relation for $(z^2)^n \bar{\mathbf{P}}(z^2)$ can be considered where the zeroth degree term is $i\sigma_2 \mathbf{P}_n^{(n)*}$ so that

$$\mathbf{P}_n^{(n)} = \frac{1 + |\chi_{n+1}|^2 \omega_n}{1 + |\chi_{n+1}|^2 \omega_n^2} \begin{pmatrix} -\omega_n \chi_{n+1}^* \\ 1 \end{pmatrix} \mu_{n+1}^{-1} \mathbf{P}_{2,n+1}^{(n+1)}. \quad (82)$$

Remark 5.1. In the discrete inverse scattering case, the two formulas (69) and (75) remain invariant under any scaling of the polynomial $\mathbf{P}_{n+1}(z^2)$. Therefore, knowledge of either $\mathbf{P}_{n+1}(z^2)$ or $\mathbf{P}_{n+1}(z^2)/\sqrt{-W_{n+1}}$ is sufficient to determine the transfer matrix $M_{n+1}(z^2)$.

The discussion above regarding the discrete inverse scattering step can be summarized in the following lemma:

Lemma 5.3. Given $\mathbf{P}_{n+1}(z^2)/\sqrt{-W_{n+1}} \in \mathcal{P}(d; \mathbb{C}^2)$ where $d \in \{n+1, n\}$ and $\omega_n \in \mathbb{R}_+$, there exists a unique unitary matrix $M_{n+1}(z^2)/\sqrt{C_{n+1}}$ for $z \in \mathbb{T}$ and a polynomial $\mathbf{P}_n(z^2)/\sqrt{-W_n} \in \mathcal{P}(d-1; \mathbb{C}^2)$ such that

$$\frac{\mathbf{P}_{n+1}(z^2)}{\sqrt{-W_{n+1}}} = \frac{M_{n+1}(z^2)}{\sqrt{C_{n+1}}} \frac{\mathbf{P}_n(z^2)}{\sqrt{-W_n}}.$$

Further, if $\omega_n \leq 1$, then

$$\left[(1 + |A_{n+1}|^2)(1 + |B_{n+1}|^2) \right]^{1/2} \leq \frac{P_{1,0}^{(n)}/\sqrt{-W_n}}{P_{1,0}^{(n+1)}/\sqrt{-W_{n+1}}}. \quad (83)$$

Proof. The first part of the lemma is evident from the discussion above. The second part follows from the inequality

$$\frac{1 + |\chi_{n+1}|^2 \omega_n}{1 + |\chi_{n+1}|^2 \omega_n^2} \geq 1,$$

for $\omega_n \leq 1$.

Next, we consider some of special cases where it is possible to obtain unique solution of the discrete inverse scattering problem. It is worth noting that these special cases belong to a certain choice of the values $\{\omega_n\}_{n \in \mathbb{Z}}$.

5.1. Case I: $A_n = B_{n+1}$

Let $A_n = B_{n+1}$ and assume $A_n \in \mathbb{D}$. Then the forward scattering problem described in Lemma 5.1 always yields a polynomial $\mathbf{P}_n(z^2)/\sqrt{-W_n} \in \mathcal{P}(n; \mathbb{C}^2)$ on account of Lemma 5.2.

For discrete inverse scattering, the condition $A_n = B_{n+1}$ amounts to $B_{n+1} = \chi_{n+1} \omega_n$. From (80), we have

$$|\chi_{n+1}|^2 \omega_n^2 + 2\omega_n - 1 = 0,$$

which yields

$$\omega_n = \frac{1}{1 + \sqrt{1 + |\chi_{n+1}|^2}} \quad (84)$$

as the admissible solution (the other root violates the positivity constraint in (79)). For this case, the expression (81) for the zeroth degree coefficient simplifies to

$$\mathbf{P}_0^{(n)} = \frac{1}{2\mu_{n+1}\omega_n} \begin{pmatrix} 1 \\ \omega_n \chi_{n+1} \end{pmatrix} \mathbf{P}_{1,0}^{(n+1)}, \quad (85)$$

In the Lemma 5.3, we favor the case of $d = n$ so that number of (vector) coefficients associated with $\mathbf{P}_n(z^2)$ be n . If the steps described in the aforementioned lemma are carried out recursively to the point $n = 0$, we obtain

$$\mathbf{P}_0^{(0)} = \frac{1}{2\mu_1\omega_0} \begin{pmatrix} 1 \\ \omega_0 \chi_1 \end{pmatrix} \mathbf{P}_{1,0}^{(1)}.$$

Note that $\chi_1 = 0$ on account of $\mathbf{P}_1^{(1)} = 0$; therefore,

$$\frac{\mathbf{P}_0(z^2)}{\sqrt{-W_0}} = \begin{pmatrix} 1 \\ 0 \end{pmatrix} \frac{P_{1,0}^{(1)}}{\sqrt{-W_1}} \sqrt{1 + |A_1|^2} = \begin{pmatrix} 1 \\ 0 \end{pmatrix}. \quad (86)$$

Finally, we state the main result of this section which is a now merely a consequence of the preceding lemmas applied to the case at hand:

Proposition 5.4. Let $\mathbf{A} = (A_1, A_2, \dots, A_N) \in \mathbb{D}^N$ be an arbitrary vector. Let the transfer matrices $\{M_n(z^2)\}_{n=1}^N$ be determined by (67) using \mathbf{A} together with $\mathbf{B} \in \mathbb{D}^N$ given

by $B_1 = 0$ and $B_n = A_{n-1}$ for $1 < n \leq N$. Then, corresponding to the initial condition $\mathbf{P}_0(z^2) = (1, 0)^\top$, the recurrence relation

$$\mathbf{P}_n(z^2) = M_n(z^2)\mathbf{P}_{n-1}(z^2), \quad 1 \leq n \leq N,$$

yields a unique polynomial $\mathbf{P}_N(z^2)/\sqrt{-W_N} \in \mathbb{P}(N-1; \mathbb{C}^2)$ with $(-W_N) = \prod_{n=1}^N C_n > 0$ such that

$$|P_{2,0}^{(N)}/P_{1,0}^{(N)}| < 1.$$

Conversely, for any given polynomial $\check{\mathbf{P}}_N(z^2) \in \mathbb{P}(N-1; \mathbb{C}^2)$ such that

$$|\check{P}_{2,0}^{(N)}/\check{P}_{1,0}^{(N)}| < 1,$$

there exists a unique vector $\mathbf{A} = (A_1, A_2, \dots, A_N) \in \mathbb{D}^N$ which determines the the transfer matrices $\{\tilde{M}_n(z^2)/\sqrt{C_n}\}_{n=1}^N$ as stated above such that the recurrence relation

$$\check{\mathbf{P}}_{n-1}(z^2) = \frac{z^{-2}}{\sqrt{C_n}} \tilde{M}_n(z^2) \check{\mathbf{P}}_n(z^2),$$

starting from $n = N$ yields $\check{\mathbf{P}}_0(z^2) = (1, 0)^\top$.

Putting $\check{\mathbf{P}}_N(z^2) = \mathbf{P}_N(z^2)/\sqrt{-W_N}$, note that the condition

$$|P_{2,0}^{(N)}/P_{1,0}^{(N)}| = |\check{P}_{2,0}^{(N)}/\check{P}_{1,0}^{(N)}| < 1,$$

corresponds to the fact that $A_N \in \mathbb{D}$ in the direct part of the last proposition. The condition above is imposed explicitly in the converse part in order to ensure $A_N \in \mathbb{D}$.

Corollary 5.5. *Let $\mathbf{A} = (A_1, A_2, \dots, A_N) \in \mathbb{D}^N$ correspond to $\check{\mathbf{P}}_N(z^2) \in \mathbb{P}(N-1; \mathbb{C}^2)$ as in the converse part of the last proposition. Then the following estimate holds:*

$$\|\mathbf{A}\|_2 = \left(\sum_{n=1}^N |A_n|^2 \right)^{1/2} \leq \left(\frac{1}{\check{P}_{1,0}^{(N)}} - 1 \right)^{1/2}.$$

Proof. The proof follows from the relation (83) of Lemma 5.3. \square

We conclude this section with the discussion of the trapezoidal rule which corresponds to the case at hand. Let $\mathbf{Q} = (Q_1, Q_2, \dots, Q_N) \in \mathbb{D}^N$. In the case of trapezoidal rule, it follows from the description in Sec. 3.1.3 that the coefficients A_n and B_n introduced in (65) satisfy

$$A_n = B_{n+1} = R_n = -Q_n^*, \quad 0 < n < N,$$

with $A_N = Q_N$ and we choose $Q_0 = B_1 = 0$. It also follows that the quantities $\mu_n \in \mathbb{R}_+$ introduced in (65) are given by

$$\mu_n = \Theta_n^{-1} = (1 + |Q_n|^2)^{-1}, \quad 0 < n \leq N.$$

Further, we have

$$C_n = \frac{1 + |Q_{n-1}|^2}{1 + |Q_n|^2} = \frac{\Theta_{n-1}}{\Theta_n}, \quad 1 < n \leq N,$$

while $C_1 = \Theta_1^{-1}$.

5.2. Case II: $A_n \neq B_{n+1}$

First, let us assume that $B_n = 0$. The discussion of the forward scattering problem is identical to that of the previous case. For discrete inverse scattering, this case corresponds to $\omega_n = 1$. The expression for the zeroth degree coefficient (81) simplifies to

$$\mathbf{P}_0^{(n)} = \frac{1}{\mu_{n+1}} \begin{pmatrix} 1 \\ \chi_{n+1} \end{pmatrix} \mathbf{P}_{1,0}^{(n+1)}. \quad (87)$$

As in the last section, we favor the case of $d = n$ in the Lemma 5.3. Again, if the steps described in the aforementioned lemma are carried out recursively to the point $n = 0$, it is easy to conclude that

$$\frac{\mathbf{P}_0(z^2)}{\sqrt{-W_0}} = \begin{pmatrix} 1 \\ 0 \end{pmatrix}. \quad (88)$$

The necessary and sufficient condition for discrete inverse scattering in this case can be stated as:

Proposition 5.6. *Let $\mathbf{A} = (A_1, A_2, \dots, A_N) \in \mathbb{C}^N$ be an arbitrary vector. Let the transfer matrices $\{M_n(z^2)\}_{n=1}^N$ be determined by (67) using \mathbf{A} together with $B_n = 0$ for $1 \leq n \leq N$. Then, corresponding to the initial condition $\mathbf{P}_0(z^2) = (1, 0)^\top$, the recurrence relation*

$$\mathbf{P}_n(z^2) = M_n(z^2)\mathbf{P}_{n-1}(z^2), \quad 1 \leq n \leq N,$$

yields a unique polynomial $\mathbf{P}_N(z^2)/\sqrt{-W_N} \in \mathbb{P}(N-1; \mathbb{C}^2)$ with $(-W_N) = \prod_{n=1}^N C_n > 0$.

Conversely, for any given polynomial $\check{\mathbf{P}}_N(z^2) \in \mathbb{P}(N-1; \mathbb{C}^2)$ there exists a unique vector $\mathbf{A} = (A_1, A_2, \dots, A_N) \in \mathbb{C}^N$ which determines the the transfer

matrices $\{\tilde{M}_n(z^2)/\sqrt{C_n}\}_{n=1}^N$ as stated above such that the recurrence relation

$$\check{P}_{n-1}(z^2) = \frac{z^{-2}}{\sqrt{C_n}} \tilde{M}_n(z^2) \check{P}_n(z^2),$$

starting from $n = N$ yields $\check{P}_0(z^2) = (1, 0)^\top$.

Corollary 5.7. Let $\mathbf{A} = (A_1, A_2, \dots, A_N) \in \mathbb{C}^N$ correspond to $\check{P}_N(z^2) \in \mathcal{P}(N-1; \mathbb{C}^2)$ as in the converse part of the last proposition. Then the following estimate holds:

$$\|\mathbf{A}\|_2 = \left(\sum_{n=1}^N |A_n|^2 \right)^{1/2} \leq \left(\frac{1}{[\check{P}_{1,0}^{(N)}]^2} - 1 \right)^{1/2}.$$

Secondly, let us assume that $A_n = 0$. The discussion of the forward scattering problem is identical to that of the previous case. For discrete inverse scattering, this case corresponds to $\omega_n = 0$. The expression for the zeroth degree coefficient (81) simplifies to

$$P_0^{(n)} = \frac{1}{\mu_{n+1}} \begin{pmatrix} 1 \\ 0 \end{pmatrix} P_{1,0}^{(n+1)}. \quad (89)$$

Here, we favor the case of $d = n + 1$ in the Lemma 5.3. Again, if the steps described in the aforementioned lemma are carried out recursively to the point $n = 0$, it is easy to conclude that

$$\frac{P_0(z^2)}{\sqrt{-W_0}} = \begin{pmatrix} 1 \\ 0 \end{pmatrix}. \quad (90)$$

The expression for the highest degree coefficient (82), simplifies to

$$P_n^{(n)} = \frac{1}{\mu_{n+1}} \begin{pmatrix} 0 \\ 1 \end{pmatrix} P_{2,n+1}^{(n+1)}. \quad (91)$$

The necessary and sufficient condition for discrete inverse scattering in this case can be stated as:

Proposition 5.8. Let $\mathbf{B} = (B_1, B_2, \dots, B_N) \in \mathbb{C}^N$ be an arbitrary vector. Let the transfer matrices $\{M_n(z^2)\}_{n=1}^N$ be determined by (67) using \mathbf{B} together with $A_n = 0$ for $1 \leq n \leq N$. Then, corresponding to the initial condition $P_0(z^2) = (1, 0)^\top$, the recurrence relation

$$P_n(z^2) = M_n(z^2) P_{n-1}(z^2), \quad 1 \leq n \leq N,$$

yields a unique polynomial $P_N(z^2)/\sqrt{-W_N} \in \mathcal{P}(N; \mathbb{C}^2)$ with $(-W_N) = \prod_{n=1}^N C_n > 0$.

Conversely, for any given polynomial $\check{P}_N(z^2) \in \mathcal{P}(N; \mathbb{C}^2)$ there exists a unique vector $\mathbf{B} = (B_1, B_2, \dots, B_N) \in \mathbb{C}^N$ which determines the the transfer matrices $\{\tilde{M}_n(z^2)/\sqrt{C_n}\}_{n=1}^N$ as stated above such that the recurrence relation

$$\check{P}_{n-1}(z^2) = \frac{z^{-2}}{\sqrt{C_n}} \tilde{M}_n(z^2) \check{P}_n(z^2),$$

starting from $n = N$ yields $\check{P}_0(z^2) = (1, 0)^\top$.

Corollary 5.9. Let $\mathbf{B} = (B_1, B_2, \dots, B_N) \in \mathbb{C}^N$ correspond to $\check{P}_N(z^2) \in \mathcal{P}(N; \mathbb{C}^2)$ as in the converse part of the last proposition. Then the following estimate holds:

$$\|\mathbf{B}\|_2 = \left(\sum_{n=1}^N |B_n|^2 \right)^{1/2} \leq \left(\frac{1}{[\check{P}_{1,0}^{(N)}]^2} - 1 \right)^{1/2}.$$

5.2.1. Implicit Euler method

Let $\mathbf{Q} = (Q_1, Q_2, \dots, Q_N) \in \mathbb{C}^N$. For the implicit Euler method, it is evident from the discussion in Sec. 3.1.2 that

$$A_n = R_n = -Q_n^*, \quad B_n = 0, \quad 1 \leq n \leq N,$$

and

$$\mu_n = \Theta_n^{-1} = (1 + |Q_n|^2)^{-1}.$$

Further,

$$C_n = (1 + |Q_n|^2)^{-1} = \Theta_n^{-1}.$$

5.2.2. Split-Magnus method

For the split-Magnus method, we consider the samples on a staggered grid so that $\mathbf{Q} = (Q_{1/2}, Q_{3/2}, \dots, Q_{N-1/2}) \in \mathbb{C}^N$. It is evident from the discussion in Sec. 4.2 that

$$A_n = R_{n-1/2} = -Q_{n-1/2}^*, \quad B_n = 0, \quad 1 \leq n \leq N,$$

and

$$\mu_n = \Theta_{n-1/2}^{-1/2} = (1 + |Q_{n-1/2}|^2)^{-1/2}.$$

Further, $C_n = 1$.

5.2.3. Forward Euler method

Let $\mathbf{Q} = (Q_0, Q_1, \dots, Q_{N-1}) \in \mathbb{C}^N$. For the implicit Euler method, it is evident from the discussion in Sec. 3.1.1 that

$$A_n = 0, \quad B_n = R_{n-1} = -Q_{n-1}^*, \quad 1 \leq n \leq N,$$

and $\mu_n = 1$. Further,

$$C_n = (1 + |Q_{n-1}|^2) = \Theta_{n-1}.$$

6. Stability and convergence analysis

The main objective of this section is to carry out an error-analysis for various steps involved in the algorithms proposed in Sec. 3.

Notations

The class of m -times differentiable complex-valued functions is denoted by \mathcal{C}^m . A function of class \mathcal{C}^m is said to belong to $\mathcal{C}_0^m(\Omega)$, if the function and its derivatives up to order m have a compact support in Ω and if they vanish on the boundary $(\partial\Omega)$. Complex-valued functions (with support in Ω) of bounded variation over \mathbb{R} is denoted by BV and the variation of any function $f \in \text{BV}$ over $\Omega \in \mathbb{R}$ is denoted by $\mathcal{V}[f; \Omega]$. If $q \in \text{BV}$, then $\partial_x q \in L^1$ exists almost everywhere such that $\|\partial_x q\|_{L^1} \leq \mathcal{V}[q; \Omega]$ [58, Chap. 16]. Let $q^{(1)}$ to be equivalent to $\partial_x q$ so that $\|q^{(1)}\|_{L^1} = \|\partial_x q\|_{L^1}$.

Let $J = (-\infty, L]$ and $d > 0$. A complex-valued function $f(x)$ is said to belong to the class $E_d(J)$ if $\text{supp } f \subset J$ and there exists a constant $\kappa_\infty > 0$ such that the estimate $|f(x)| \leq \kappa_\infty e^{-2d|x|}$ holds almost everywhere in J . Clearly, $E_d(J) \subset L^p(J)$ for $1 \leq p \leq \infty$. Define $\mathbb{S}_-(\mu) = \{\zeta \in \mathbb{C}_- | \text{Im } \zeta \geq -\mu\}$.

6.1. Compactly supported and one-sided potentials

The Jost solution for compactly supported and one-sided potential are known to have analytic continuation into the upper-half of the complex plane. We detail some of these analyticity and decay properties of the Jost solutions required for our purpose. This discussion is motivated by the fact that our fast Darboux transformation (FDT) algorithm discussed in Sec. 3.8.2 proceeds by computing the Jost solutions of a truncated potential which

can be interpreted as one-sided (if it does not have a compact support). Further, the analyticity properties of the Jost solutions also determine the behavior of the Lubich coefficients as discussed in Sec. 3.6.

We begin with a study of the modified Jost solutions defined by

$$\tilde{P}(x; \zeta) = \Phi(x; \zeta) e^{i\zeta x} - \begin{pmatrix} 1 \\ 0 \end{pmatrix}.$$

Let $\Omega = [L_1, L_2]$ in the following unless stated otherwise. The system of equations (17) can be transformed into a set of Volterra integral equations of the second kind for the modified Jost solution $\tilde{P}(x; \zeta)$:

$$\tilde{P}(x; \zeta) = \Phi(x; \zeta) + \int_{\Omega} \mathcal{K}(x, y; \zeta) \tilde{P}(y; \zeta) dy, \quad (92)$$

where $\Phi(x; \zeta) = (\Phi_1, \Phi_2)^T \in \mathbb{C}^2$ with

$$\begin{aligned} \Phi_1(x; \zeta) &= \int_{L_1}^x dz \int_{L_1}^z dy q(z) r(y) e^{2i\zeta(z-y)} dy, \\ \Phi_2(x; \zeta) &= \int_{L_1}^x r(y) e^{2i\zeta(x-y)} dy, \end{aligned} \quad (93)$$

and the Volterra kernel $\mathcal{K}(x, y; \zeta) = \text{diag}(\mathcal{K}_1, \mathcal{K}_2) \in \mathbb{C}^{2 \times 2}$ is such that

$$\begin{aligned} \mathcal{K}_1(x, y; \zeta) &= r(y) \int_y^x q(z) e^{2i\zeta(z-y)} dz, \\ \mathcal{K}_2(x, y; \zeta) &= q(y) \int_y^x r(z) e^{2i\zeta(x-z)} dz, \end{aligned} \quad (94)$$

with $\mathcal{K}(x, y; \zeta) = 0$ for $y > x$.

Theorem 6.1. *Let $q \in L^1$ be supported in $\Omega = [L_1, L_2]$ with $\kappa = \|q\|_{L^1}$. Then the estimate*

$$\|\tilde{P}(x; \zeta)\|_{L^\infty(\Omega)} \leq \begin{cases} C, & \zeta \in \overline{\mathbb{C}}_+, \\ C e^{-2 \text{Im}(\zeta)(L_2 - L_1)}, & \zeta \in \mathbb{C}_-. \end{cases} \quad (95)$$

holds with $C = \|\mathbf{D}\| \cosh \kappa$ where $\mathbf{D} = (\kappa^2/2, \kappa)^T$.

Proof. The proof can be obtained using the same method as in [2, 59]. For fixed $\zeta \in \overline{\mathbb{C}}_+$, let \mathcal{K} denote the Volterra integral operator in (92) corresponding to the kernel $\mathcal{K}(x, y; \zeta)$ such that

$$\begin{aligned} \mathcal{K}[\tilde{P}](x; \zeta) &= \int_{\Omega} \mathcal{K}(x, y; \zeta) \tilde{P}(y; \zeta) dy \\ &= \int_{L_1}^x dz \int_{L_1}^z dy \begin{pmatrix} q(z) r(y) e^{2i\zeta(z-y)} \tilde{P}_1(y; \zeta) \\ q(y) r(z) e^{2i\zeta(x-z)} \tilde{P}_2(y; \zeta) \end{pmatrix}. \end{aligned} \quad (96)$$

Consider the $L^\infty(\Omega)$ -norm [60, Chap. 9] of \mathcal{K} given by

$$\|\mathcal{K}\|_{L^\infty(\Omega)} = \operatorname{ess\,sup}_{x \in \Omega} \int_{\Omega} \|\mathcal{K}(x, y; \zeta)\| dy, \quad (97)$$

so that $\|\mathcal{K}\|_{L^\infty(\Omega)} \leq \kappa^2/2$. The resolvent \mathcal{R} of this operator exists and is given by the Neumann series $\mathcal{R} = \sum_{n=1}^{\infty} \mathcal{K}_n$ where $\mathcal{K}_n = \mathcal{K} \circ \mathcal{K}_{n-1}$ with $\mathcal{K}_1 = \mathcal{K}$. It can also be shown using the methods in [2, 59] that $\|\mathcal{K}_n\|_{L^\infty(\Omega)} \leq \kappa^{2n}/(2n)!$, yielding the estimate $\|\mathcal{R}\|_{L^\infty(\Omega)} \leq [\cosh(\kappa) - 1]$. Therefore, for any $\Phi(x; \zeta) \in L^\infty(\Omega)$, the relationship $\tilde{P}(x; \zeta) = \Phi(x; \zeta) + \mathcal{R}[\Phi](x; \zeta)$ implies, for $\zeta \in \bar{\mathbb{C}}_+$,

$$\|\tilde{P}(x; \zeta)\|_{L^\infty(\Omega)} \leq \cosh(\kappa) \|\Phi(x; \zeta)\|_{L^\infty(\Omega)}. \quad (98)$$

The result for $\bar{\mathbb{C}}_+$ in (95) follows from the observation that, for $\zeta \in \bar{\mathbb{C}}_+$, $\|\Phi(x; \zeta)\|_{L^\infty(\Omega)} \leq \|\mathbf{D}\|$ where $\mathbf{D} = (\kappa^2/2, \kappa)^\top$. Therefore, C can be chosen to be $\|\mathbf{D}\| \cosh \kappa$. For the case \mathbb{C}_- of (95), we consider $\tilde{P}_-(x; \zeta) = \tilde{P}(x; \zeta)e^{-2i\zeta x}$. The Volterra integral equations then reads as $\tilde{P}_-(x; \zeta)$:

$$\tilde{P}_-(x; \zeta) = \Phi_-(x; \zeta) + \int_{\Omega} \mathcal{K}_-(x, y; \zeta) \tilde{P}_-(y; \zeta) dy, \quad (99)$$

where $\Phi_-(x; \zeta) = \Phi(x; \zeta)e^{-2i\zeta x} \in \mathbb{C}^2$ and the Volterra kernel $\mathcal{K}_-(x, y; \zeta) = \operatorname{diag}(\mathcal{K}_1^{(-)}, \mathcal{K}_2^{(-)}) \in \mathbb{C}^{2 \times 2}$ is such that

$$\begin{aligned} \mathcal{K}_1^{(-)}(x, y; \zeta) &= r(y) \int_y^x q(z) e^{-2i\zeta(x-z)} dz, \\ \mathcal{K}_2^{(-)}(x, y; \zeta) &= q(y) \int_y^x r(z) e^{-2i\zeta(z-y)} dz, \end{aligned} \quad (100)$$

with $\mathcal{K}_-(x, y; \zeta) = 0$ for $y > x$. Using the approach outlined above, it is possible to show that, for $\zeta \in \mathbb{C}_-$, $\|\tilde{P}_-(x; \zeta)\|_{L^\infty(\Omega)} \leq \cosh(\kappa) \|\Phi_-(x; \zeta)\|_{L^\infty(\Omega)}$. The result for the case $\zeta \in \mathbb{C}_-$ in (95) then follows from the observation that $\|\Phi_-(x; \zeta)\|_{L^\infty(\Omega)} \leq \|\mathbf{D}\| e^{2\operatorname{Im}(\zeta)L_1}$ for $\zeta \in \mathbb{C}_-$. \square

Theorem 6.2. *Let $q \in \operatorname{BV}$ with support in $\Omega = [L_1, L_2]$ such that $q(x) = 0$ for $x \in \partial\Omega$. Then, there exists a constant $C > 0$ independent of $\zeta \in \mathbb{C}$ such that the estimate*

$$\|\tilde{P}(x; \zeta)\|_{L^\infty(\Omega)} \leq \frac{C}{1 + |\zeta|} \times \begin{cases} 1 & \zeta \in \bar{\mathbb{C}}_+, \\ e^{-2\operatorname{Im}(\zeta)(L_2 - L_1)} & \zeta \in \mathbb{C}_-, \end{cases} \quad (101)$$

holds.

Proof. Consider the first term on the RHS of (92): Integrating by parts, we obtain

$$\begin{aligned} \Phi_1(x; \zeta) &= \int_{L_1}^x q(z) e^{2i\zeta z} dz \int_{L_1}^z r(y) e^{-2i\zeta y} dy \\ &= \frac{-1}{2i\zeta} \int_{L_1}^x r(z) q(z) dz \\ &\quad + \frac{1}{2i\zeta} \int_{L_1}^x q(z) e^{2i\zeta z} dz \int_{L_1}^z [\partial_y r(y)] e^{-2i\zeta y} dy, \end{aligned}$$

so that

$$\begin{aligned} 2(1 + |\zeta|)|\Phi_1| &\leq \int_{L_1}^x |q(z)|^2 dz \\ &\quad + \int_{L_1}^x |q(z)| e^{-2\operatorname{Im}(\zeta)z} dz \int_{L_1}^z [2|r(y)| + |\partial_y r(y)|] e^{2\operatorname{Im}(\zeta)y} dy. \end{aligned}$$

Setting $2D_1 = \|q\|_2^2 + \|q\|_1^2 + \|q\|_1 \|q^{(1)}\|_1$, we have

$$|\Phi_1(x; \zeta)| \leq \frac{D_1}{1 + |\zeta|} \times \begin{cases} 1, & \zeta \in \bar{\mathbb{C}}_+, \\ e^{-2\operatorname{Im}(\zeta)(L_2 - L_1)}, & \zeta \in \mathbb{C}_-. \end{cases}$$

Again, integrating by parts, we have

$$\begin{aligned} \Phi_2(x; \zeta) &= \int_{L_1}^x r(y) e^{2i\zeta(x-y)} dy \\ &= \frac{-1}{2i\zeta} r(x) + \frac{1}{2i\zeta} \int_{L_1}^x [\partial_y r(y)] e^{2i\zeta(x-y)} dy, \end{aligned}$$

so that

$$2(1 + |\zeta|)|\Phi_2| \leq |r(x)| + \int_{L_1}^x [2|r(y)| + |\partial_y r(y)|] e^{-2\operatorname{Im}(\zeta)(x-y)} dy.$$

Putting $2D_2 = \|q\|_\infty + 2\|q\|_1 + \|q^{(1)}\|_1$, then

$$|\Phi_2(x; \zeta)| \leq \frac{D_2}{1 + |\zeta|} \times \begin{cases} 1, & \zeta \in \bar{\mathbb{C}}_+, \\ e^{-2\operatorname{Im}(\zeta)(L_2 - L_1)}, & \zeta \in \mathbb{C}_-. \end{cases}$$

Now, proceeding as in the proof of Theorem 6.1, we conclude that the estimate (101) holds with $C = \|\mathbf{D}\| \cosh(\|q\|_1)$ where $\mathbf{D} = (D_1, D_2)^\top$. \square

Finally, let us extend the preceding two results to the one-sided potentials:

Theorem 6.3. Let $q \in E_d(J)$ for some $d > 0$ with $J = (-\infty, L]$. Let $\kappa_1 = \|q\|_{L^1(J)}$ and $\kappa_\infty > 0$ be the constant such that $|q(x)| \leq \kappa_\infty e^{-2d|x|}$. Then, for every $\mu \in (0, d)$, the estimate

$$\|\tilde{P}(x; \zeta)\|_{L^\infty(J)} \leq \begin{cases} C_1, & \zeta \in \overline{\mathbb{C}}_+, \\ \frac{C_2 e^{-2\operatorname{Im}(\zeta)L}}{[d^2 - (\operatorname{Im} \zeta)^2]}, & \zeta \in \mathbb{S}_-(\mu). \end{cases} \quad (102)$$

holds with constants C_1 and C_2 given by

$$C_1 = \|\mathbf{D}\| \cosh \kappa_1, \quad C_2 = \|\mathbf{E}\| \cosh \kappa_1,$$

where $\mathbf{D} = (\kappa_1^2/2, \kappa_1)^\top$ and $\mathbf{E} = (\kappa_\infty^2, d\kappa_\infty)^\top$.

In addition, if $\partial_x q \in E_d(J)$, then there exists a constant $C > 0$ independent of $\zeta \in \mathbb{C}$ such that the estimate

$$\|\tilde{P}(x; \zeta)\|_{L^\infty(J)} \leq \frac{C}{1 + |\zeta|}, \quad \zeta \in \overline{\mathbb{C}}_+, \quad (103)$$

holds.

6.1.1. Error due to domain-truncation

For the purpose of numerical solution of the ZS-problem posed on a unbounded domain, it is mandatory to choose a computational domain that is bounded. This requires truncation of the original unbounded domain to a bounded domain, say, $[-L_-, L_+]$ where $L_-, L_+ > 0$. Let us observe here that the estimates obtained in Theorem 6.3 can be improved slightly in order to give us a better control of the domain truncation error. Let \mathcal{K}_j denote the Volterra integral operator corresponding to the kernel \mathcal{K}_j for $j = 1, 2$ defined in (94). Set the domain to be $J = (-\infty, -L_-]$ and assume the conditions stated in the first part of Theorem 6.3 to be true. Then it can be shown that, for $\zeta \in \overline{\mathbb{C}}_+$, we have

$$\begin{aligned} \|\tilde{P}_1\|_{L^\infty(J)} &= \|\Phi_1 + \mathcal{K}_1[\Phi_1]\|_{L^\infty(J)} \leq [\cosh(\kappa_1) - 1], \\ \|\tilde{P}_2\|_{L^\infty(J)} &= \|\Phi_2 + \mathcal{K}_2[\Phi_2]\|_{L^\infty(J)} \leq \sinh \kappa_1. \end{aligned} \quad (104)$$

Now in any numerical scheme, one would take $(1, 0)^\top$ as the initial value for the Jost solution $\phi(x; \zeta)e^{i\zeta x}$ at $x = -L_-$. This step introduces an error which is bounded by $\max(\|\tilde{P}_1\|_{L^\infty(J)}, \|\tilde{P}_2\|_{L^\infty(J)})$. Let $L_- > 0$ be a free parameter and assume $q \in E_d(\mathbb{R})$. Now, if we require the maximum error to be equal to $\epsilon > 0$, then it suffices to have $\sinh[\|q\chi_{(-\infty, -L_-)}\|_{L^1}] = \epsilon$ which works out to be

$$\|q\chi_{(-\infty, -L_-)}\|_{L^1} \leq \log[\epsilon + \sqrt{1 + \epsilon^2}]. \quad (105)$$

Similar result can be obtained for truncation from the right side by using the property in Remark 2.1.

6.2. Discretization in the spectral domain

Let the grid points be as defined in Sec. 3.1. In this section we discuss of the stability and convergence properties of the numerical methods developed in Sec. 3.1. To this end, we closely follow the terminology introduced in [32] adapted to the problem at hand.

The general form of a one-step method for (17) can be stated as

$$\tilde{v}_{n+1} = [\sigma_0 + h\Lambda(x_n; h)]\tilde{v}_n, \quad (106)$$

where dependence on the spectral parameter, ζ , is suppressed. We keep the spectral parameter fixed in the following discussion or allow it to vary over any compact domain of \mathbb{C} . The function $\Lambda(x_n; h)$ is referred to as the *update function* of the one-step method. The truncation error of this method is defined as

$$\mathbf{T}(x, \mathbf{y}; h) = \frac{1}{h}[\tilde{v}(x+h) - \tilde{v}(x)] - \Lambda(x; h)\tilde{v}(x), \quad (107)$$

with $\tilde{v}(x) = \mathbf{y}$. A method is called *consistent* if $\lim_{h \rightarrow 0} \mathbf{T}(x, \mathbf{y}; h) = 0$. The necessary and sufficient condition for consistency in this case is $\Lambda(x; 0) = \tilde{U}(x)$. A method is said to have an order p if, for some vector norm $\|\cdot\|$, $\|\mathbf{T}(x, \mathbf{y}; h)\| \leq Ch^p$ holds uniformly over $\Omega \times \Gamma$ where $\Gamma \subset \mathbb{C}^2$ is a compact set and C is independent of x, \mathbf{y} and h . Let $\mathbf{x}_h = (x_n)_{0 \leq n \leq N}$ represent the grid. Let us introduce a vector-valued grid-function as $\mathbf{u} = \{\mathbf{u}_n\}_{n=0}^N$ where $\mathbf{u}_n \in \mathbb{C}^2$ such that value of \mathbf{u} at x_n is \mathbf{u}_n . The class of such solutions is denoted by $\mathbf{G}(\mathbf{x}_h)$. Define the infinity-norm of any grid-function as

$$\|\mathbf{u}\|_\infty = \max_{0 \leq n \leq N} \|\mathbf{u}_n\|. \quad (108)$$

In order to introduce the concept of stability of the one-step method, let us define the residue operator as

$$(\mathcal{R}_h \mathbf{u})_n = \frac{1}{h}[\mathbf{u}_{n+1} - \mathbf{u}_n] - \Lambda(x_n; h)\mathbf{u}_n \quad (109)$$

for any grid-function $\mathbf{u} \in \mathbf{G}(\mathbf{x}_h)$ and $n < N$ (we set $(\mathcal{R}_h \mathbf{u})_N = (\mathcal{R}_h \mathbf{u})_{N-1}$). A method is said to be *stable* if there exists a constant C_0 for $h_0 > 0$ such that for any two arbitrary grid-functions, $\mathbf{u}, \mathbf{w} \in \mathbf{G}(\mathbf{x}_h)$, we have

$$\|\mathbf{u} - \mathbf{w}\|_\infty \leq C_0(\|\mathbf{u}_0 - \mathbf{w}_0\| + \|\mathcal{R}_h \mathbf{u} - \mathcal{R}_h \mathbf{w}\|_\infty), \quad (110)$$

for all $h \leq h_0$.

Remark 6.1. The intuition behind this definition, as explained in [32] is as follows: if $\mathbf{u} \in \mathbf{G}(\mathbf{x}_h)$ denotes the grid-function obtained by the one-step method using infinite-precision arithmetic (so that $\mathcal{R}_h \mathbf{u} = 0$) and if $\mathbf{w} \in \mathbf{G}(\mathbf{x}_h)$ denotes the grid-function obtained using finite-precision arithmetic (initial conditions being the same, i.e., $\mathbf{u}_0 = \mathbf{w}_0$), then any stable method must yield $\|\mathbf{u} - \mathbf{w}\|_\infty = \mathcal{O}(\epsilon)$ where ϵ is the machine precision in the latter case.

Let $q \in \mathbf{BV}(\Omega)$, then there exist a constants C and $h_0 > 0$ independent of x and h such that $\|\Lambda(x; h)\| < C$ for all $h \in [0, h_0]$, (where $\|\cdot\|$ is the induced matrix norm). This shows that for any two arbitrary vectors, $\mathbf{u}, \mathbf{w} \in \mathbb{C}^2$ and $h \in [0, h_0]$, the Lipschitz condition,

$$\|\Lambda(x; h)\mathbf{u} - \Lambda(x; h)\mathbf{w}\| \leq \|\Lambda(x; h)\| \|\mathbf{u} - \mathbf{w}\| \leq C\|\mathbf{u} - \mathbf{w}\|,$$

is satisfied. Therefore, the stability of the one-step method (106) easily follows from [32, Theorem 5.3.1]. Further, for any grid-function $\mathbf{u} \in \mathbf{G}(\mathbf{x}_h)$, we have

$$\|\mathbf{u}_n\| \leq (1 + Ch) \|\mathbf{u}_{n-1}\| \leq (1 + Ch)^n \|\mathbf{u}_0\|.$$

Then using the inequality $(1 + Ch)^N < e^{ChN}$, it follows that $\|\mathbf{u}\|_\infty \leq e^{C(L_2 - L_1)} \|\mathbf{u}_0\|$ which also guarantees the boundedness of the numerical solution when computed using infinite precision.

Finally, consistency and stability for any given one-step method imply global convergence. Moreover, if $\tilde{\mathbf{v}} = \{\tilde{\mathbf{v}}(x_n)\}_{n=0}^N$, denotes the grid-function determined by the exact solution and $\mathbf{u} \in \mathbf{G}(\mathbf{x}_h)$ be any grid-function obtained using the one-step method (106) with initial condition $\mathbf{u}_0 = \tilde{\mathbf{v}}(x_0)$, then $\|\mathbf{u} - \tilde{\mathbf{v}}\|_\infty = \mathcal{O}(h^p)$ where p is the order of the one-step method [32, Theorem 5.3.2].

6.2.1. Implicit Euler method

Continuing from Sec. 3.1.2, we have

$$\tilde{\mathbf{v}}_{n+1} = (\sigma_0 - h\tilde{U}_{n+1})^{-1} \tilde{\mathbf{v}}_n,$$

which determines the update function to be

$$\Lambda(x_n; h) = \frac{-h(\det \tilde{U}_{n+1})\sigma_0 + \tilde{U}_{n+1}}{[1 + (\det \tilde{U}_{n+1})h^2]}.$$

It is easy to verify that $\Lambda(x_n; 0) = \tilde{U}_n$, therefore, the method is consistent. Using the Taylor's theorem

$$\mathbf{T}(x, \mathbf{y}; h) = (\sigma_0 - h\tilde{U}(x + h))^{-1} \left[-\frac{h}{2} \partial_x^2 \tilde{\mathbf{v}}(x') \right], \quad \tilde{\mathbf{v}}(x) = \mathbf{y},$$

where $x \leq x' \leq x + h$. Assuming that $q(x) \in \mathbf{C}_0^1(\Omega)$, we have $\partial_x^2 \tilde{\mathbf{v}} = e^{i\sigma_3 \zeta x} (\partial_x U + U^2 + 2i\zeta[\sigma_3, U])\mathbf{v}$, therefore, the order of the method is $p = 1$. If the Jost solution under consideration is $\mathbf{v} = \boldsymbol{\phi}$ then $\|e^{i\zeta x} \boldsymbol{\phi}\|$ is bounded for $\zeta \in \overline{\mathbb{C}}_+$ (see Theorem 6.1), consequently, the truncation error coefficient to the leading order in ζ is $|\zeta| h e^{2\text{Im}(\zeta)x} \|[\sigma_3, U]\|$. Evidently, the method is stable which together with its consistency imply convergence (with order $p = 1$).

6.2.2. Trapezoidal rule

Continuing from Sec. 3.1.3, we have

$$\tilde{\mathbf{v}}_{n+1} = \left(\sigma_0 - \frac{h}{2} \tilde{U}_{n+1} \right)^{-1} \left(\sigma_0 + \frac{h}{2} \tilde{U}_n \right) \tilde{\mathbf{v}}_n \quad (111)$$

so that the update function is given by

$$\Lambda(x_n; h) = \frac{h(\tilde{U}_{n+1} \tilde{U}_n - \sigma_0 \det \tilde{U}_{n+1}) + 2(\tilde{U}_n + \tilde{U}_{n+1})}{[4 + (\det \tilde{U}_{n+1})h^2]}.$$

Again, it is easy to verify that $\Lambda(x_n; 0) = \tilde{U}_n$, therefore, the method is consistent. Using the Taylor's theorem

$$\mathbf{T}(x, \mathbf{y}; h) = \left[-\frac{h^2}{12} \partial_x^3 \tilde{\mathbf{v}}(x) \right] + \mathcal{O}(h^3), \quad \tilde{\mathbf{v}}(x) = \mathbf{y}.$$

Assuming that $q(x) \in \mathbf{C}_0^2(\Omega)$, we have

$$\partial_x^3 \tilde{\mathbf{v}} = -4\zeta^2 e^{i\sigma_3 \zeta x} ([\sigma_3, [\sigma_3, U]] + \mathcal{O}(1/\zeta)) \mathbf{v},$$

therefore, the order of the method is $p = 2$. Again, if the Jost solution under consideration is $\mathbf{v} = \boldsymbol{\phi}$ then $\|e^{i\zeta x} \boldsymbol{\phi}\|$ is bounded for $\zeta \in \overline{\mathbb{C}}_+$ (see Theorem 6.1), consequently, the truncation coefficient to the leading order in ζ is $|\zeta|^2 h^2 e^{2\text{Im}(\zeta)x} \|[\sigma_3, [\sigma_3, U]]\|/3$. Evidently, the method is stable which together with its consistency imply convergence (with order $p = 2$).

6.2.3. Split-Magnus method

For the convergence analysis of the split-Magnus method described in Sec. 4.2, let us observe that an equivalent form of the integrator is

$$\sqrt{(\sigma_0 - h\tilde{U}_{n+1/2})} \tilde{\mathbf{v}}_{n+1} = \sqrt{(\sigma_0 + h\tilde{U}_{n+1/2})} \tilde{\mathbf{v}}.$$

Using Taylor's theorem for matrix functions, we have

$$\mathbf{T}(x, \mathbf{y}; h) = \frac{h^2}{24} (\partial_x^3 \tilde{\mathbf{v}} - 3\tilde{U} \partial_x^2 \tilde{\mathbf{v}} - 3\tilde{U}^2 \partial_x \tilde{\mathbf{v}}) + \mathcal{O}(h^3).$$

Assuming U is twice differentiable on $[x, x + h]$, we conclude that the order of the method is $p = 2$. Further, this one-step method is consistent and stable, therefore, also convergent for fixed ζ (or ζ varying in a compact domain). The truncation error coefficient to the leading order in ζ is $|\zeta|^2 h^2 e^{2\text{Im}(\zeta)x} \|[\sigma_3, [\sigma_3, U]]\|/6$. This value can be seen to be twice as small as that of the trapezoidal rule. Let us note that it is not seem straightforward to determine which of the two one-step methods has smaller total truncation error coefficient (for fixed ζ); however, the trapezoidal rule appears to exhibit smaller total truncation error in the numerical tests.

6.3. Computation of norming constants

In Sec. 3.2.1, it was stated that the computation of norming constants from the discrete b -coefficients $b_N(z^2)$ is ill-conditioned. This can be attributed to the nature of the truncation error coefficients in the underlying one-step method for complex values of ζ . It is evidenced by the presence of a factor of the form $\exp[2\text{Im}(\zeta)x]$ in the truncation error coefficient which tends to grow for $x > 0$ (see Sec. 6.2). Therefore, it is better to “truncate” the scattering potential at the origin¹² and solve the corresponding one-sided ZS-problems as discussed in Sec. 3.2.1. Finally, let us note that there are other discretization schemes such as the *exponential time-differencing* (ETD) scheme [31] which may alleviate these problems; however, it may come at a cost of increased operational complexity. These ideas will be explored in a future publication.

6.4. Lubich’s method

Starting from the functions $a(\zeta)$ and $\check{b}(\zeta)$ analytic in the upper-half of the complex plane, Lubich’s construction as described in Sec. 3.6 allows us to compute the polynomials associated with the discrete scattering coefficients $\mathbf{P}_N(z^2) = \{\mathbf{P}(z^2)\}_N$. Note that, in the preceding section, we discussed the necessary and sufficient condition for discrete inverse scattering with polynomials (which can be seen as a finite-support sequence of coefficients). However, Lubich’s method yields infinite series that needs to be truncated. Therefore, the compatibility of Lubich’s construction with the layer-peeling algorithm cannot be

studied within the framework of finite-support sequences. However, it is possible to determine if $\mathbf{P}(z^2)$ can be associated to a Jost solution prior to truncation of the series. If the coefficients of the series decay sufficiently fast, the truncation introduces a negligible error so that the layer-peeling criteria can be satisfied to a sufficient degree of accuracy.

Let us first consider the case of compactly supported potential. Define the vector $\mathbf{P}(z^2) = (P_1, P_2)^\top$ as

$$P_1(z^2) = a\left(\frac{i\delta(z^2)}{2h}\right), \quad P_2(z^2) = \check{b}\left(\frac{i\delta(z^2)}{2h}\right),$$

which can be expanded into a convergent Taylor series as in Sec. 3.6 on account of the analyticity of the scattering coefficients over whole of the complex plane. Further note that

$$P_1^*(1/z^{*2}) = a^*\left(\frac{i\delta(1/z^{*2})}{2h}\right), \quad P_2^*(1/z^{*2}) = \check{b}^*\left(\frac{i\delta(1/z^{*2})}{2h}\right).$$

Therefore, for $z \in \mathbb{T}$, we have¹³

$$\mathbf{P}(z^2) \cdot \mathbf{P}^*(z^2) = (aa^* + \check{b}\check{b}^*) \circ \left(\frac{i\delta(z^2)}{2h}\right) = 1.$$

Note that here we have used the fact that $a(\zeta)\bar{a}(\zeta) + b(\zeta)\bar{b}(\zeta) = 1$ for all $\zeta \in \mathbb{C}$, however, such a relationship would not hold if we relax the requirement of compact support of the potential.

Let $f(\zeta)$ denote either $a(\zeta) - 1$ or $\check{b}(\zeta)$. When $f(\zeta)$ is analytic in the upper-half of the complex plane, then on any compact domain $\Gamma \subset \overline{\mathbb{C}}_+$ the functions can be regarded as Lipschitz continuous. Observing that $\delta(e^{-h})/h = 1 + \mathcal{O}(h^p)$ where $p = 1$ for BDF1 and $p = 2$ for TR, we have

$$\left|\zeta - \frac{i}{2h}\delta(e^{2i\zeta h})\right| \leq Ch^p, \quad (112)$$

on any compact domain of $\Gamma \subset \overline{\mathbb{C}}_+$ and $h \in [0, h_0]$ ($h_0 > 0$) where $C > 0$ depends only on Γ and h_0 . Therefore, using the estimate (112) and the Lipschitz continuity of $f(\zeta)$ one can assert that there exists a constant $C' > 0$ for a given Γ and h_0 such that [41]

$$\left|f(\zeta) - f\left(\frac{i\delta(e^{2i\zeta h})}{2h}\right)\right| \leq C'h^p.$$

¹²If the growth behavior of the potential is known before-hand, then it is possible to choose an optimal point of truncation.

¹³For sufficiently small h , it can be verified that $|P_{1,0}| \neq 0$. Other conditions pertaining to the specific discretization schemes can be explicitly verified using the results in Sec. 3.6.

Therefore, the Wronskian relationship, $|a(\xi)|^2 + |b(\xi)|^2 = 1$ for $\xi \in \mathbb{R}$ can only be satisfied upto $\mathcal{O}(h^p)$ on any bounded interval in \mathbb{R} .

Finally, as far as the truncation of the infinite series is concerned, let us note that for the kind problems considered in this article, Lubich's method is applied to rational functions with known poles in \mathbb{C}_- which makes it easy to determine the decay behavior of these coefficients using the method of partial-fractions (see Sec. 3.7).

6.5. Darboux transformation

In this section, we study convergence behavior of the Darboux transformation with numerically computed Jost solutions. Continuing from Sec. 2.3, let $(\zeta_k, b_k) \in \mathfrak{S}_K$ denote the discrete eigenvalue and the corresponding norming constant. Define the Vandermonde matrix

$$F = \{F_{jk}\}_{K \times K} = \{\zeta_j^k\}_{j=1,2,\dots,K, k=0,1,\dots,K-1},$$

the diagonal matrix $\Gamma = \text{diag}(\gamma_1, \gamma_2, \dots, \gamma_K)$ and the vectors

$$\mathbf{f} = \begin{pmatrix} \zeta_1^K \\ \zeta_2^K \\ \vdots \\ \zeta_K^K \end{pmatrix}, \quad \mathbf{g} = \Gamma \mathbf{f} = \begin{pmatrix} \zeta_1^K \gamma_1 \\ \zeta_2^K \gamma_2 \\ \vdots \\ \zeta_K^K \gamma_K \end{pmatrix}, \quad (113)$$

where

$$\gamma_k = \frac{\phi_2^{(0)}(0, 0; \zeta_k) - b_k \psi_2^{(0)}(0, 0; \zeta_k)}{\phi_1^{(0)}(0, 0; \zeta_k) - b_k \psi_1^{(0)}(0, 0; \zeta_k)}. \quad (114)$$

The unknown Darboux coefficients can be put into the vector form

$$\mathbf{D}_0 = \begin{pmatrix} d_0^{(0,K)} \\ d_0^{(1,K)} \\ \vdots \\ d_0^{(K-1,K)} \end{pmatrix}, \quad \mathbf{D}_1 = \begin{pmatrix} d_1^{(0,K)} \\ d_1^{(1,K)} \\ \vdots \\ d_1^{(K-1,K)} \end{pmatrix}, \quad (115)$$

then the linear system of equations (10) which determines the coefficients of the Darboux matrix can be written as

$$\underbrace{\begin{pmatrix} \mathbf{f} \\ \mathbf{g}^* \end{pmatrix}}_{\mathbf{w}} = \underbrace{\begin{pmatrix} F & \Gamma F \\ -\Gamma^* F^* & F^* \end{pmatrix}}_{\mathcal{W}} \underbrace{\begin{pmatrix} \mathbf{D}_0 \\ \mathbf{D}_1 \end{pmatrix}}_{\mathbf{D}}. \quad (116)$$

Note that the quantities \mathbf{f} and F are known exactly while Γ (and in turn \mathbf{g}) is determined only up to $\mathcal{O}(h^p)$, where

p is the order of convergence of the one-step method. Let $\|\cdot\|$ denote the Euclidean norm for vectors and the induced spectral norm for matrices. Define $\kappa(\mathcal{W}) = \|\mathcal{W}^{-1}\| \cdot \|\mathcal{W}\|$ to be the condition number of \mathcal{W} , then, under the assumption $\|\mathcal{W}^{-1}\| \cdot \|\Delta \mathcal{W}\| < 1$ (which can be satisfied for sufficiently small h), the standard perturbation theory [61, Chap. 11] yields the estimate

$$\frac{\|\Delta \mathbf{D}\|}{\|\mathbf{D}\|} \leq \frac{\kappa(\mathcal{W})}{1 - \kappa(\mathcal{W}) \frac{\|\Delta \mathcal{W}\|}{\|\mathcal{W}\|}} \left(\frac{\|\Delta \mathbf{w}\|}{\|\mathbf{w}\|} + \frac{\|\Delta \mathcal{W}\|}{\|\mathcal{W}\|} \right). \quad (117)$$

Given that the perturbations are of $\mathcal{O}(h^p)$, from above equation it follows that the coefficients of the Darboux matrix can be determined up to $\mathcal{O}(h^p)$.

In order to determine the convergence behavior of the fast Darboux transformation (FDT) algorithm as described in Sec. 3.8.1, we need to study the convergence of the corresponding Lubich coefficients. To this end, let us denote by $\widetilde{D}_K(\zeta, \mathfrak{S}_K)$ the approximation to the Darboux matrix $D_K(\zeta, \mathfrak{S}_K)$. Now, using the partial fraction expansion as in (42), we have

$$\begin{aligned} & \mu_K(\zeta) [\widetilde{D}_K(\zeta, \mathfrak{S}_K) - D_K(\zeta, \mathfrak{S}_K)] \\ &= \sum_{k=0}^K \frac{\text{Res}[\mu_K, \zeta_k^*]}{(\zeta - \zeta_k^*)} [\widetilde{D}_K(\zeta_k^*, \mathfrak{S}_K) - D_K(\zeta_k^*, \mathfrak{S}_K)]. \end{aligned} \quad (118)$$

In order to establish the relationship between the error in the Darboux matrix as stated above and the error in the coefficients of the Darboux matrix, we need the following lemma:

Lemma 6.4. *For a given discrete spectrum \mathfrak{S}_K where K is finite, the inequality*

$$\|\widetilde{D}_K(\zeta, \mathfrak{S}_K) - D_K(\zeta, \mathfrak{S}_K)\| \leq 2 \|\Delta \mathbf{D}\| G_K(|\zeta|^2),$$

holds for any $\zeta \in \mathbb{C}$ where

$$G_K(\xi) = \begin{cases} \sqrt{\frac{\xi^K - 1}{\xi - 1}}, & \xi \neq 1, \\ \sqrt{K}, & \xi = 1. \end{cases}$$

Proof. From the the definition of the Darboux matrix, we have

$$\|\widetilde{D}_K(\zeta, \mathfrak{S}_K) - D_K(\zeta, \mathfrak{S}_K)\| \leq \sum_{k=0}^{K-1} \|\widetilde{D}_k^{(K)} - \widetilde{D}_k^{(K)}\| |\zeta|^k,$$

for $\zeta \in \mathbb{C}$. Now, using the Cauchy-Schwartz inequality, we obtain

$$\sum_{k=0}^{K-1} \|\tilde{D}_k^{(K)} - \bar{D}_k^{(K)}\| |\zeta|^k \leq \sqrt{\sum_{k=0}^{K-1} \|\tilde{D}_k^{(K)} - \bar{D}_k^{(K)}\|^2} \sqrt{\sum_{k=0}^{K-1} |\zeta|^{2k}}.$$

Note that this inequality does not change on replacing the spectral norm ($\|\cdot\|$) with the Euclidean norm ($\|\cdot\|_E$) and it is easy to see

$$\sqrt{\sum_{k=0}^{K-1} \|\tilde{D}_k^{(K)} - \bar{D}_k^{(K)}\|_E^2} = 2\|\Delta\mathbf{D}\|,$$

which concludes the proof. \square

Let $\mathcal{D}_K(\tau, \mathfrak{S}_K)$ and $\tilde{\mathcal{D}}_K(\tau, \mathfrak{S}_K)$ denote the inverse Fourier-Laplace transform of $\mu_K(\zeta)D_K(\zeta, \mathfrak{S}_K) - \sigma_0$ and $\mu_K(\zeta)\tilde{D}_K(\zeta, \mathfrak{S}_K) - \sigma_0$, respectively; then, we have the following proposition for the rate of convergence:

Proposition 6.5. *Consider the discrete spectrum \mathfrak{S}_K with finite K . If $\|\Delta\mathbf{D}\| = \mathcal{O}(h^p)$ where p is order of the underlying one-step method, then*

$$\|\tilde{\mathcal{D}}_K(\tau, \mathfrak{S}_K) - \mathcal{D}_K(\tau, \mathfrak{S}_K)\| = \mathcal{O}(h^p).$$

Proof. Let the set of eigenvalues be \mathfrak{E}_K corresponding to \mathfrak{S}_K and define

$$R = 2 \max_{\zeta \in \mathfrak{E}_K} |\text{Res}[\mu_K, \zeta^*]| G_K(|\zeta|^2),$$

where G_K is as defined in the forgoing lemma. From (118) and the forgoing lemma, we have

$$\begin{aligned} & \|\tilde{\mathcal{D}}_K(\tau, \mathfrak{S}_K) - \mathcal{D}_K(\tau, \mathfrak{S}_K)\| \\ & \leq R\|\Delta\mathbf{D}\| \sum_{k=1}^K \left| \frac{1}{2\pi} \int_{-\infty+ic}^{\infty+ic} \frac{e^{-i\zeta\tau} d\zeta}{\zeta - \zeta_k^*} \right| \leq R\|\Delta\mathbf{D}\| \sum_{k=1}^K e^{-\eta_k\tau} \\ & \leq RK\|\Delta\mathbf{D}\|, \end{aligned}$$

where $\eta_k = \text{Im} \zeta_k > 0$. The result follows by setting $\|\Delta\mathbf{D}\| = \mathcal{O}(h^p)$. \square

Let the matrix-valued Lubich coefficients for $D_K(\zeta, \mathfrak{S}_K)$ and $\tilde{D}_K(\zeta, \mathfrak{S}_K)$ be defined as

$$\begin{aligned} \mu_K\left(\frac{i\delta(z^2)}{2h}\right) D_K\left(\frac{i\delta(z^2)}{2h}, \mathfrak{S}_K\right) &= \sum_{k=0}^{\infty} \Lambda_k(\mathfrak{S}_K; h) z^{2k}, \\ \mu_K\left(\frac{i\delta(z^2)}{2h}\right) \tilde{D}_K\left(\frac{i\delta(z^2)}{2h}, \mathfrak{S}_K\right) &= \sum_{k=0}^{\infty} \tilde{\Lambda}_k(\mathfrak{S}_K; h) z^{2k}, \end{aligned} \quad (119)$$

respectively. The zeroth Lubich coefficient is obtained by evaluating the Darboux matrix at $\zeta = i\delta(0)/2h$. Therefore,

$$\|\Lambda_0 - \tilde{\Lambda}_0\| \leq 2hR\|\Delta\mathbf{D}\| \sum_{k=1}^K \frac{1}{|i\delta(0) - 2h\zeta_k^*|},$$

leading to $\|\Lambda_0 - \tilde{\Lambda}_0\| = \mathcal{O}(h^{p+1})$. In view of [39, Theorem 4.1] and the forgoing proposition, it follows that

$$\|\Lambda_k - \tilde{\Lambda}_k\| = \mathcal{O}(h^{p+1}), \quad k \in \mathbb{Z}_+.$$

7. Numerical Tests

In this section, we present several numerical tests to demonstrate the performance of the numerical algorithms developed in this paper. For better numerical conditioning, we scale the scattering potential $q(x)$ of the ZS-problem by a suitable scaling parameter such that $\|q\|_{L^2}$ is unity or close to unity. Let us briefly review the effect of this scaling to (3): For some $\kappa > 0$, let $\tilde{U} = U/\kappa$, $y = \kappa x$ and $\lambda = \zeta/\kappa$ then

$$\begin{aligned} v_y(y/\kappa; \zeta) &= i(\zeta/\kappa)\sigma_3 v(y/\kappa; \zeta) + \tilde{U}(y/\kappa) v(y/\kappa; \zeta), \\ w_y &= -i\lambda\sigma_3 w + \tilde{U}(y) w, \end{aligned}$$

where $w(y; \lambda) = v(y/\kappa; \lambda\kappa)$.

For the sake of clarity, let us specify the acronyms used to denote the one-step methods considered in this article for testing: *implicit Euler method (BDF1)*, *trapezoidal rule (TR)*, *Magnus method with one-point Gauss quadrature (MG1)* and *split-Magnus method (SM)*. The main focus of this section is to study the dependence of the total numerical error on the free parameters of a given algorithm together with its total run-time. In particular, we have considered the test cases that test the performance of the new methods introduced in this article against the so called benchmarking methods (MG1 and SM) wherever possible. In all of the test cases described below, N represents the number of samples which is taken from the set $\mathfrak{N} = \{2^j, j = 10, 11, \dots, 20\}$.

7.1. Examples

Our test cases are derived from following examples for which the exact value of the quantities to be analyzed are known in a closed form or can be evaluated to the machine precision by a known method.

7.1.1. Multi-solitons

Define a sequence of angles for $J \in \mathbb{Z}_+$ by choosing $\Delta\theta = (\pi - 2\theta_0)/(J-1)$, $\theta_0 > 0$, and $\theta_j = \theta_0 + (j-1)\Delta\theta$, $j = 1, 2, \dots, J$ so that $\theta_j \in [\theta_0, \pi - \theta_0]$. Then the eigenvalues for our numerical experiment are chosen as

$$\zeta_{j+J(l-1)} = le^{i\theta_j}, \quad l = 1, 2, \dots, 8, \quad j = 1, 2, \dots, J. \quad (120)$$

The norming constants are chosen as

$$b_j = e^{i\pi(j-1)/(8J-1)}, \quad j = 1, 2, \dots, 8J. \quad (121)$$

Here we choose, $\theta_0 = \pi/3$ and $J = 4$. Then we consider a sequence of discrete spectra defined as

$$\mathfrak{S}_K = \{(\zeta_k, b_k), k = 1, 2, \dots, K\}, \quad K = 4, 8, \dots, 32. \quad (122)$$

Let \mathfrak{S}_K be the set of all the eigenvalues. The potential can be computed with machine precision using the CDT algorithm which is taken as the reference for error analysis in this case. For fixed K , the eigenvalues are scaled by the scaling parameter $\kappa = 2\sqrt{\sum_{k=0}^K \text{Im } \zeta_k}$. Let $\eta_{\min} = \min_{\zeta \in \mathfrak{S}_K} \text{Im } \zeta$, then the computational domain for this example is chosen as $[-L, L]$ where $L = 11\kappa/\eta_{\min}$.

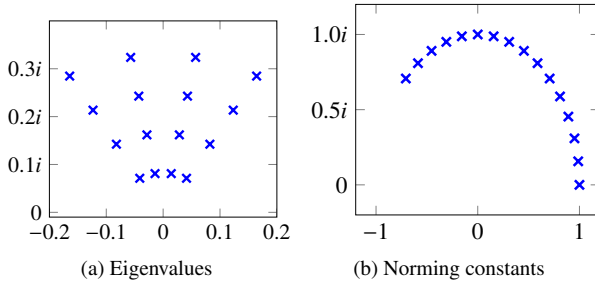


Figure 6: The figure shows the discrete spectrum, \mathfrak{S}_{16} , defined by (122).

7.1.2. Secant-hyperbolic potential

The exact solution of the ZS-problem for the secant-hyperbolic potential was first reported in [62]. We summarize the results required for our purpose as follows: Let the potential be written as

$$q(x) = A \operatorname{sech} x, \quad (123)$$

where A is referred to as the amplitude. The scattering coefficients are then given by

$$a(\zeta) = \frac{\Gamma\left(\frac{1}{2} - i\zeta\right)^2}{\Gamma\left(A + \frac{1}{2} - i\zeta\right)\Gamma\left(-A + \frac{1}{2} - i\zeta\right)}, \quad \zeta \in \overline{\mathbb{C}}_+,$$

$$b(\zeta) = -\sin \pi A \operatorname{sech} \pi \zeta, \quad |\operatorname{Im} \zeta| < 1/2.$$

The eigenvalues are given by

$$\zeta_k = i(\tilde{A} - k), \quad k = 1, 2, \dots, K,$$

where K is the largest integer smaller than $\tilde{A} = (A + 1/2)$. Putting $\tilde{A}_f = \tilde{A} - K$, the non-integer part of \tilde{A} , the a -coefficient can be written as a product of solitonic and radiative parts as follows

$$a(\zeta) = \underbrace{\left(\prod_{k=1}^K \frac{\zeta - \zeta_k}{\zeta - \zeta_k^*}\right)}_{a_S(\zeta)} \underbrace{\frac{\Gamma\left(\frac{1}{2} - i\zeta\right)^2}{\Gamma(\tilde{A}_f - i\zeta)\Gamma(1 - \tilde{A}_f - i\zeta)}}_{a_R(\zeta)}.$$

Note that $a_R(\zeta)$ belongs to a secant-hyperbolic potential with amplitude $A_R = \tilde{A}_f - 1/2 (> 0)$. The corresponding norming constants are given by $b_k = (-1)^k$.

This example allows one to test the CDT and the FDT algorithms where the seed potential can be taken as $q_0(x) = A_R \operatorname{sech}(x)$ and the sequence of discrete spectra to be added,

$$\mathfrak{S}_K = \{(\zeta_k, b_k), k = 1, 2, \dots, K\}, \quad K = 4, 8, \dots, 32, \quad (124)$$

where we set $A_R = 0.4$. Corresponding to \mathfrak{S}_K , the amplitude of the augmented secant-hyperbolic potential is given by $A = 0.4 + K$ and $\tilde{A} = 0.9 + K$. As in the last example, for fixed K , the eigenvalues are scaled by the scaling parameter given by $\kappa = 2\sqrt{\sum_{k=0}^K \text{Im } \zeta_k}$.

In order to choose the computational domain $[-L, L]$ for the sech-potential (123) with the aforementioned scaling, we can use the relation (105). Choosing $\eta_{\min} = \min_{\zeta \in \mathfrak{S}_K} \text{Im } \zeta$ where \mathfrak{S}_K is the set of all the eigenvalues and observing that

$$\|q\chi_{(-\infty, -L/\kappa]}\|_{L^1} = A \tan^{-1} \left[\frac{1}{\sinh(L/\kappa)} \right],$$

we have $L \approx [\eta_{\min} \log(2A/\epsilon)](\kappa/\eta_{\min})$ which rounds to $L \approx 30(\kappa/\eta_{\min})$ for $\epsilon = 10^{-12}$.

7.2. Test cases

7.2.1. Discrete spectrum

For multi-soliton potentials described in Sec. 7.1.1, we test the convergence behavior with regard to the discrete spectrum for various discretization schemes, namely, BDF1, TR, SM and MG1. For the convergence behavior of the numerically computed norming constants, we assume that the eigenvalues are known exactly. The error in the norming constants is quantified by

$$e_{\text{rel}} = \sqrt{\frac{\sum_{k=1}^K |b_k^{(\text{num.})} - b_k|^2}{\sum_{k=1}^K |b_k|^2}}. \quad (125)$$

For the convergence behavior with regard to the eigenvalues, we compute $a^{(\text{num.})}(\zeta_k)$ where the a -coefficient is computed numerically. The error is then quantified by

$$e_{\text{rel}} = \lim_{\eta \rightarrow \infty} \sqrt{\frac{1}{K} \sum_{k=1}^K \left| \frac{a^{(\text{num.})}(\zeta_k)}{a^{(\text{num.})}(i\eta)} \right|^2}. \quad (126)$$

For MG1, the limit is evaluated by setting $\eta = 100$. For others $\lim_{\eta \rightarrow \infty} a(i\eta) = P_{1,0}^{(N)}$. Except for MG1, all other schemes are implemented using the fast forward scattering algorithm (see Sec. 3.5.1). The computation of the norming constant is discussed in Sec. 3.2.1 and Sec. 4.

7.2.2. Multi-soliton potential

In this test case, we carry out the convergence analysis and a comparison of run-time (per sample) of different variants of the FDT algorithm for multi-solitons as described in Sec. 7.1.1. Note that the CDT algorithm in this case gives the exact potential which allows us to compute the total numerical error for the FDT algorithm for arbitrary discrete spectra. The error is quantified by

$$e_{\text{rel}} = \frac{\|q^{(\text{num.})} - q\|_{L^2}}{\|q\|_{L^2}}, \quad (127)$$

where the integrals are evaluated numerically using the trapezoidal rule.

The different variants of the FDT algorithm are described as follows: any one-step method for the ZS-problem can be combined with any one-step method for

the Lubich coefficients to obtain the FDT algorithm. In particular the relevant combinations are: BDF1-BDF1, BDF1-TR and TR-TR. We also consider the partial-fraction variant of the TR-TR combination which is labeled as TR-TR-PF. Note that the combination of a first order method for the ZS-problem with a second order method for the Lubich coefficients or vice versa should lead to a first order FDT algorithm. A second order method for the ZS-problem must be combined with a second order method or higher for the Lubich coefficients in order to obtain a second order FDT algorithm.

Parameters for the Lubich method are as follows: $M = 8N$ and $N_{\text{th}} = N/8$ (for the PF-variant). For the Cauchy integral, the radius of the circular contour is $\varrho = \exp[-8/(N/2 - 1)]$.

7.2.3. General Darboux transformation

In this test case, we carry out the convergence analysis and a comparison of run-time (per sample) of different variants of the CDT/FDT algorithm for the secant-hyperbolic potential as described in Sec. 7.1.2. Note that, in the case of the secant-hyperbolic potential, the soliton-free seed potential as well as the augmented potential can be stated in a closed form.

The variants of the CDT/FDT algorithm are determined by the underlying one-step method. Unlike in the last test case (Sec. 7.2.2), Lubich method uses the same one-step method as that of the ZS-problem. The total numerical error is quantified by (127). Parameters for the Lubich method are the same as in the last test case.

7.3. Results and discussion

7.3.1. Discrete spectrum

For a given multi-soliton, this test case was designed to assess the performance of the discretization schemes, namely, BDF1, TR, SM and MG1 in the determination of the discrete spectrum. The results are plotted in Fig. 7 where it can be easily seen that all the methods considered show convergence at a rate that is determined by the underlying one-step method. However, the rate of convergence of BDF1 with regard to discrete eigenvalues seems to be better than expected as evident from the plots in the bottom row of Fig 7. The overall accuracy of MG1 is evidently superior to that of others while TR turns out to be a close second.

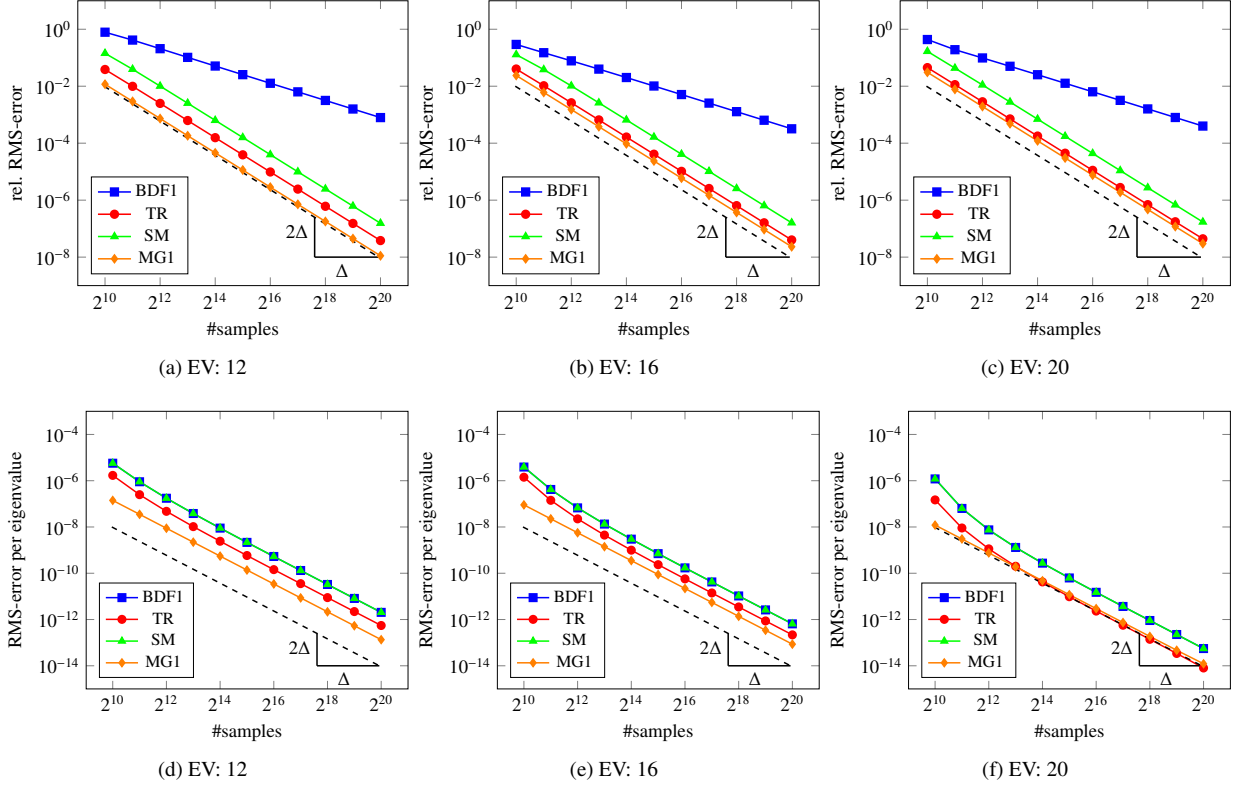


Figure 7: The figure depicts the convergence analysis for the norming constants (top row) and the discrete eigenvalues (bottom row). The numerical test (as described in Sec. 7.2.1) is carried out for fixed number of eigenvalues (EV).

7.3.2. Multi-soliton potential

This test case was designed to study the convergence and run-time behavior of different variants of the FDT algorithm for multi-solitons. The results for fixed number of eigenvalues and varying number of samples is shown in Fig. 8. The second order of convergence of the schemes BDF1-TR, TR-TR and TR-TR-PF can be identified from the plots in the top row of Fig. 8. The scheme BDF1-TR shows better rate of convergence than expected.

The run-time behavior of CDT for fixed number of eigenvalues is clearly superior to all of the method as evident from Fig. 8 (bottom row). The scheme TR-PF however becomes very competitive with the CDT algorithm.

The error and the run-time (per sample) as a function of the number of eigenvalues keeping the number of samples fixed is shown in Fig. 9. Here, the FDT algorithm

outperforms the CDT algorithm with TR-TR-PF variant being the fastest as evident from the plots in the top row of Fig. 9. It is interesting to note that the error as a function of number of eigenvalues as shown in plots at the bottom row of Fig. 9 exhibits exponentially increasing behavior. This puts an upper limit to the number of eigenvalues that can be handled with the FDT algorithm within a given precision.

7.3.3. General Darboux transformation

This test case was designed to study the convergence and run-time behavior of different variants of the CDT/FDT algorithm for a soliton-free seed potential. The results for fixed number of eigenvalues (that are meant to be added) and varying number of samples is shown in Fig. 11. The second order of convergence of the TR vari-

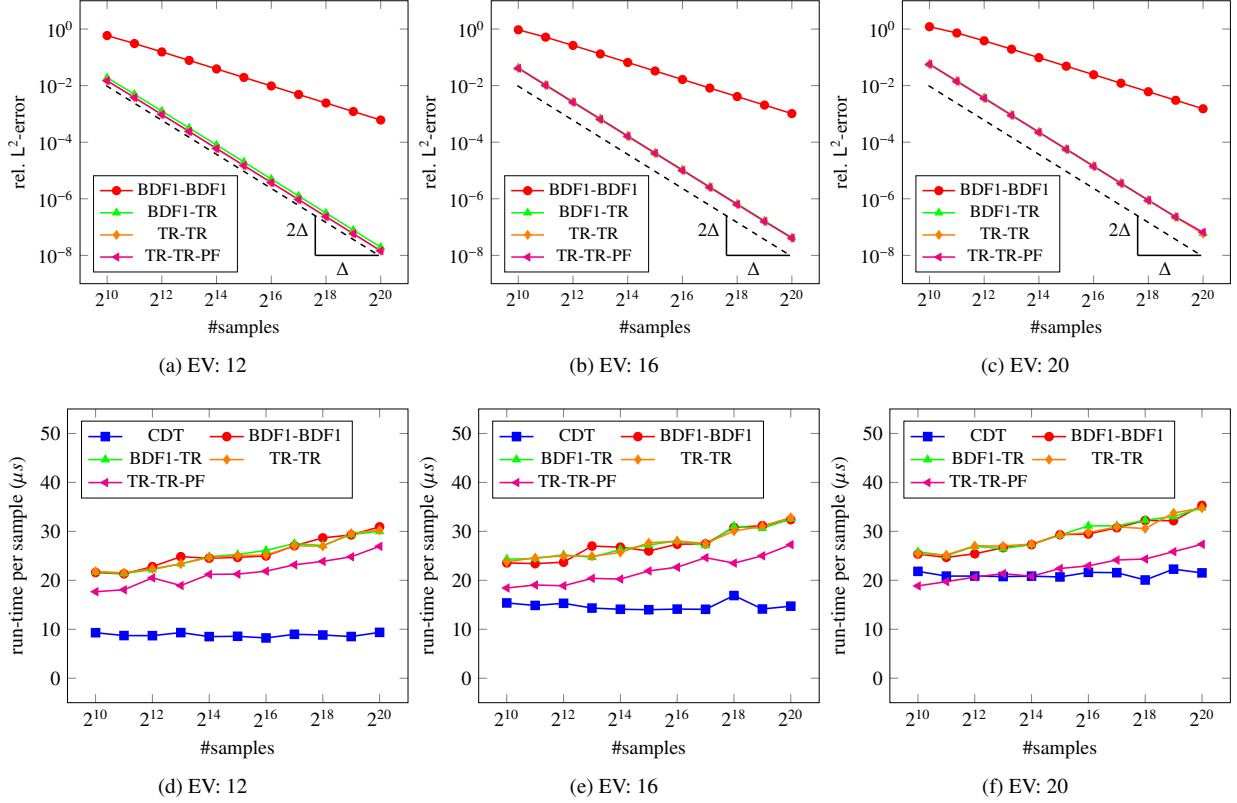


Figure 8: The figure depicts the convergence analysis (top row) and the run-time behavior (bottom row) for multi-solitons. The numerical test (as described in Sec. 7.2.2) is carried out with fixed number of eigenvalues (EV).

ant of the CDT/FDT algorithm can be identified from the plots in the top row of Fig. 11. However, the TR variant of the CDT algorithm performs not only worse as compared to that of the FDT algorithm but it also becomes unstable with increasing number of eigenvalues. Further, unlike the CDT algorithm, the BDF1 and TR variant of FDT shows convergence (at an expected rate) with increasing number of samples.

The run-time behavior of CDT for fixed number of eigenvalues is clearly superior to that of FDT as evident from Fig. 12 (bottom row). The scheme TR-PF however becomes very competitive to the CDT-TR variant. Note that CDT in this case is reliable *only* for small number of eigenvalues.

The error and the run-time (per sample) as a function of the number of eigenvalues keeping the number of sam-

ples fixed is shown in Fig. 12. Here, the FDT algorithm outperforms the CDT algorithm with TR-TR-PF variant being the fastest as evident from the plots in the top row of Fig. 12. As in the last test case, the error as a function of number of eigenvalues as shown in plots at the bottom row of Fig. 12 exhibits exponentially increasing behavior. Note that FDT not only outperforms CDT in terms of accuracy, it also exhibits superior numerical conditioning with increasing number of eigenvalues as evident from Fig. 12 (bottom row).

Remark 7.1. For the CDT algorithm, the root cause of the numerical instability witnessed in the test cases above can be traced back to the truncation error coefficients of the underlying one-step method for complex values of ζ . In Sec. 6.2, it is shown that, for $\zeta \in \mathbb{C}_+$, the evaluation of

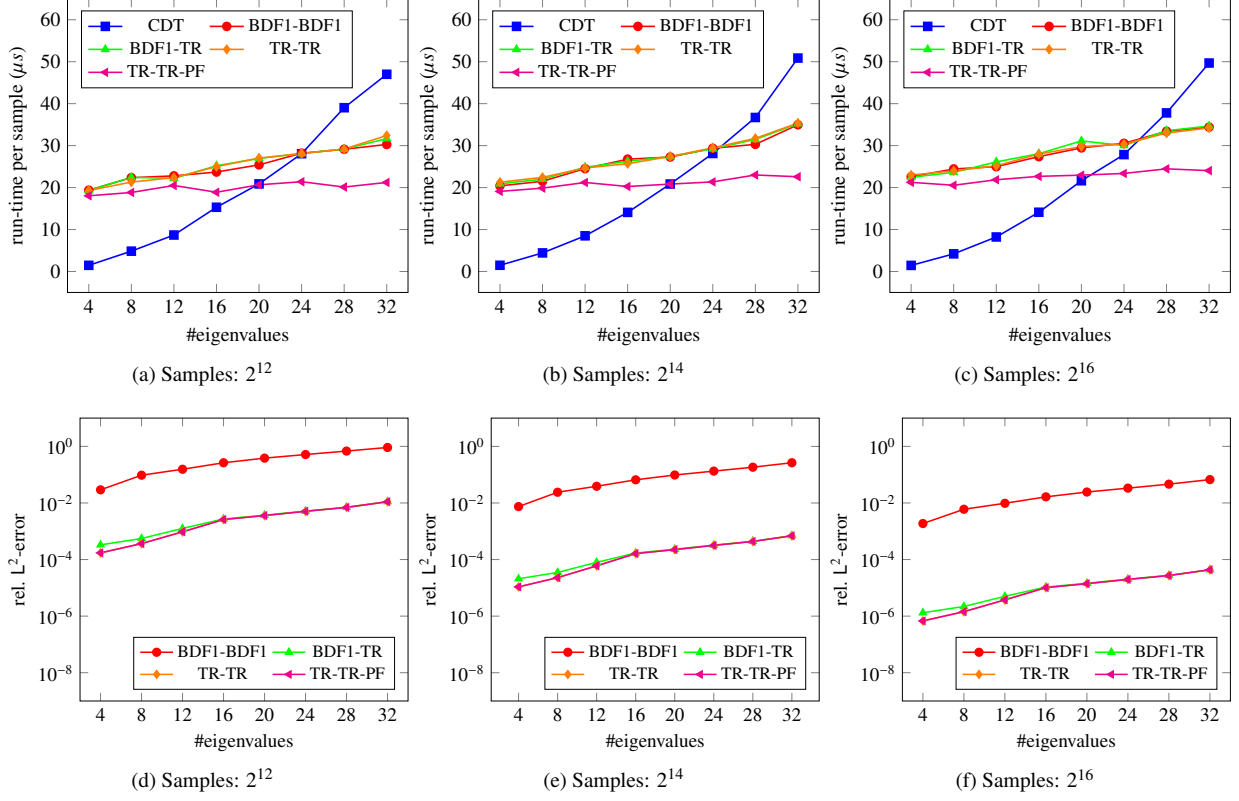


Figure 9: The figure depicts the run-time (top row) and the relative numerical error (bottom row) for multi-solitons as a function of number of eigenvalues. The numerical test (as described in Sec. 7.2.2) is carried out with fixed number of samples.

the Jost function ϕ_n may suffer from exponential amplification of the truncation error for $x > 0$. This observation also implies ψ_n may become very inaccurate for $x < 0$. Therefore, the failure of CDT can be attributed to inaccuracy of one of the Jost solutions for a given x . The FDT algorithm on the other hand requires the aforementioned Jost solutions to be computed at the point $x = 0$ and nowhere else. Therefore, FDT circumvents the problem that causes CDT to fail. Note that there is nothing unique about the point $x = 0$ but one can rely on the rule of thumb that the origin should be placed in the middle of an effective support of the potential.

8. Conclusion

To conclude, we have presented a systematic approach to discretize the non-Hermitian Zakharov-Shabat (ZS) problem that provides a favorable framework for the fast forward and inverse $SU(2)$ -nonlinear Fourier transformation (NFT). As a first step towards developing a fast inverse NFT, we have presented several ways to obtain a fast Darboux transformation (FDT) algorithm with an operational complexity of $\mathcal{O}(KN + N \log^2 N)$ where K is the number of eigenvalues to be added to a seed potential and N is the number of samples of the potential. This algorithm exhibits an order of convergence that matches the underlying exponential one-step method. In particular, if one uses the *trapezoidal rule* of integration, the order of convergence is $\mathcal{O}(N^{-2})$. The strength of this algorithm

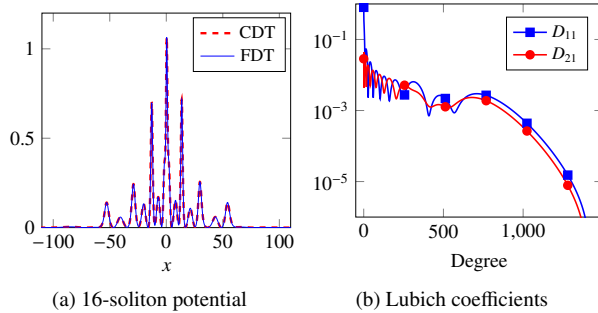


Figure 10: The figure on the left shows the multi-soliton potential corresponding to the discrete spectrum, \mathfrak{S}_{16} , defined by (122). The Lubich coefficients for the Darboux matrix is shown on the right. The underlying one-step method for the FDT algorithm here is the trapezoidal rule (TR).

was demonstrated by exhaustive numerical tests where we could successfully add 32 eigenvalues to a soliton-free seed potential. It must be noted that the FDT algorithm shows a promising route to a fast inverse NFT which is confirmed empirically in [18]—this forms the subject matter of the second part of this paper.

Furthermore, we have also presented a second approach that naively tries to mimic the classical Darboux transformation (CDT) scheme in the discrete framework developed for the ZS-problem with an arbitrary seed potential. This algorithm affords a complexity of $\mathcal{O}(K^2N)$; however, it turns out to be less accurate and numerically unstable beyond certain number of eigenvalues.

Finally, let us emphasize that, based on the ideas presented in this paper and drawing on the pioneering work of Lubich on convolution quadrature, it seems plausible to anticipate the existence of higher-order convergent fast forward/inverse NFT algorithms using (exponential) linear multistep methods such as various order BDF-schemes—we hope to return to this theme in the future.

References

- [1] V. E. Zakharov, A. B. Shabat, Exact theory of two-dimensional self-focusing and one-dimensional self-modulation of waves in nonlinear media, *Sov. Phys. JETP* 34 (1972) 62–69.
- [2] M. J. Ablowitz, D. J. Kaup, A. C. Newell, H. Segur,

The inverse scattering transform - Fourier analysis for nonlinear problems, *Studies in Applied Mathematics* 53 (4) (1974) 249–315. doi:10.1002/sapm1974534249.

- [3] M. Ablowitz, H. Segur, *Solitons and the Inverse Scattering Transform*, Society for Industrial and Applied Mathematics, 1981. doi:10.1137/1.9781611970883.
- [4] Y. Kodama, A. Hasegawa, Nonlinear pulse propagation in a monomode dielectric guide, *Quantum Electronics, IEEE Journal of* 23 (5) (1987) 510–524. doi:10.1109/JQE.1987.1073392.
- [5] G. Agrawal, *Nonlinear Fiber Optics*, Academic Press, Academic Press, 2013.
- [6] A. Hasegawa, Y. Kodama, Guiding-center soliton in optical fibers, *Opt. Lett.* 15 (24) (1990) 1443–1445. doi:10.1364/OL.15.001443.
- [7] A. Hasegawa, Y. Kodama, Guiding-center soliton, *Phys. Rev. Lett.* 66 (1991) 161–164. doi:10.1103/PhysRevLett.66.161.
- [8] S. K. Turitsyn, B. G. Bale, M. P. Fedoruk, Dispersion-managed solitons in fibre systems and lasers, *Physics Reports* 521 (4) (2012) 135–203, dispersion-Managed Solitons in Fibre Systems and Lasers. doi:10.1016/j.physrep.2012.09.004.
- [9] R. Feced, M. N. Zervas, Efficient inverse scattering algorithm for the design of grating-assisted codirectional mode couplers, *J. Opt. Soc. Am. A* 17 (9) (2000) 1573–1582. doi:10.1364/JOSAA.17.001FZ2000573.
- [10] J. K. Brenne, J. Skaar, Design of grating-assisted codirectional couplers with discrete inverse-scattering algorithms, *J. Lightwave Technol.* 21 (1) (2003) 254.
- [11] D. E. Rourke, P. G. Morris, The inverse scattering transform and its use in the exact inversion of the Bloch equation for noninteracting spins, *Journal of Magnetic Resonance* (1969) 99 (1) (1992) 118–138. doi:10.1016/0022-2364(92)90159-5.

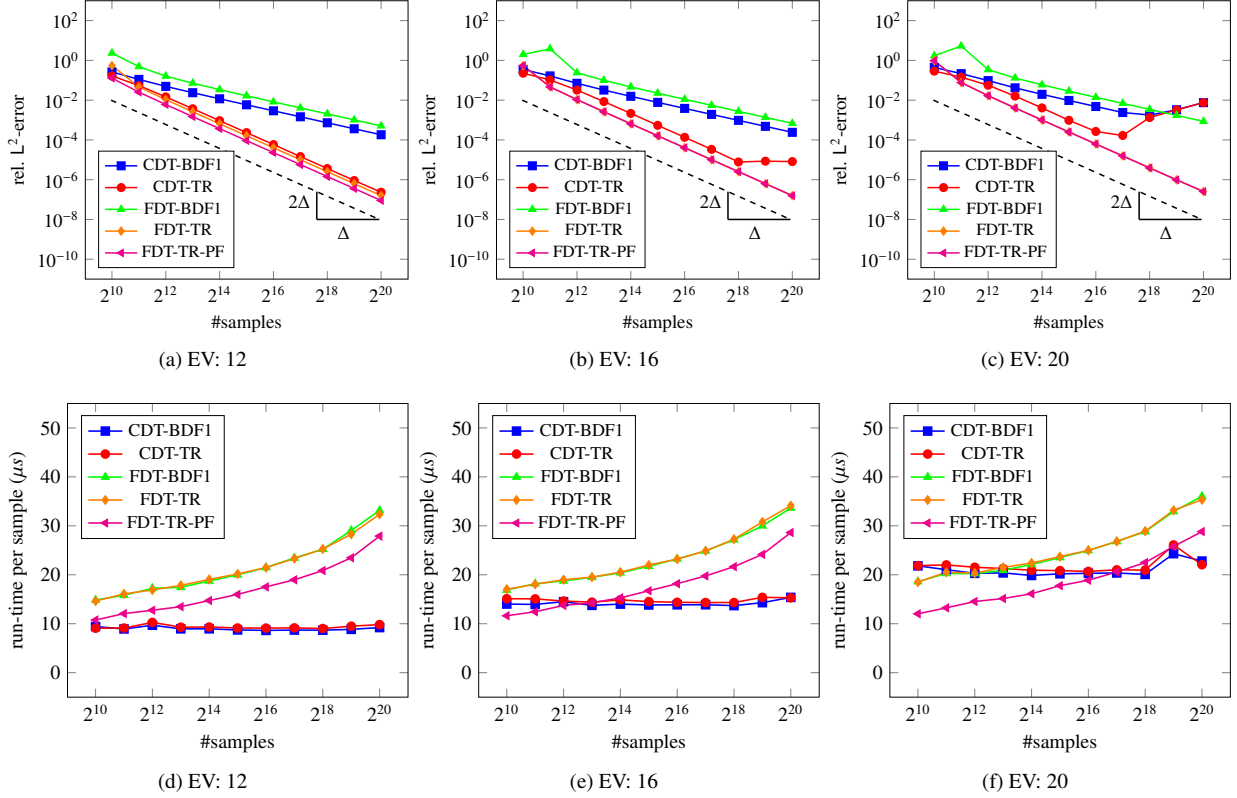


Figure 11: The figure depicts convergence analysis (top row) and run-time behavior for general Darboux transformation. The numerical test is carried out with a soliton-free sech-potential as seed and fixed number of eigenvalues to be added to the profile (see Sec. 7.2.3).

- [12] D. E. Rourke, P. G. Morris, Half solitons as solutions to the Zakharov-Shabat eigenvalue problem for rational reflection coefficient with application in the design of selective pulses in nuclear magnetic resonance, *Phys. Rev. A* 46 (1992) 3631–3636. doi:10.1103/PhysRevA.46.3631.
- [13] D. E. Rourke, J. K. Saunders, Half solitons as solutions to the Zakharov-Shabat eigenvalue problem for rational reflection coefficient. II. Potentials on infinite support, *Journal of Mathematical Physics* 35 (2) (1994) 848–872. doi:10.1063/1.530617.
- [14] A. Hasegawa, T. Nyu, Eigenvalue communication, *J. Lightwave Technol.* 11 (3) (1993) 395–399. doi:10.1109/50.219570.
- [15] M. I. Yousefi, F. R. Kschischang, Information transmission using the nonlinear Fourier transform, Parts I–III, *IEEE Trans. Inf. Theory* 60 (7) (2014) 4312–4369.
- [16] V. Aref, S. T. Le, H. Büelow, Demonstration of fully nonlinear spectrum modulated system in the highly nonlinear optical transmission regime, in: *ECOC 2016 - Post Deadline Paper; 42nd European Conference on Optical Communication*, 2016, pp. 1–3.
- [17] S. K. Turitsyn, J. E. Prilepsky, S. T. Le, S. Wahls, L. L. Frumin, M. Kamalian, S. A. Derevyanko, Nonlinear Fourier transform for optical data processing and transmission: advances and perspectives, *Optica* 4 (3) (2017) 307–322. doi:10.1364/OPTICA.4.000307.

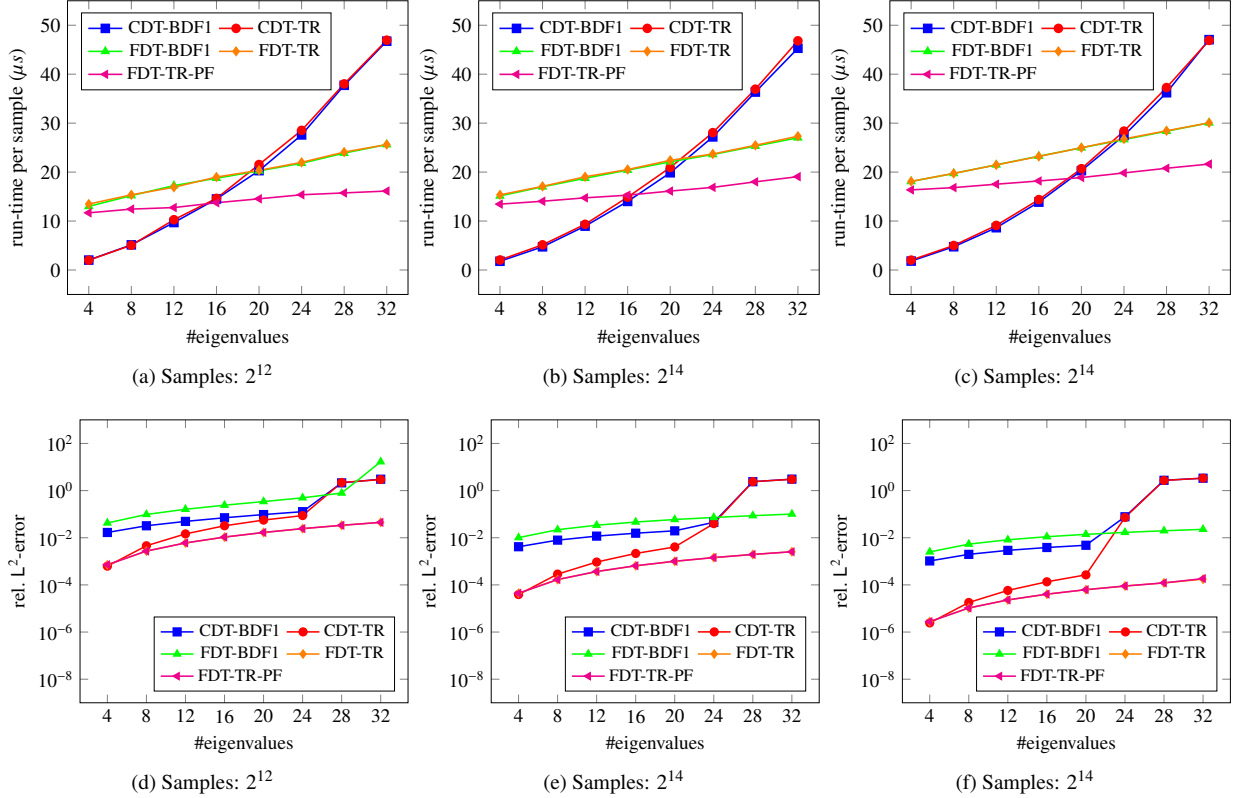


Figure 12: The figure depicts the run-time (top row) and the relative numerical error (bottom row) for the general Darboux transform as a function of number of eigenvalues. The numerical test (as described in Sec. 7.2.3) is carried out with fixed number of samples.

- [18] V. Vaibhav, S. Wahls, Introducing the fast inverse NFT, in: Optical Fiber Communication Conference, Optical Society of America, 2017, p. Tu3D.2. doi: [10.1364/OFC.2017.Tu3D.2](https://doi.org/10.1364/OFC.2017.Tu3D.2).
- [19] J. Lin, Evolution of the scattering data under the classical Darboux transform for SU(2) soliton systems, Acta Mathematicae Applicatae Sinica 6 (4) (1990) 308–316. doi: [10.1007/BF02015338](https://doi.org/10.1007/BF02015338).
- [20] C. Gu, A. Hu, Z. Zhou, Darboux Transformations in Integrable Systems: Theory and their Applications to Geometry, Mathematical Physics Studies, Springer Netherlands, 2005. doi: [10.1007/1-4020-3088-6](https://doi.org/10.1007/1-4020-3088-6).
- [21] S. Hari, F. Kschischang, M. Yousefi, Multi-eigenvalue communication via the nonlinear Fourier transform, in: Communications (QBSC), 2014 27th Biennial Symposium on, 2014, pp. 92–95. doi: [10.1109/QBSC.2014.6841191](https://doi.org/10.1109/QBSC.2014.6841191).
- [22] Z. Dong, S. Hari, T. Gui, K. Zhong, M. I. Yousefi, C. Lu, P.-K. A. Wai, F. R. Kschischang, A. P. T. Lau, Nonlinear frequency division multiplexed transmissions based on NFT, Photonics Technology Letters, IEEE 27 (15) (2015) 1621–1623. doi: [10.1109/LPT.2015.2432793](https://doi.org/10.1109/LPT.2015.2432793).
- [23] S. Hari, F. R. Kschischang, Bi-directional algorithm for computing discrete spectral amplitudes in the NFT, Journal of Lightwave Technology 34 (15) (2016) 3529–3537. doi: [10.1109/JLT.2016.2577702](https://doi.org/10.1109/JLT.2016.2577702).

- [24] H. Terauchi, A. Maruta, Eigenvalue modulated optical transmission system based on digital coherent technology, in: OECC/PS, 2013 18th, 2013, pp. 1–2.
- [25] H. Bülow, Experimental assessment of nonlinear Fourier transformation based detection under fiber nonlinearity, in: Optical Communication (ECOC), 2014 European Conference on, 2014, pp. 1–3. doi: [10.1109/ECOC.2014.6963840](https://doi.org/10.1109/ECOC.2014.6963840).
- [26] H. Bülow, Experimental demonstration of optical signal detection using nonlinear Fourier transform, J. Lightwave Technol. 33 (7) (2015) 1433–1439.
- [27] Y. Matsuda, H. Terauchi, A. Maruta, Design of eigenvalue-multiplexed multi-level modulation optical transmission system, in: Optical Fibre Technology, 2014 OptoElectronics and Communication Conference and Australian Conference on, 2014, pp. 1016–1018.
- [28] V. Aref, H. Bülow, K. Schuh, W. Idler, Experimental demonstration of nonlinear frequency division multiplexed transmission, arXiv:1508.02577[cs.IT] (2015).
- [29] H. Bülow, V. Aref, W. Idler, Transmission of waveforms determined by 7 eigenvalues with psk-modulated spectral amplitudes, arXiv:1605.08069[physics.optics] (2016).
- [30] S. Wahls, V. Vaibhav, Fast inverse nonlinear Fourier transforms for continuous spectra of Zakharov-Shabat type, arXiv:1607.01305v2[cs.IT] (2016).
- [31] S. M. Cox, P. C. Matthews, Exponential time differencing for stiff systems, Journal of Computational Physics 176 (2) (2002) 430–455. doi: [10.1006/jcph.2002.6995](https://doi.org/10.1006/jcph.2002.6995).
- [32] W. Gautschi, Numerical Analysis, Birkhäuser Boston, 2012. doi: [10.1007/978-0-8176-8259-0](https://doi.org/10.1007/978-0-8176-8259-0).
- [33] M. Born, E. Wolf, Principles of Optics: Electromagnetic Theory of Propagation, Interference and Diffraction of Light, seventh Edition, Cambridge University Press, 1999.
- [34] P. Henrici, Applied and Computational Complex Analysis, Volume 3: Discrete Fourier Analysis, Cauchy Integrals, Construction of Conformal Maps, Univalent Functions, Applied and Computational Complex Analysis, John Wiley & Sons, Inc., 1993.
- [35] A. M. Bruckstein, T. Kailath, Inverse scattering for discrete transmission-line models, SIAM Review 29 (3) (1987) 359–389. doi: [10.1137/1029075](https://doi.org/10.1137/1029075).
- [36] M. J. Ablowitz, B. Prinari, A. D. Trubatch, Discrete and Continuous Nonlinear Schrödinger Systems, Vol. 302 of London Mathematical Society Lecture Note Series, Cambridge University Press, 2004.
- [37] S. Wahls, H. V. Poor, Fast numerical nonlinear Fourier transforms, IEEE Transactions on Information Theory 61 (12) (2015) 6957–6974. doi: [10.1109/TIT.2015.2485944](https://doi.org/10.1109/TIT.2015.2485944).
- [38] S. Wahls, H. V. Poor, Fast inverse nonlinear Fourier transform for generating multi-solitons in optical fiber, in: Information Theory (ISIT), 2015 IEEE International Symposium on, 2015, pp. 1676–1680. doi: [10.1109/ISIT.2015.7282741](https://doi.org/10.1109/ISIT.2015.7282741).
- [39] C. Lubich, Convolution quadrature and discretized operational calculus. I, Numerische Mathematik 52 (2) (1988) 129–145. doi: [10.1007/BF01398686](https://doi.org/10.1007/BF01398686).
- [40] C. Lubich, Convolution quadrature and discretized operational calculus. II, Numerische Mathematik 52 (4) (1988) 413–425. doi: [10.1007/BF01462237](https://doi.org/10.1007/BF01462237).
- [41] C. Lubich, On the multistep time discretization of linear initial-boundary value problems and their boundary integral equations, Numerische Mathematik 67 (3) (1994) 365–389. doi: [10.1007/s002110050033](https://doi.org/10.1007/s002110050033).
- [42] G. Neugebauer, R. Meinel, General N-soliton solution of the AKNS class on arbitrary background, Physics Letters A 100 (9) (1984) 467–470. doi: [10.1016/0375-9601\(84\)90827-2](https://doi.org/10.1016/0375-9601(84)90827-2).

- [43] V. Vaibhav, W. Wahls, Multipoint newton-type non-linear Fourier transform for detecting multi-solitons, in: Optical Fiber Communication Conference, Optical Society of America, 2016, p. W2A.34. doi: [10.1364/OFC.2016.W2A.34](https://doi.org/10.1364/OFC.2016.W2A.34).
- [44] G. L. Lamb, Elements of soliton theory, Pure and applied mathematics, John Wiley & Sons, Inc., 1980.
- [45] H. Steudel, Scattering at truncated solitons and inverse scattering on the semiline, Contemporary Mathematics 301 (2002) 331–338. doi: [10.1088/0266-5611/24/2/025015](https://doi.org/10.1088/0266-5611/24/2/025015).
- [46] H. Steudel, D. J. Kaup, Inverse scattering for an AKNS problem with rational reflection coefficients, Inverse Problems 24 (2) (2008) 025015. doi: [10.1088/0266-5611/24/2/025015](https://doi.org/10.1088/0266-5611/24/2/025015).
- [47] S. Wahls, H. V. Poor, Introducing the fast nonlinear Fourier transform, in: Proc. IEEE Int. Conf. Acoust. Speech Signal Process. (ICASSP), Vancouver, Canada, 2013.
- [48] V. Aref, Control and detection of discrete spectral amplitudes in nonlinear Fourier spectrum, arXiv:1605.06328[math.NA] (2016).
- [49] W. K. McClary, Fast seismic inversion, Geophysics 48 (10) (1983) 1371–1372. doi: [10.1190/1.1441417](https://doi.org/10.1190/1.1441417).
- [50] W. Magnus, On the exponential solution of differential equations for a linear operator, Communications on Pure and Applied Mathematics 7 (4) (1954) 649–673. doi: [10.1002/cpa.3160070404](https://doi.org/10.1002/cpa.3160070404).
- [51] A. Iserles, S. Nørsett, On the solution of linear differential equations in Lie groups, Philosophical Transactions of the Royal Society of London A: Mathematical, Physical and Engineering Sciences 357 (1754) (1999) 983–1019. doi: [10.1098/rsta.1999.0362](https://doi.org/10.1098/rsta.1999.0362).
- [52] M. Hochbruck, C. Lubich, On Magnus integrators for time-dependent Schrödinger equations, SIAM Journal on Numerical Analysis 41 (3) (2003) 945–963. doi: [10.1137/S0036142902403875](https://doi.org/10.1137/S0036142902403875).
- [53] E. Hairer, C. Lubich, G. Wanner, Geometric Numerical Integration: Structure-Preserving Algorithms for Ordinary Differential Equations, 2nd Edition, Springer Series in Computational Mathematics, Springer-Verlag Berlin Heidelberg, 2006. doi: [10.1007/3-540-30666-8](https://doi.org/10.1007/3-540-30666-8).
- [54] G. Boffetta, A. R. Osborne, Computation of the direct scattering transform for the nonlinear Schrödinger equation, Journal of Computational Physics 102 (2) (1992) 252–264. doi: [10.1016/0021-9991\(92\)90370-E](https://doi.org/10.1016/0021-9991(92)90370-E).
- [55] S. Burtsev, R. Camassa, I. Timofeyev, Numerical algorithms for the direct spectral transform with applications to nonlinear Schrödinger type systems, Journal of Computational Physics 147 (1) (1998) 166–186. doi: [10.1006/jcph.1998.6087](https://doi.org/10.1006/jcph.1998.6087).
- [56] G. Strang, On the construction and comparison of difference schemes, SIAM Journal on Numerical Analysis 5 (3) (1968) 506–517. doi: [10.1137/0705041](https://doi.org/10.1137/0705041).
- [57] A. M. Bruckstein, B. C. Levy, T. Kailath, Differential methods in inverse scattering, SIAM Journal on Applied Mathematics 45 (2) (1985) 312–335. doi: [10.1137/0145017](https://doi.org/10.1137/0145017).
- [58] F. Jones, Lebesgue Integration on Euclidean Space, Jones and Bartlett books in mathematics, Jones and Bartlett, 2001.
- [59] S. Novikov, S. V. Manakov, L. P. Pitaevskii, V. E. Zakharov, Theory of Solitons: The Inverse Scattering Method, Contemporary Soviet Mathematics, Consultant Bureau, New York and London, 1984.
- [60] G. Gripenberg, S. O. Londen, O. Staffans, Volterra Integral and Functional Equations, Vol. 34 of Encyclopedia of Mathematics and Its Applications, Cambridge University Press, 1990.
- [61] P. Lancaster, M. Tismenetsky, The Theory of Matrices: With Applications, 2nd Edition, Computer Science and Scientific Computing Series, Academic Press, 1985.

- [62] J. Satsuma, N. Yajima, B. initial value problems of one-dimensional self-modulation of nonlinear waves in dispersive media, Progress of Theoretical Physics Supplement 55 (1974) 284–306. [doi: 10.1143/PTPS.55.284](https://doi.org/10.1143/PTPS.55.284).